KU LEUVEN

ARENBERG DOCTORAL SCHOOL
Faculty of Engineering Technology

Design parameters for construction of dikes with treated sludge at redevelopment of sludge reservoirs

Kristof Verreydt

Supervisors:
prof. dr. ir. Pieter Rauwoens
em. prof. dr. ir. Dionys Van Gemert

Dissertation presented in partial fulfillment of the requirements for the degree of Doctor of Engineering Technology (PhD)

May 2021

Design parameters for construction of dikes with treated sludge at redevelopment of sludge reservoirs

Kristof VERREYDT

Examination committee:
prof. dr. ir. Jan Van Impe, chair
prof. dr. ir. Pieter Rauwoens, supervisor
em. prof. dr. ir. Dionys Van Gemert, supervisor
prof. ir. Noël Huybrechts
prof. dr. Jan Elsen
em. prof. dr. Noël Vandenberghe
dr. ir. Jules Houtmeyers
(Tessenderlo Group)
prof. dr. ir. Hanbing Bian
(ULille, France)

Dissertation presented in partial fulfillment of the requirements for the degree of Doctor of Engineering Technology (PhD)

May 2021

© 2021 KU Leuven – Faculty of Engineering Technology
Uitgegeven in eigen beheer, Kristof Verreydt, Kasteelpark Arenberg 40, box 2448, B-3001 Leuven (Belgium)

Alle rechten voorbehouden. Niets uit deze uitgave mag worden vermenigvuldigd en/of openbaar gemaakt worden door middel van druk, fotokopie, microfilm, elektronisch of op welke andere wijze ook zonder voorafgaande schriftelijke toestemming van de uitgever.

All rights reserved. No part of the publication may be reproduced in any form by print, photoprint, microfilm, electronic or any other means without written permission from the publisher.

Le talent n'existe pas.
Le talent, c'est d'avoir l'envie de faire quelque chose
... tout le restant, c'est de la sueur.

Jacques Brel

Preface

After finishing my education in engineering technology, I started working at Triconsult nv, a spin-off of KU Leuven, founded by em. prof. dr. ir. Dionys van Gemert. After a few years, prof. Dionys Van Gemert proposed to expand the boundaries of my knowledge with an interesting project on industrial sludge. Because of the size and complexity of the project, I had the opportunity to convert my experiences into a doctoral research project. Hence, my great thanks goes to prof. Dionys Van Gemert not only for the opportunities given but also for chairing knowledge and insights on engineering. Without his guidance and contributions, this work would not have been possible.

My appreciation goes to my promoter prof. dr. ir. Pieter Rauwoens for his critical view and change of perspective, which has taken my research to a higher level.

I would like to thank all the members of the Examination Committee. First of all, prof. ir. Noël Huybrechts and prof. dr. ir. Jan Elsen for their interest in the project and their useful constructive remarks throughout the years. Secondly, thanks to em. prof. dr. Noël Vandenberghe and prof. dr. ir. Hanbing Bian (ULille) for their willingness to make participate in the Examination Committee. I also like to thank prof. dr. ir. Jan Van Impe for being available to chair the Examination Committee. My special thanks to dr. ir. Jules Houtmeyers (Tessenderlo Group) for his enthusiasm towards the project and his support in many ways.

I wish to express my gratitude to Tessenderlo Group, for the opportunities given and the investments in the soil research. Thanks to the staff at Tessenderlo Group, Ham, for their involvement and support, in particular Tom Claes, Johan Van Waelderen and Geert Peeters.

Furthermore, I would like to thank Jan van Broekhoven and the crane operators at Envi nv for their assistance in conducting small or large soil tests.

I thank my colleagues at Triconsult nv. Sven, Kris, Gert and Timo, thanks for the useful tips and (psychological) support. Special thanks to Timo, who assisted me in most of the field testing in the sludge.

I would also like to thank my family and family in law for their unconditional support. Thank you, mum and dad, for all the opportunities you've granted me and guidance and advice which you've given me, making me who I am today.

An extraordinary thank you goes to my wife for her permanent support. Nicky, despite me renovating our house and spending weekends on analysing data and writing text, you kept up my motivation and encouraged me to persevere. Thanks for relieving me of household chores, which put much more burden on you. I promise to make this right in the (many) years to come.

I couldn't be more thankful about my children. Finn, for keeping me fit by playing tag and Ella with her beautiful smile, turning a frown upside down. I will be happy to leave behind this extra workload and spend more time with them.

Kristof Verreydt

May 2021

Abstract

Reliable data on the shear resistance are essential in slope stability calculations. When elevations are made with documented soils (sand, clay, ...), literature data can be used. However, if the material deviates from common soil types, field and/or laboratory tests are required to characterise the soil.

This research deals with the (physical) characterisation of (historical) industrial sludge, arising from the production of phosphate fertilizer and feed phosphate at the chemical producer, Tessenderlo Group. The sludge mainly consists of calcium-fluoride (CaF_2), bound to silicon-dioxide (SiO_2).

Throughout the years, the produced sludge was stored at several deposits located in the vicinity of the factory at Ham (Belgium), among others at deposit Veldhoven (75 ha), deposit Kepkensberg (30 ha) and Old Deposit (7.5 ha). The existing deposits are being reconverted, which includes clearing and redeveloping one deposit site and optimising the storage capacity of the others by creating sludge embankments on top of the current sludge levels.

By performing an elaborate material investigation and executing full-scale test setups, a suitable method will be developed to analyse and determine the characteristics of the industrial sludge. These methods may well be applied to similar material such as dredging sludge. The results are used to evaluate the stability issues of embankments constructed with and on the industrial sludge.

First of all, a soil investigation was conducted, in which a series of laboratory and field tests were carried out. The sludge has a low permeability. Hence, the emphasis of the soil tests is on the undrained soil parameters.

The stored material consists of a combination of naturally consolidated sludge with a highly variable fraction of glauconite containing sand. During the construction of the sludge elevations, the water content of the sludge is reduced by allowing sludge drying by wind and sun.

This method is applied layer by layer and the layering rate strongly depends on the initial water content of the particular sludge and the weather conditions. This resulted in an embankment with varying parameters, whereby layers with a high water content (weak layers) may alternate with layers with low water content (strong layers). Because of the heterogeneous composition of the embankment, investigating the subsurface at various locations and depths is considered more valuable than performing high-quality tests at individual points.

In the second stage of the research, the accuracy of in situ tests was evaluated and compared with a full-scale slope failure test. The elevation of the terrain and the influence of consolidation were simulated by the construction of a test embankment measuring 30 m $\times$ 60 m $\times$ 4 m.

Field vane tests were used to estimate the undrained shear strength. The theoretical failure load at the test embankment was calculated with the results of the vane tests. The crest load consisted of water tight containers, placed on crane mats. Filling the containers with water was done step by step to increase the load. Between the loading steps, deformations of the slope were measured with two theodolites that registered the movement of various reference points. The containers were filled until slope failure occurred.

By means of a finite element analysis, a back-calculation of the full-scale test was done. The various influence parameters, such as 3D-effects, anisotropy and strain rate effect were analysed and estimated. On the one hand, a classic Mohr-Coulomb material model was used for the back-calculation. On the other hand, the recently developed material model NGI-ADP (Norwegian Geotechnical Institute - Active, Direct simple shear, Passive) by [Andresen and Jostad, 1999], was applied. The NGI-ADP material model allows to simulate the anisotropic behaviour of the soil.

The analysis indicated the importance of the influence of anisotropic soil behaviour of the sludge on the short-term stability of the test embankment. The NGI-ADP material model predicted quite accurately the actual failure load, using anisotropic conversion factors. These anisotropic conversion factors are based on literature data by [Ladd, 1991], [Terzaghi et al., 1996] and [Skempton, 1957].

Finally, the most suitable test method is implemented in a finite element analysis for an embankment with dimensions 260 m $\times$ 135 m $\times$ 16 m on sludge deposit Veldhoven. The soil investigation included piezocone penetration tests (CPTu) at locations where also field vane tests had been made, to enable determination of the cone factor.

In addition, the derived anisotropic conversion factors are applied on the CPTu for the determination of the shear parameters for the different anisotropic stress states in the sludge embankment.

Different material models are available for simulating soil behaviour. The frequently applied models (Mohr-Coulomb, Hardening Soil, ...) are compared with the recently developed NGI-ADP material model.

Beknopte samenvatting

Kennis van de schuifweerstand is van fundamenteel belang voor het berekenen van de taludstabiliteit bij ophogingen. Als een ophoging met gedocumenteerde gronden (zand, klei, ...) wordt uitgevoerd, kunnen gegevens uit de literatuur gebruikt worden. Indien het gebruikte materiaal echter sterk afwijkt van frequent voorkomende grondsoorten, zijn terrein- en/of laboratoriumproeven noodzakelijk voor het karakteriseren van de grond.

Voorliggend doctoraatsonderzoek handelt over industrieel slib o.a. afkomstig van de productie van fosfaten (dierenvoedingssupplementen). Het restproduct bestaat hoofdzakelijk uit calciumfluoride (CaF_2), gebonden aan siliciumdioxide (SiO_2). Doorheen de jaren werd het geproduceerde slib opgeslagen in verschillende opslagbekkens in de omgeving van de chemische fabriek te Ham (België): slibbekken Veldhoven (75 ha), slibbekken Kepkensberg (30 ha) en Oud Bekken (7.5 ha). De bestaande slibbekkens ondergaan de komende jaren een reconversie waarbij sommige bekkens volledig ontruimd worden. De opslagcapaciteit van de andere bekkens wordt geoptimaliseerd door opstapeling van slib bovenop het huidig slibpeil.

Met een uitgebreid materiaalonderzoek en diverse proefopstellingen wordt getracht een gepaste methode te ontwikkelen voor het analyseren en bepalen van de karakteristieken van het industrieel slib. Deze kunnen ook van toepassing zijn op soortgelijke materialen zoals baggerslib. De proefresultaten worden aangewend om de stabiliteitszekerheid te evalueren van de ophogingen op en met industrieel slib.

In eerste instantie werden diverse veld- en laboproeven uitgevoerd op het CaF_2 slib. De waterdoorlatendheid van het slib is vergelijkbaar met deze van klei, en daarom wordt er in het bijzonder aandacht besteed aan de ongedraineerde grondparameters.

Het gestockeerde materiaal bestaat uit een combinatie van natuurlijk geconsolideerd slib met een sterk variërende fractie glauconiethoudend zand. Om het watergehalte van het slib te reduceren wordt het aan de zon en de lucht gedroogd, tijdens de bouw van de ophoging. Deze methode wordt laag per laag toegepast en is sterk afhankelijk van het initiële watergehalte van het aangevoerde slib en van de weersomstandigheden. Finaal heeft deze methode geleid tot een ophoging met sterk variërende eigenschappen waarbij lagen met een hoog waterhalte (zwakke laag) afwisselen met lagen met een laag watergehalte (sterke laag). Door de heterogene samenstelling van de ophoging, wordt geoordeeld dat het onderkennen van de ondergrond op diverse locaties en dieptes betrouwbaarder is dan het uitvoeren van hoge kwaliteitsproeven op individuele punten.

In een tweede stap werd de nauwkeurigheid van in situ proeven geëvalueerd en vergeleken met een bezwijkproef op ware grootte. Een ophoging van het terrein en de invloed van consolidatie werd gesimuleerd door de bouw van een proefdijk (30 m $\times$ 60 m $\times$ 4 m).

Een inschatting van de ongedraineerde schuifsterkte van het slib gebeurde voorafgaandelijk door middel van in situ vinproeven. De theoretische bezwijklast werd berekend met de verkregen resultaten van de vinproeven. De belasting op de proefdijk bestond uit waterdichte containers, geplaatst op houten rijplaten. De belasting werd verhoogd door het stapsgewijs vullen van de container met water. Tussen de belastingstappen werden de vervormingen van het talud opgemeten met behulp van twee theodolieten die de verplaatsing registreerden van een groot aantal piketten aangebracht op het talud en achter de containers. De containers werden verder gevuld met water tot bezwijken optrad in het slibmassief.

Een eindige elementen analyse werd toegepast voor een back-calculation van de bezwijkproef. De verschillende invloedparameters zoals 3D-effecten, anisotropie en strain rate effect werden geanalyseerd en begroot. Voor de modellering van de bezwijkproef werd enerzijds een klassiek Mohr-Coulomb materiaalmodel toegepast. Anderzijds werd er gebruik gemaakt van het recent ontwikkeld materiaal model NGI-ADP (Norwegian Geotechnical Institute - Active, Direct simple shear, Passive; [Andresen and Jostad, 1999]). Het NGI-ADP materiaal model laat toe om het anisotrope gedrag van het slibmateriaal te simuleren.

De analyse van de bezwijkproef toont aan dat het anisotrope grondgedrag van het slib een belangrijke invloed heeft op de korte termijn stabiliteit van de proefdijk. Het NGI-ADP materiaal model benaderde de werkelijke bezwijklast, gebruikmakend van anisotrope conversiefactoren, gebaseerd op literatuur gegevens van [Ladd, 1991], [Terzaghi et al., 1996] en [Skempton, 1957].

Finaal wordt de gekozen onderzoeksmethode toegepast op een intussen opgebouwde ophoging. De resultaten worden geïmplementeerd in een eindige elementen analyse voor een ophoging met afmetingen 260 m $\times$ 135 m $\times$ 16 m gebouwd op slibbekken Veldhoven. Het grondonderzoek omvatte piëzocone sonderingen (CPTu), waarbij de conusfactor werd gedefinieerd op basis van in situ vinproeven. Tevens worden de gedefinieerde anisotrope conversie factoren toegepast op de CPTu voor de bepaling van de afschuifparameters voor de verschillende anisotrope spanningstoestanden in de slibophoging.

Verschillende materiaalmodellen zijn beschikbaar voor het voorspellen van het afschuifgedrag van gronden. Frequent toegepaste modellen (Mohr-Coulomb, Hardening Soil, ...) worden vergeleken met het recentelijk ontwikkelde NGI-ADP materiaalmodel.

Nomenclature

Symbols – Latin characters

Symbol	Description	Unit
a	CPTu area ratio factor	-
b	Time factor	-
c	Cohesion	kN/m^2
c_{BST}	Cohesion at borehole shear test	kN/m^2
C_c	Compressibility index	-
C_r	Swelling or reloading stiffness	-
c_u	Undrained shear strength	kN/m^2
D	Depth	m
D	Drainage length	m
e	Void ratio	-
E	Young's modulus	kN/m^2
E'_{50}	Effective triaxial compression modulus	kN/m^2
E_{50}^{ref}	Reference triaxial stiffness	kN/m^2
E_{oed}	Oedometer modulus	kN/m^2
E_{oed}^{ref}	Reference oedometer stiffness	kN/m^2
E_u	Undrained triaxial modulus	kN/m^2
E_{ur}^{ref}	Reference un/reloading stiffness	kN/m^2
FS_{2D}	Factor of safety at plain strain or 2D geometry	-
FS_{3D}	Factor of safety at 3D geometry	-
G	Shear modulus	kN/m^2
G/s_u	Ratio shear modulus over undrained shear strength	-

Symbol	Description	Unit
G/s_u^A	Ratio shear modulus over (plane strain) active shear strength	-
G_{ur}	Unload/reload shear modulus	kN/m^2
G_{ur}/s_u^A	Ratio unloading/reloading shear modulus over (plane strain) active shear strength	-
I_p	Plasticity index	%
J_2	Second deviatoric stress invariant	-
k	Permeability	m/s
K	Earth pressure coefficient	-
K_0	Coefficient of earth pressure at rest	-
L	Length	m
M	Friction constant	-
m	Strength increase exponent	-
n	Number of tests	-
N_c	Theoretical cone factor	-
$N_{\Delta u}$	Empirical cone factor for excess pore water pressure	-
N_k	Empirical cone factor	-
N_{ke}	Empirical cone factor for effective cone resistance	-
N_{kt}	Empirical cone factor for net cone resistance	-
$N_{kt,FV}$	Empirical cone factor for net cone resistance, with field vane test as reference	-
N_{kt}^A	Empirical cone factor correlated to the undrained active shear strength	-
$N_{kt,CAUC}$	Empirical cone factor correlated to the anisotropic consolidated undrained compression shear strength	-
N_{kt}^{DSS}	Empirical cone factor correlated to the undrained direct simple shear strength	-
$N_{kt,Lab}$	Empirical cone factor correlated to the average undrained laboratory shear strength	-
N_{kt}^P	Empirical cone factor correlated to the undrained passive shear strength	-
$N_{kt,TC}$	Empirical cone factor correlated to the undrained triaxial compression shear strength	-

Symbol	Description	Unit
$N_{kt,TE}$	Empirical cone factor correlated to the undrained triaxial extension shear strength	-
OCR	Over-consolidation ratio	-
OCR_{min}	Minimum over-consolidation ratio	-
p	Mean total stress	kN/m^2
p'	Mean effective stress	kN/m^2
POP_{min}	Minimum pre-overburden pressure	kN/m^2
p_w	Pore water pressure	kN/m^2
q	Deviatoric stress	kN/m^2
q_c	Cone tip resistance	kN/m^2
q_{net}	Net cone resistance	kN/m^2
q_t	Cone tip resistance corrected for pore pressure effects	kN/m^2
R_f	Friction ratio	-
R_{inter}	Interface strength	-
S	Normally consolidated shear strength ratio	-
s	Standard deviation	-
s'	Mean effective stress	kN/m^2
S_{FV}	Shear strength ratio at field vane test	-
S_{peak}	Shear strength ratio at peak strength	-
S_t	Sensitivity of soil	-
S_{TC}	Shear strength ratio at triaxial compression test	-
s_u	Undrained shear strength	kN/m^2
s_u^A	Undrained plain strain active shear strength	kN/m^2
s_u^A/s_u^P	Ratio of (plane strain) passive shear strength over (plane strain) active shear strength	-
$s_{u,ave}$	Undrained average shear strength	kN/m^2
$s_{u,ave,char}$	Characteristic average undrained shear strength	kN/m^2
$s_{u,ave,char}^A$	Characteristic average active undrained shear strength	kN/m^2
$s_{u,claycover}$	Undrained shear strength of clay cover	kN/m^2
$s_{u,CPTu}$	Undrained shear strength at piezocone test	kN/m^2
$s_u^{C,TX}/s_u^A$	Ratio of triaxial compressive shear strength over (plane strain) active shear strength	-
$s_{u,DSS}$	Undrained shear strength at direct simple shear	kN/m^2

Symbol	Description	Unit
s_u^{DSS}	Undrained direct simple shear strength	kN/m^2
s_u^{DSS}/s_u^A	Ratio of direct simple shear strength over (plane strain) active shear strength	-
$s_{u,FV}$	Undrained shear strength at field vane test	kN/m^2
$s_{u,inc}^A$	Increase of shear strength with depth	kPa/m
$s_{u,Lab}$	Average laboratory undrained shear strength	kN/m^2
S_{ult}	Shear strength ratio at ultimate strain	-
$s_{u,min}$	Minimum undrained shear strength	kN/m^2
$s_{u,NC}$	Undrained shear strength at normal consolidation	kN/m^2
$s_{u,OC}$	Undrained shear strength at over-consolidation	kN/m^2
s_u^P	Undrained plain strain passive shear strength	kN/m^2
$s_{u,ref}^A$	Reference (plane strain) active shear strength	kN/m^2
s_{u,t_0}	Undrained shear strength with time to failure t_0	kN/m^2
$s_{u,TC}$	Undrained shear strength at triaxial compression	kN/m^2
$s_{u,TE}$	Undrained shear strength at triaxial extension	kN/m^2
s_{u,t_f}	Undrained shear strength with time to failure t_f	kN/m^2
S_α	Shear strength ratio at a certain stress state	-
T	Dimensionless time factor	-
t	Construction time	sec
t	Shear strength	kN/m^2
t_0	Time to failure at reference time	sec
$t_{0,95}^{n-1}$	Student t-distribution at confidence level of 95% and (n-1) degrees of freedom	-
t_f	Time to failure	sec
U	Degree of consolidation	-
u	Pore water pressure	kN/m^2
u_0	Pore water pressure at equilibrium	kN/m^2
u_1	Pore water pressure at face of piezocone	kN/m^2
u_2	Pore water pressure at shoulder position of piezocone	kN/m^2
u_3	Pore water pressure behind friction sleeve of piezocone	kN/m^2
w	Water content	$\%$
w_L	Liquid limit	$\%$
y	Reference depth	m

Symbols – Greek characters

Symbol	Description	Unit
α	Coefficient for normally consolidated shear strength ratio	-
α	Angle between major principal stress and vertical axis	$^\circ$
Γ	Specific volume of a point on the critical state line at a certain pressure	-
Γ	Spread reduction factor	-
γ	Shear strain	-
γ	Unit weight	kN/m^3
γ_f^C	Shear strain at failure in triaxial compression	%
γ_f^{DSS}	Shear strain at failure in direct simple shear	%
γ_f^E	Shear strain at failure in triaxial extension	%
γ'_{sand}	Unit weight of sand	kN/m^3
γ_{sat}	Saturated unit weight	kN/m^3
γ_{unsat}	Unsaturated unit weight	kN/m^3
γ_w	Unit weight of water	kN/m^3
Δu	Excess pore water pressure	kN/m^2
ϵ_v	Vertical strain	-
θ	Lode angle	$^\circ$
κ	Hardening parameter	-
λ	Gradient of compression line	-
λ_a	Active horizontal earth pressure coefficient	-
μ	Correction factor	-
μ_B	Field vane correction factor by Bjerrum	-
$\mu_{DSS/FV}$	Anisotropic conversion factor from field vane to direct simple shear	-
$\mu_{Lab/FV}$	Anisotropic conversion factor from field vane to average laboratory shear	-
μ_R	Strain rate correction factor	-
$\mu_{TC/FV}$	Anisotropic conversion factor from field vane to triaxial compression	-

Symbol	Description	Unit
$\mu_{TE/FV}$	Anisotropic conversion factor from field vane to triaxial extension	-
μ_{α}	Anisotropic conversion factor	-
ν	Specific volume	-
ν'	Poisson's ratio	-
ν_u	Undrained Poisson's ratio	-
ν_{ur}	Poisson's ratio for un/reloading	-
σ	Total stress	kN/m^2
σ'_h	Horizontal effective stress	kN/m^2
σ'	Effective stress	kN/m^2
σ'_1	Major principle effective stress	kN/m^2
$\sigma'_{1,max}$	Maximum major principle effective stress ever reached	kN/m^2
σ'_h	Horizontal effective stress	kN/m^2
σ_n	Total normal stress	kN/m^2
σ'_p	Effective pre-consolidation stress	kN/m^2
σ_v	Total vertical stress	kN/m^2
σ'_v	Effective vertical stress	kN/m^2
σ'_{v0}	Effective vertical overburden stress	kN/m^2
σ_{v0}	Total vertical overburden stress	kN/m^2
σ'_{vc}	Effective vertical consolidation stress	kN/m^2
σ'_{vi}	In situ vertical effective stress	kN/m^2
$\sigma_{vy,peak}$	Vertical peak stress	kN/m^2
σ'_{xx}	Effective horizontal stress	kN/m^2
σ'_{yy}	Effective vertical stress	kN/m^2
τ	Shear stress	kN/m^2
τ_0	Initial in situ shear stress	kN/m^2
τ_0/s_u^A	Initial mobilization of shear strength	-
τ_{max}	Maximum shear stress	kN/m^2
τ_{xy}	Shear stress	kN/m^2
ϕ'	Effective angle of friction	$^{\circ}$
ϕ'_{BST}	Effective angle of friction at borehole shear test	$^{\circ}$
ϕ'_{CS}	Effective angle of friction of critical state line	$^{\circ}$
ϕ'_{sand}	Effective angle of friction of sand	$^{\circ}$

Symbol	Description	Unit
ψ'	Dilatancy angle	°

Abbreviations and acronyms

Symbol	Description
BST	Borehole shear test
CAU	Anisotropically consolidated undrained shear test
CAUC	Anisotropically consolidated undrained TC test
CIU	Isotropically consolidated undrained shear test
CK_0U	K_0 consolidated undrained shear test
COV	Coefficient of variation
CPT	Cone penetration test
CPTu	Piezocone penetration test
CRS	Constant rate of strain
CSSM	Critical state soil mechanics
CSL	Critical state line
CUU	Unconsolidated undrained test
DSS	Direct simple shear
ESP	Effective stress path
FEM	Finite element method
FS	Factor of safety
FVT	Field vane test
HS	Hardening Soil
LL	Liquid limit
MC	Mohr-Coulomb
NC	Normal consolidation
NGI-ADP	Norwegian Geotechnical Institution - Active, DSS, Passive
OC	Over-consolidation
PI	Plasticity index
PL	Plastic limit
SD	Standard deviation

Symbol	Description
SHANSEP	Stress History And Normalised Soil Engineering Properties
SS	Soft Soil
TAW	Tweede Algemene Waterpassing (dutch): Second general leveling
TC	Triaxial compression
TE	Triaxial extension
TSP	Total stress path
WC	Water content

Contents

Abstract v

Beknopte samenvatting ix

Nomenclature xiii

Contents xxi

List of Figures xxv

List of Tables xxxi

1 Introduction 1

1.1 General considerations 1
1.2 Redevelopment of sludge deposits at Tessenderlo Group 2
1.3 Research methods and objectives 5
1.4 Layout of the dissertation 6

2 Background information - History 9

2.1 Introduction 9
2.2 Sludge handling 10
2.3 Encountered problems 13
2.3.1 Differential settlements and heave 13
2.3.2 Documented slope failures 14
2.4 Conclusions 18

3 Literature survey: State of the art **19**
3.1 Introduction 19
3.2 Geotechnical characterisation of an industrial sludge 20
3.3 Literature references 23
3.3.1 Performance of a test embankment constructed on an organic clayey silt deposit 23
3.3.2 Failure of a trial embankment on peat in Booneschans, the Netherlands 25
3.3.3 Effective Stress Finite Element Stability Analysis of an Old Railway Embankment on Soft Clay in Perniö, Finland 29
3.4 Conclusions 31

4 Undrained soil behaviour **33**
4.1 Introduction 33
4.2 Drained vs undrained analysis 34
4.3 Critical state soil mechanics 36
4.3.1 CSSM theory 36
4.3.2 Shear strength in CSSM 39
4.4 SHANSEP 42
4.4.1 General 42
4.4.2 SHANSEP test procedure 43
4.4.3 Discussion 46
4.5 Anisotropy 46
4.5.1 General 46
4.6 Material models 49
4.6.1 Introduction 49
4.6.2 SHANSEP MC 50
4.6.3 NGI-ADP 52
4.6.4 SHANSEP NGI-ADP 55
4.7 Other shear phenomena 56
4.7.1 Peak shear 56
4.7.2 Strain compatibility 57
4.8 Conclusions 59

5 Field investigation and test procedures 61
5.1 Introduction . . . 61
5.2 Field investigation and laboratory testing program . . . 62
5.2.1 Borehole shear test . . . 62
5.2.2 Piezocone penetration test . . . 64
5.2.3 Field vane test . . . 66
5.2.4 Triaxial testing . . . 67
5.2.5 One-dimensional consolidation test . . . 68
5.3 Results of field investigation and laboratory testing program . . . 70
5.3.1 BST results . . . 70
5.3.2 CPTu results . . . 71
5.3.3 Field vane test results . . . 76
5.3.4 Triaxial test results . . . 79
5.3.5 One-dimensional consolidation test results . . . 81
5.4 Determination of cone factor from TC and FV tests . . . 83
5.4.1 Determination of cone factor with field vane test . . . 83
5.4.2 Determination of cone factor with triaxial tests . . . 86
5.4.3 Comparison between triaxial and field vane test method 87
5.4.4 Comparison of cone factor with literature findings . . . 89
5.5 Conclusions . . . 92

6 Full-scale slope failure test 95
6.1 Introduction . . . 95
6.2 Geometry and construction of test embankment . . . 96
6.3 Geotechnical characterisation . . . 99
6.3.1 Field vane tests . . . 99
6.3.2 Unconsolidated undrained triaxial compression tests . . . 101
6.4 Results of the large scale slope failure test . . . 101
6.5 Back-calculation of slope failure test . . . 105
6.5.1 Correction factors . . . 105
6.5.2 Material models . . . 110
6.5.3 Results of back-calculation . . . 113
6.5.4 Slope failure test after consolidation . . . 116
6.6 Conclusions . . . 118

7 Stability analysis of a sludge embankment on Veldhoven deposit 121
7.1 Introduction . . . 121
7.2 Geometry . . . 122
7.3 Soil investigations . . . 125
7.3.1 Anisotropic transformations for cone factor . . . 125
7.3.2 Determining characteristic value of undrained shear strength 127
7.4 Numerical analysis of embankment . . . 130
7.4.1 Geometry . . . 130
7.4.2 Material parameters . . . 131
7.4.3 NGI-ADP . . . 131
7.4.4 Hardening Soil . . . 132
7.4.5 Results of slope analysis . . . 135
7.4.6 Sensitivity analysis . . . 136
7.5 Conclusions . . . 138

8 Summary of results and discussion 141
8.1 Overview . . . 141
8.2 Conclusions . . . 142
8.2.1 Soil characterisation . . . 142
8.2.2 Full-scale slope failure test . . . 145
8.2.3 Stability analysis of a sludge embankment . . . 145
8.3 Recommendations for design, soil investigations and practice for construction of sludge embankments . . . 147
8.4 Recommendations for further research . . . 148

A Results of piezocone penetration tests 151

B Results of field vane tests 157

C Determination of cone factor based on field vane tests 161

Bibliography 165

Curriculum vitae 173

List of publications 175

List of Figures

1.1 Aerial view on sludge deposits in the vicinity of Tessenderlo Chemie 3
1.2 Aerial photograph of Veldhoven deposit (2014) 4

2.1 Chamber filter press at Veldhoven deposit 10
2.2 Cross-section of surrounding dike of Veldhoven deposit S1, design plan for elevation of dike, 1977 11
2.3 Ripping of top sludge layer by crane with a customized fork . . 12
2.4 Principle of conversion of wet sedimentation pond with the occurrence of heave and slope failure 13
2.5 Measurement of local heave of the terrain at Veldhoven S3 . . . 14
2.6 Sheared zone along dewatering trench at Veldhoven S1, 2009 . 14
2.7 Documented failure zone at deposit Kepkensberg: Monitoring beacons (A) before sliding; (B) after slope failure in January 2013 15
2.8 Aerial view on failure zone at deposit Kepkensberg 15
2.9 View on slope failure at Veldhoven S3-3, July 3 2014 16
2.10 Aerial view on dry (S3-3) and wet deposit (S3-1) 17

3.1 SEM micrograph illustration of sludge at $\times$8000 magnification and SEM micrograph illustration of a typical kaolinite clay . . 20
3.2 Cross section trough a new embankment constructed with filter cakes 21
3.3 Settlement measurements under trial embankment 2 from 2002 till 2008 22

3.4 Cross section of embankment with layout of instrumentation and sequence of construction 24
3.5 Cross section of embankment with layout of instrumentation and sequence of construction 25
3.6 Typical subsoil profile at test location 26
3.7 Illustration of failure mechanism at IJkdike failure 27
3.8 Cross section of test setup 30
3.9 Predicted failure load with different calculation methods 31

4.1 Degree of consolidation 35
4.2 Drained and undrained stress paths 36
4.3 Definition of critical state 37
4.4 Graphic presentation of the critical state soil mechanic principle 38
4.5 Three dimensional presentation of CSSM with the upper half of the state boundary surface 39
4.6 Shear strength in the Critical State Soil Mechanics framework . 40
4.7 Soil behaviour in CSSM for four common stress paths 41
4.8 Hypothetical stress path during tube sampling and specimen preparation 43
4.9 SHANSEP-method for re-consolidation of soil samples 44
4.10 Variation of s_u/σ'_{v0} over OCR for five different clays 45
4.11 Orientation of major principle stress along a circular shear plane 47
4.12 Typical stress paths and stress-strain curves for triaxial compression and extension tests with definition of stress/strain quantities 48
4.13 Undrained strength anisotropy from CK_0U tests on normally consolidated clays and silts 48
4.14 Effective and total stress paths of real soft soil behaviour and for Mohr-Coulomb Undrained A and B model 51
4.15 Effective stress paths of real soft soil and SHANSEP MC model 52
4.16 Typical deviatoric plane strain plot of equal shear strength contours for NGI-ADP model 54
4.17 Effective stress paths of real soft soil behaviour and for SHANSEP NGI-ADP model 56
4.18 Normalized stress-strain data of clay for PSC, DSS and PSE . . 57

4.19 Mechanism of progressive failure on an excavated slope in over-consolidated clay 58

5.1 Components of borehole shear test device 62
5.2 Stress path during various stages of the borehole shear test . . 63
5.3 Positions for pore pressure measurements at piezocone 65
5.4 Bjerrum's field vane correction factor 67
5.5 Principle compression curve from one-dimensional compression test and triaxial test 69
5.6 Areal view on sludge deposit Veldhoven, section S3-3 72
5.7 CPTu results for locations S01 and S02 73
5.8 Profile of over-consolidation ratio based on CPTu results of S01, at location A (S01) 75
5.9 Field vane test results at locations A and B on sludge deposit Veldhoven S3-3 77
5.10 Results of borehole samples from location B 78
5.11 Graphical presentation of undrained shear strength ratio (S) from triaxial compression test 80
5.12 Detail of stress paths for consolidated undrained triaxial tests on samples E 81
5.13 Sludge samples taken by pushing in PVC tubes 82
5.14 Graphical presentation of cone factor calculation from results of piezocone and field vane test 85
5.15 Comparison of undrained shear strength with a cone factor of 11.0 and field vane and triaxial compression test results 88

6.1 Test setup of large scale slope failure test 97
6.2 Cross-section of setup of large scale slope failure test 97
6.3 Sludge dumped in ridges during the construction of test embankment to enhance drying by wind and sun 98
6.4 Location of field vane tests at areas A and B of the test embankment 99
6.5 Undrained shear strength from vane shear test at test area A and B, at different depths 100

6.6 Grid of measuring points for horizontal deformations during slope failure test 102
6.7 Horizontal displacements of measuring points at row C 102
6.8 Bulge formed below container 1, just above the interface between the sand layer and the sludge 103
6.9 Vertical displacements of containers, monitored with two reference points on container 3 and one point on each of containers 1 and 2 104
6.10 Horizontal displacements of containers, monitored with two reference points on container 3 and one point on each of containers 1 and 2 104
6.11 Open cracks adjacent to crane mats, after termination of test . 105
6.12 Relation between triaxial extension, direct simple shear and triaxial compression and orientation of failure surface for different shapes of embankments. 107
6.13 Influence of anisotropy on undrained shear strength of CK_0U tests on normally consolidated clay and loam 108
6.14 Anisotropic conversion factors for conversion of shear strength ratio of undrained shear resistance 108
6.15 Calculated FS (3D) of the sludge embankment with a load of 33 kN/m^2 for a range of undrained (field vane) shear strength with MC and NGI–ADP material models 113
6.16 Calculated FS (3D) of the sludge embankment during the different steps of the slope failure test with MC and NGI–ADP material models 114
6.17 Shear stress and shear strain in elevation in the MC and NGI–ADP model at a crest load of 33 kN/m^2. 115
6.18 Average and SD of undrained shear strength from vane shear test at location B over a period of 10 months 117

7.1 Aerial photos of deposit Veldhoven, S3 123
7.2 Profile of slope at elevation of sludge deposit Veldhoven, subsection S3-3, at location B 124

7.3 Schematic presentation of the characteristic value of two mechanisms with a different problem scale compared to the fluctuation scale 128
7.4 Result of active average undrained shear strength from CPTu S01 to S05 129
7.5 Finite element model of sludge embankment 130
7.6 Indication of shear plane by visualisation of incremental shear strain at failure, NGI-ADP material model 135
7.7 Indication of shear plane by visualisation of incremental shear strain at failure, HS material model 135
7.8 Influence of variation in cone factor ($N_{kt,FV}$) and plasticity index (I_p) on factor of safety for NGI-ADP material model calculations 137

List of Tables

4.1 Additional parameters in the SHANSEP MC material model . 50
4.2 Specific parameters in the NGI-ADP material model 54
4.3 Additional SHANSEP parameters in the SHANSEP NGI-ADP material model 55

5.1 Results of borehole shear tests at deposits Veldhoven and Kepkensberg 71
5.2 Over-consolidation ratio for S01 to S05 (locations A to E) . . . 75
5.3 Plasticity index for test locations A to E on deposit Veldhoven S3 77
5.4 Results of consolidated undrained triaxial compression tests . . 79
5.5 Results of one-dimensional consolidation tests 82
5.6 Calculation of N_{kt} at location A, based on field vane test . . . 84
5.7 Undrained shear strength based on triaxial tests and one-dimensional consolidation test 87
5.8 Cone factors from field vane test and triaxial compression test . 87
5.9 Summary of literature data regarding the cone factor 90
5.10 Cone factor for CaF_2 sludge according to methods by [Löfroth, 2008] and [Karlsrud et al., 2005] 91

6.1 Model input data for sludge elevation (Mohr-Coulomb and NGI-ADP) 112

7.1 Various anisotropic conversion factors at different plasticity indexes 126
7.2 Cone factors for various stress states at different plasticity indexes 127

7.3 Material properties of NGI-ADP material model for industrial sludge elevation and foundation 133
7.4 Material properties of hardening soil material model for industrial sludge elevation and foundation 134

Chapter 1

Introduction

1.1 General considerations

The evaluation of the stability of slopes and other types of earth structures requires the understanding of the complex behaviour of soils. Over the past decades, research methods have evolved, resulting in the availability of a range of laboratory and in situ test methods for determining the mechanical behaviour of soils, and in particular their shear resistance. Each method, however, has its limitations and downsides, which are to be kept in mind when studying a certain soil.

When relying solely on laboratory tests, the dataset will commonly be limited due to the time-consuming and relatively costly tests, which have to be executed in well-equipped laboratories. Furthermore, high-quality data will only be available for the examined points, but the variation of the investigated properties on site remains unknown. On the other hand, when performing large series of in situ tests (i.e. vane shear test, cone penetration test, borehole shear test, ...), data are gathered on various locations and depths, which provides information on the variation of the properties across the investigated area. The parameters obtained from in situ test are often less accurate and fewer parameters can be determined. For in situ testing, strength parameters are easier to determine compared to deformation parameters (shear strain, Young's modulus, ...) because displacement measurements in situ are difficult to perform. The positive and negative aspects of laboratory and in situ testing are to be considered when analysing soil structures.

Engineering judgement and lessons learned from experience, often involving failures, are still of great importance. Relying blindly on numbers may result in loss of the broader picture and the understanding of the true mechanism of soil behaviour, which can deviate from the devised mathematical model.

The present study deals with the (physical) characterisation of (historical) industrial sludge, resulting from the production of phosphate fertiliser and animal feed phosphate at a chemical processing plant in Ham (Belgium). With the reorganization of several sludge deposits, significant volumes of sludge must be re-stacked. To create the necessary extra storage capacity, the capacity of a wet industrial sludge deposit near the processing plant is being increased by elevating the deposit with an embankment built solely with naturally as well as with mechanically consolidated sludge. The consolidated sludge has a permeability similar to clay ($\pm$ $1{\cdot}10^{-9}$ m/s) and a high water content (35% to 140%). Furthermore, the method of re-stacking the sludge material results in a mixture of highly and only slightly consolidated sludge with varying water content.

The low permeability and relatively fast elevation pace necessitates an undrained analysis whereas the re-stacking of previously consolidated sludge causes a highly unpredictable behaviour and varying parameters. Hence, the content of the required investigation (field and laboratory) must be adapted to the specific details of the material in question.

1.2 Redevelopment of sludge deposits at Tessenderlo Group

Tessenderlo Chemie started the producing of sulphuric acid, sulphates, phosphates and electrolyse products in 1919 at Tessenderlo, Belgium. Over the years several sludge deposits were installed in the vicinity of the plant to store the waste products generated by the production.

In 1993, the remaining storage capacity at that time was considered to be insufficient for the future production. Research concentrated on optimizing the current deposits by stacking the sludge up to higher levels.

Due to changing in demands on the international market, the phosphate production has declined. At the end of 2013 internal reorganizations led to the reduction of the annual sludge production. Before the reorganization the sludge output was around 45 000 tonnes per year (dry matter). The remaining annual sludge production is reduced to about 2 000 tonnes (dry matter) and will be reduced furthermore.

In the current perspective the footprint of the deposits is too large and considered not economical. Therefore a reorganization of the sludge deposits is scheduled. Some deposits are being closed, cleared and redeveloped as industrial area. Other deposits are reorganized to compensate the capacity loss of closed deposits or to prepare for final covering.

A view on the sludge deposits is given in Figure 1.1. The reorganization of Tessenderlo Chemie comprises three deposits: Old Deposit, Veldhoven and Kepkensberg.

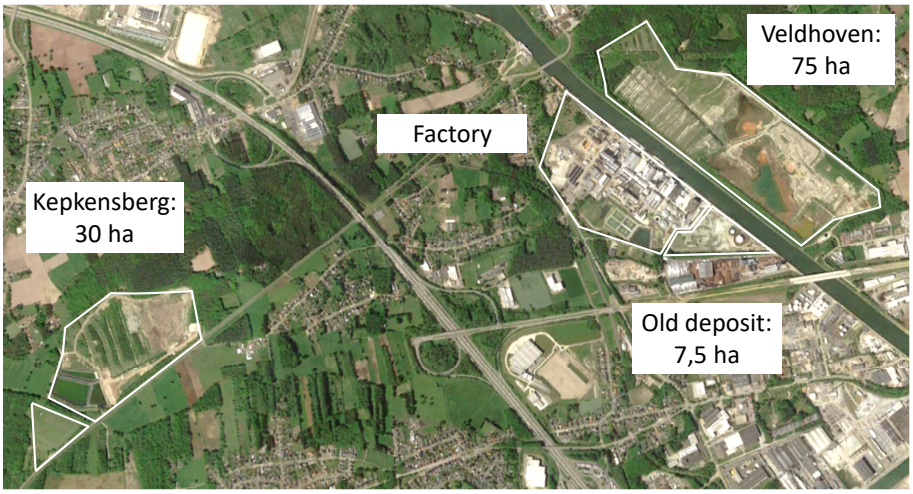

Figure 1.1: Aerial view on sludge deposits in the vicinity of Tessenderlo Chemie [Google earth, 5/05/2018]

A basic element in the reorganization is the "dry" storage of old, wet sludge. The objective is to use a combination of naturally dried and consolidated sludge, filter pressed sludge and accelerated naturally dried sludge as construction material for elevated embankments. By using the dried sludge itself as building material, space occupied by the actual deposits can be decreased.

Sludge deposit Veldhoven measures roughly 1500 m by 440 m. It is divided in three zones named S1, S2 and S3, as presented in Figure 1.2. The oldest area, S1, contains naturally dried sludge, which has been left to consolidate naturally since 1987. Area S2 is a small sedimentation basin where the watery sludge coming from the factory is received. After sedimentation, the settled particles are dredged and pumped to a filter pressing station (Figure 1.2, circle). The filter cakes are transported back to S3 with conveyor belts.

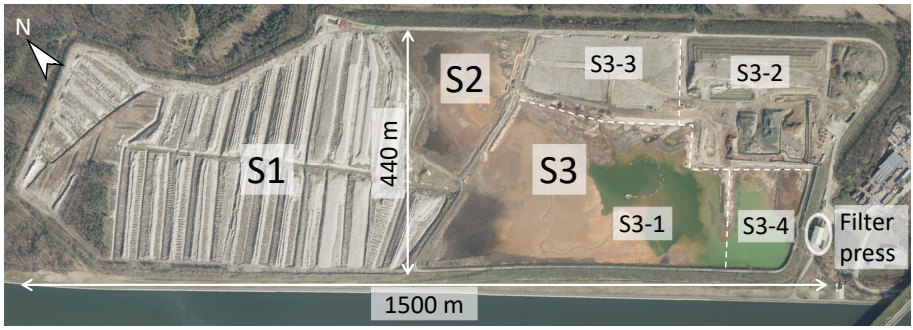

Figure 1.2: Aerial photograph of Veldhoven deposit, subdivided into S1, S2 and S3 [Geopunt Vlaanderen, 9/03/2014]

Deposit area S3 is divided in four sub zones. S3-1 is a sedimentation basin where the watery sludge from the plant is stored (overflow from S2). The second part (S3-2) is a solid sludge area with a bottom layer of filter cakes (8 to 9 m thick) and an elevation of 10 m built with a combination of filter cakes and naturally dried sludge. A real size test embankment (200 m $\times$ 60 m $\times$ 10 m) has been the topic of an earlier research by Tennekoon [Tennekoon, 2007].

A second, smaller, sedimentation basin is located at S3-4. Here, clear water is separated and pumped back to the factory and reused as transportation water for sludge. The majority of the present research was executed in subsection S3-3.

S3-3 was converted over the past years from a wet sedimentation basin to an embankment consisting of naturally dried sludge. The area has been reclaimed by dumping filter cakes or dried sludge in the settling pond (former area S3-1) and hereby elevating the terrain above water level. When dumping the solid sludge in the water, weak watery sludge is pushed forward, as presented in Figure 1.3.

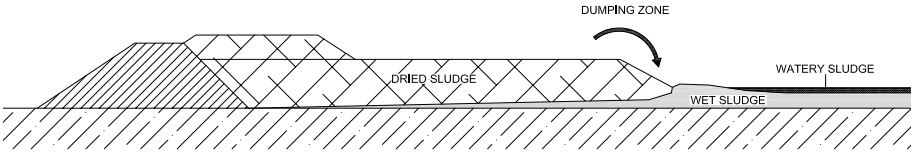

Figure 1.3: Principle of dumping dried sludge in wet deposit Veldhoven S3 to create a sludge embankment

Because deposit area S3 has been equipped with a base liner (PVC layer anno 1986), consolidation only takes place from the top. This leads to a long consolidation process of the added fill. Hence, the reduction of the water content of the sludge before stacking is an important aspect. The drying of the sludge is achieved by an accelerated drying procedure. This consist of excavating and stacking the sludge in smaller dunes and trenches (Figure 1.4), thus expanding the evaporation surface to enhance the drying by sun and wind. After a few weeks the dunes are levelled to accept the next sludge volume. The water content reduction achieved depends on the weather conditions. Therefore, layers with higher and lower water content can occur on top of each other.



Figure 1.4: Storing wet sludge in dunes and trenches to enhance drying by sun and wind

1.3 Research methods and objectives

The objective of this study is to establish a cost-efficient, fast and reliable method for determining the parameters for the analysis of the (slope) stability of embankments constructed with industrial sludge, characterized by a high water content and low permeability. Furthermore, the sludge material's high variability of consolidation and large spread of the undrained parameters must be taken into account.

The applied research methodology consisted firstly of analysing the material concerned using several commercially available testing tools. The advantages and disadvantages of these methods are evaluated regarding the specific issues of the industrial sludge.

Secondly, the accuracy of the most suitable method(s) is validated by performing a full-scale test. The stability results, obtained with the measured properties by the chosen test method, are then compared with the actual results of the full-scale test. The necessity of correction factors for the conversion from in situ or laboratory test to full-scale test are determined.

The vastness of the deposit terrain requires the extrapolation of test results. Hence, a link between the method A and method B has to be established, where method A is the most suitable method for determining the necessary material parameters and method B is the most convenient method for acquiring data on a large scale.

Lastly, when the most suitable test method has provided the necessary material properties, they are implemented in a material model for finite element analysis. A wide variety of material models exists to estimate the shear behaviour of soils. Some common material models (Mohr-Coulomb, Hardening Soil, ...) are compared to a recently developed NGI-ADP material model [Andresen and Jostad, 1999] in order to evaluate the influence of the estimation of the shear strength on the prediction of slope stability.

1.4 Layout of the dissertation

In chapter 2, background information on the process of handling the industrial sludge is given. Typical problems encountered with the stacking of the soft sludge are described as well as some documented slope failures.

Information about earlier researches on the industrial CaF_2 sludge is presented in chapter 3. The knowledge obtained from the earlier researches is also used to increase the data gathered during the present study. Research on potentially similar materials and soft soils was used to set up the research program. Results of some full-scale slope failure tests are given as they formed the base of the full-scale slope failure test on the sludge test embankment in the present research.

Chapter 4 presents the theoretical background of undrained soil behaviour. Whereas drained behaviour is common knowledge, undrained soil behaviour can exhibit some specific phenomena. The critical state soil mechanics theory is explained, along with other specific issues regarding undrained soil behaviour.

The experimental program carried out, is described in chapter 5. The various laboratory and in situ tests are explained and the test results are given and discussed. The results are compared to literature data of soft soils with similar plasticity index.

In chapter 6, the setup and execution of a full-scale slope failure test are presented. The results of in situ tests and the monitoring of the deformation during the loading of the test embankment are shown. The evaluation of the full-scale test, using a back-calculation, is presented and discussed.

The stability analysis of the entire embankment constructed on the reconverted sludge deposit Veldhoven S3-3 is presented in chapter 7. The conversion of data from soil investigation to material parameters is explained. Different types of material models are compared to evaluate the embankment slope stability.

Chapter 2

Background information - History

2.1 Introduction

The present study deals with the industrial sludge resulting from the production of phosphate fertilizer and animal feed phosphate. The phosphate obtained in the chemical process is dicalcium phosphate, described chemically as $CaH(PO_4).2H_2O$. Throughout the chemical process a waste product (industrial sludge) is formed. The industrial sludge consists of CaF_2 (50-60%), SiO_2 (12-14%), $CaSO_4$ (5-10%), water soluble $FeSO_4$ and $Al_2(SO_4)_3$ (7-8%), water soluble P_2O_5 (4-8%) and heavy metals (0.05-0.15%) [Van Autenboer, 1993]. The sludge is stored at several sludge deposits in the vicinity of the processing plant.

In this chapter, the storage methods and sludge handling are explained and illustrated. The typical problems occurring when handling with the industrial sludge are described as well as some documented slope failures.

2.2 Sludge handling

A basic element in the reorganization is the "dry" storage of old, wet sludge. The purpose is to use a combination of naturally dried and consolidated sludge, filter pressed sludge and accelerated naturally dried sludge as construction material for elevated embankments. By using the dried sludge itself as building material, space occupied by the actual deposit can be decreased. Several actions are necessary to make the sludge suitable for this purpose.

Three main forms of sludge, i.e. watery sludge, filter cakes and naturally dried sludge, are present at the active deposit Veldhoven (Figure 1.2).

The watery sludge is the waste component from the factory. The dry matter content of the watery sludge is about 5% (water content >1000%). The high water content allows the sludge to be pumped from the plant to sedimentation basis, on the deposit, several hundreds of metres away. The settled sludge on the bottom of the basin still has a high water content (300 to 400%) and has virtually no cohesion.

To reduce the volume of the watery sludge, it is being compressed in a filter pressing station at Veldhoven deposit site. With the use of a small barge, the watery sludge is dredged from the bottom and pumped from the settling ponds to the filter pressing station. Two large filter presses convert the watery sludge to so called "filter cakes". One of the two chamber filter presses is shown in Figure 2.1.



Figure 2.1: Chamber filter press at Veldhoven deposit

The filter press setup is prestressed at 600 tonnes with the use of hydraulic jacks. The sludge is then pumped into the filter bags (2 m × 2 m) aligned up to a length of several metres. The filling pump produces a pressure of 15 bars (1500 kPa), hereby forcing the water through the filters, leaving the sludge particle behind. This process results in a reduction of the water content from over 300% at the beginning of the process, to around 80% after filter pressing. The compressed filter cakes are dropped out of the filter bags onto a conveyor belt and transported to the storage facility.

The filter cakes have an increased shear strength due to the pre-compression in the filter pressing station. However, the elevated shear strength of the individual filter cakes needs to be reduced, when considering the global shear resistance of the stacked cakes, because of the (large) spaces in between the individual stiff filter cakes. Research has been conducted on the orientation and stacking of the filter cake and the influence on the shear strength [Op't Eynde and Michiels, 2005]. Furthermore, a real size test embankment with dimensions 60 m × 200 m × 10 m, built with CaF_2 sludge and filter cakes, has been the topic of an earlier study [Tennekoon, 2007].

The largest quantity of the sludge stored on the deposits is naturally dried and compacted sludge, originating from old settling basins. In the early days of Tessenderlo Chemie, production sedimentation basins in the vicinity were used to deposit the residue of the chemical processes.

Most deposits date back to the early 20th century, and were built with a simple setup. A surrounding dike was erected with soil excavated from the bottom of the deposit zone (example given in Figure 2.2). At most locations the surrounding ground level is therefore higher than the deposit bottom. When the watery sludge was then pumped in, thickening could take place from the top, by evaporation, and at the bottom, by infiltration. When the deposit was full, the surrounding dike was elevated, as shown in Figure 2.2.

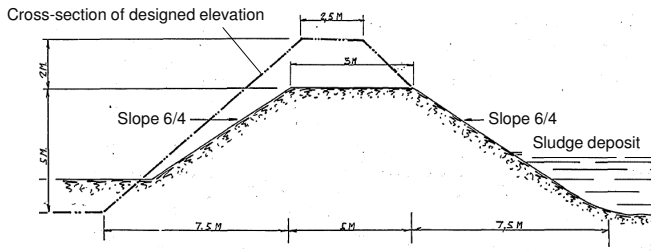

Figure 2.2: Cross-section of surrounding dike of Veldhoven deposit S1, design plan for elevation of dike, 1977

Currently built deposit sites need to be equipped with an impermeable barrier at the bottom to prevent infiltration and possible pollution of the subsoil. This, however, drastically increases the consolidation time.

Naturally dried (partially) consolidated sludge has a water content ranging from 35% up to 140%. Tests at Veldhoven S1 indicated a low water content sludge on the surface of the deposits, but increasing with depth. Beneath a depth of around 2 m under the surface, a nearly constant water content is found. An increase in water content with depth indicates that surface drying is the main reason for water content reduction.

A reduced water content is also noticed at the bottom of S1. This is due to the infiltration of excess water to the surrounding soil. Sub-deposits S2 and S3 are equipped with a bottom seal consisting of a PVC liner. Hence, consolidation can only take place at the top of the deposit, significantly increasing consolidation time.

The driest sludge is achieved with accelerated drying. Here the sludge is ploughed with a crane (Figure 2.3), turning and cutting the sludge layer to a depth of about 1 m. Another method is stacking the sludge into dunes and trenches. With both methods the evaporation surface is increased to enhance drying by sun and wind. The drying will result in a reduction of water content in this top layer. A beneficial increase in shear strength and bearing capacity is observed, making the terrain more accessible for heavy machinery and the sludge more suitable for constructing embankments.



Figure 2.3: Ripping of top sludge layer by crane with a customized fork

2.3 Encountered problems

In the process of handling, storing and stacking of the sludge at the different sites, several problems were encountered, such as (internal) sludge slope failures and the occurrence of settlements and heave.

2.3.1 Differential settlements and heave

With the reconversion of S3-3 from wet sedimentation pond to dry deposit, large quantities of weak wet sludge were entrapped by dryer sludge. The principle is presented in Figure 2.4. The wet sludge was squeezed out by increasing the load at the front. Sometimes, bulges appeared behind the front line where weak wet sludge was pressed upwards instead of horizontally (Figure 2.4). Figure 2.5 presents the topographical documentation of a bulge with a height of around 80 cm.

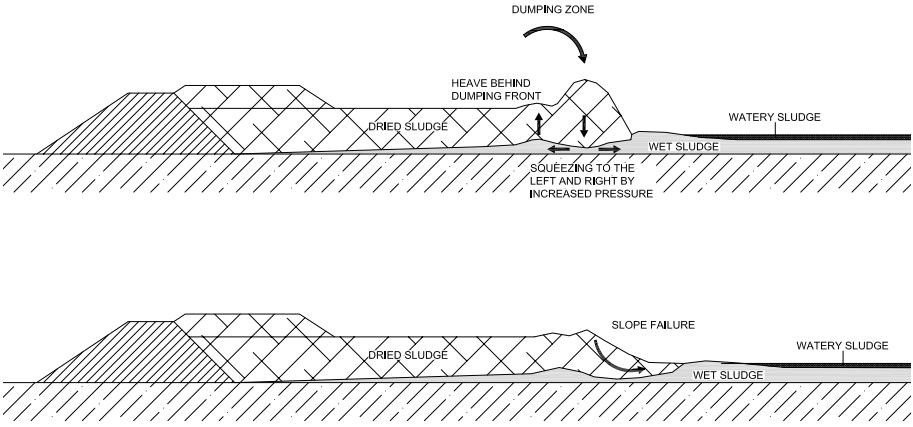

Figure 2.4: Principle of conversion of wet sedimentation pond with the occurrence of heave and slope failure

Settlement tubes were installed prior to elevation of the terrain, at a level above the external confinement dikes. However, due to significant differential settlements most of the installed tubes were damaged by heavy trucks and local settlements during elevation works, resulting in a blockage, preventing the measuring probe to pass.

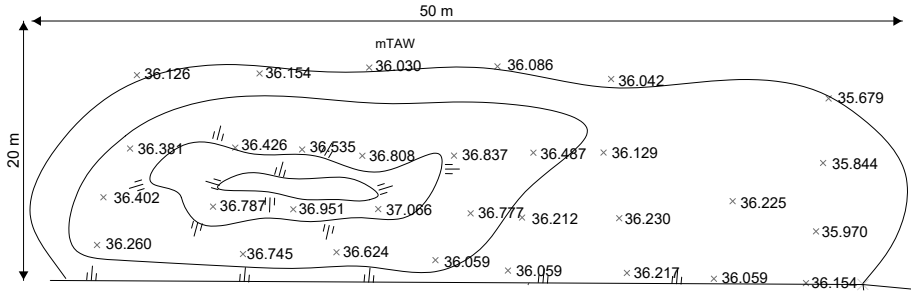

Figure 2.5: Measurement of local heave of the terrain at Veldhoven S3

2.3.2 Documented slope failures

Slope failure at Veldhoven S1, November 2009

A progressive failure zone occurred along the main dewatering trench at deposit site Veldhoven S1 in November 2009 (Figure 2.6). The cause of failure is unclear but could be attributed to the variation in pore water pressure due to a change in the water level in the trench.

Furthermore, shrinkage cracks, originated during a dry period, will cause a reduction in shear resistance along a shear plane due to loss of friction surface and will lead to a faster infiltration of water from the trench or from rainfall.



Figure 2.6: Sheared zone along dewatering trench at Veldhoven S1, 2009

Slope failure at Kepkensberg deposit, January 2013

To ensure that drying by sun and wind would not be counteracted by rain water infiltration, several drainage canals were dug in the sludge deposit. The water from the trenches is collected at the lowest point and pumped to a water treatment plant. During heavy rainfall, the canals would fill up due to the massive amount of run-off water from the vast deposits, hereby increasing the water level in the surrounding sludge. Consequently, effective stresses in the sludge diminish and increase the risk for slope failure. A view of a slope failure, occurred at sludge deposit Kepkensberg in January 2013, is given in Figure 2.7.

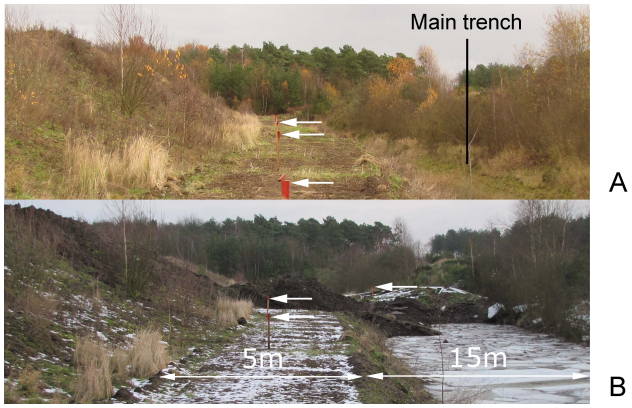

Figure 2.7: Documented failure zone at deposit Kepkensberg: Monitoring beacons (A) before sliding; (B) after slope failure in January 2013



Figure 2.8: Aerial view on failure zone at deposit Kepkensberg [Geovlaanderen, 8/06/2013]

Additional sludge was to be stored at an existing elevation of sludge near a dewatering trench with a depth of around 5 m (main dewatering trench). To monitor the movements of the old sludge volume under the added load, several wooden beacons where placed in a straight line next to the slopes (Figure 2.7 A). About 3 months later, a sliding in the slope occurred over a length of 30 m (Figure 2.7 B). An aerial view of the failed zone is presented in Figure 2.8.

Slope failure at Veldhoven S3-3, July 2014

At sludge deposit Veldhoven S3-3 a large slope failure occurred in the summer of 2014 (Figures 2.9 and 2.10). This failure was, however, actively provoked. For the reconversion of the wet deposit, dry sludge and filter cakes were dumped in the former wet deposit S3-1 to create a dry area named S3-3, illustrated in Figure 1.3.



Figure 2.9: View on slope failure at Veldhoven S3-3, July 3 2014. Horizontal and vertical displacement of dirt road near the edge of the sedimentation pond (Right). Vertical drop of about 4 m.

Initially, the dumping of dry sludge was sufficient to push forward the wet sludge. After the waterline was pushed back over several tens of metres, wet sludge accumulated at the front line. The volume of accumulating sludge did increase gradually with each push. At a certain moment the vertical pressure of the elevation became insufficient to squeeze the sludge at the bottom. This has led to the increase in residual wet sludge presence under the dumped dried sludge.



Figure 2.10: Aerial view on dry (S3-3) and wet deposit (S3-1) before (upper, 2014) and after (lower, 2015) slope failure at Veldhoven S3, on July 3 2014 [Geopunt Vlaanderen]

Squeezing is prevented by the back pressure of the accumulated wet sludge at the front line of the dried sludge elevation. To force squeezing to occur, such a high elevation was needed to develop the required vertical pressure, that slope failure occurred prior to squeezing (Figure 2.4).

By the summer of 2014, the waterline was pushed back to about 150 m, accompanied by further accumulating of wet sludge. Dried sludge had been piled at the edge up to 14 m high above water level, but still the wet sludge would not budge. Hence, it was chosen to dredge wet sludge in front of the particular area to reduce the back-pressure. As a result, a large slope failure occurred, resulting in the movement of about 5600 m^3 of sludge from the dry area into the wet zone (Figure 2.9).

The slope failure occurred over a length of about 100 m, and extended over 13 m horizontally from the edge of the slope. The top of the former dirt road was lowered by 3 to 5 m. It could be established that the settled sludge in the wet deposit was also pushed back over several decametres.

This is illustrated by the aerial photo's presented in Figure 2.10. The dredge tubes (dashed white lines) in the water follow a curve before the slope failure, whereas the line after the failure is straightened out. Behind the failed zone, cracks were noticed in the sludge elevation.

2.4 Conclusions

Slope failures are usually unintended and unwanted, and can cause damage to constructions or, in the case of hazardous material, may cause pollution issues. The failures presented above are all internal failures (inside the deposit area), hence there were no external damage or pollution risks. In fact, at Veldhoven S3-3, the slope failure mechanism was turned into a useful working principle for the reconversion of a wet deposit area.

The occurrence of slope failures gives the opportunity of gathering important information on the shear strength and failure mechanism of the sludge by analysing the failure zone. It adds to experience and improves the understanding of soil behaviour.

Chapter 3

Literature survey: State of the art

3.1 Introduction

Over the past decades, various slope failures have been well documented to improve the understanding of the complex behaviour of soils ([Rowe et al., 2001]; [Zwanenburg et al., 2012]; [Mansikkamäki, 2015]; etc.). New developments in laboratory and in situ testing have been the result, as well as the enhancement of analytical procedures and material models to perform thorough analysis. Many researchers investigated the construction and behaviour of embankments constructed on soft soils ([Indraratna et al., 2005]; [Balasubramaniam et al., 2010]; [Hunter and Fell, 2003]; [Hinchberger and Rowe, 1998]; etc.).

In this chapter, the research on soft soils and the construction of trial embankments on soft soils is discussed. First of all, earlier findings of research on the industrial CaF_2 sludge are outlined. Secondly, research using in situ test embankments is presented. The methodology and findings are discussed.

3.2 Geotechnical characterisation of an industrial sludge and numerical analysis of sludge dam behaviour, Tennekoon [2007]

Geotechnical characterisation

Various laboratory and in situ tests were carried out at Veldhoven deposit to characterise the mechanical properties of the filter pressed sludge (filter cake) as well as naturally dried sludge. It was found that the sludge is a fine grained soil, like clay. Unlike typical clays e.g. kaolinite clay, which is comprised by plate shape particles, the industrial sludge consists of microscopic spherical particles (Figure 3.1). A relatively high specific weight can be attributed to the presence of heavy metals (Cu, Cd, Hg, Zn, ...).

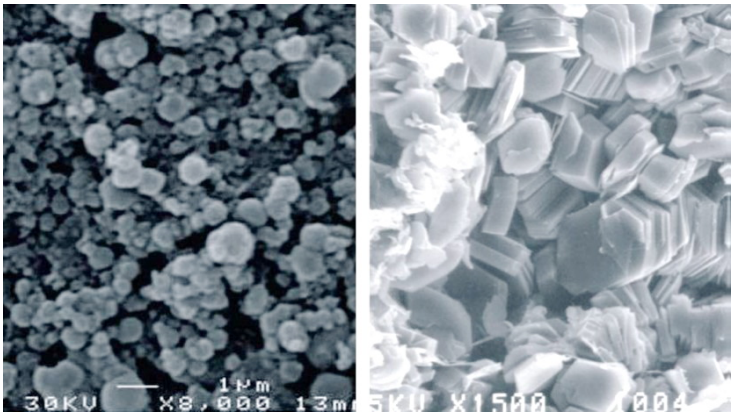

Figure 3.1: SEM micrograph illustration of sludge at ×8000 magnification [Op't Eynde and Michiels, 2005] (L) and SEM micrograph illustration of a typical kaolinite clay (R)

Undisturbed sludge samples were taken at various locations in the deposit site to carry out triaxial and direct simple shear tests. An effective angle of friction of 32° to 36° and a cohesion between 0 and 11 kPa was found. Permeability tests indicated a permeability of around $1{\cdot}10^{-9}$ m/s.

Large scale one-dimensional consolidation tests and direct shear tests were conducted to investigate the effect of filter cake orientation on the consolidation properties and shear strength properties of the sludge.

The friction angle varied between 13°, for horizontally aligned cakes, up to 29°, for vertically aligned filter cakes [Van Der Veken, 2002]. In situ, a mixture of aligning phenomena will occur due to the deposition of the cakes with dumpers and spreading with bulldozers.

Construction and monitoring of trial embankments

Two trial embankments were built to monitor the behaviour of the sludge in the dike and in the underlying sludge foundation. The dimensions of test embankment one were 60 m × 30 m × 6 m. It was equipped with settlement plates, piezometer cells and water pressure cells. It was found that the intermediate sand layers, added in one half of the embankment, enhance drainage. Furthermore, the weight of the test embankment resulted in large settlements of the embankment and surface heave around the embankment, due to squeezing of still remaining unconsolidated sludge layers in the sludge foundation under the test embankment.

The dimensions of test embankment two were 200 m by 60 m with a height of 10 m. A cross section of the embankment is given in Figure 3.2. The embankment was constructed with filter cakes and provided with intermediate sand layers for drainage.

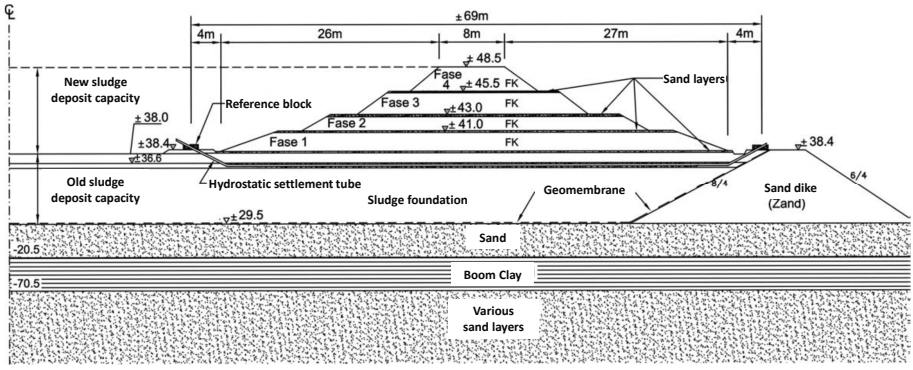

Figure 3.2: Cross section trough a new embankment constructed with filter cakes [Yonatan et al., 2009]

Hydrostatic profile gauges were used to measure settlements below the embankment through HDPE tubes installed prior to construction. Water pressure meters and piezometers were installed at different depths in the embankment foundation.

Periodic measurements were conducted during construction to measure the increase of water pressure and of deformations when sludge layers were added. Furthermore, settlement measurements were continued after construction was finished to evaluate the consolidation in time. Figure 3.3 gives a view on the settlement evolution of the sludge foundation at one of the four sections of the dike equipped with settlement tubes.

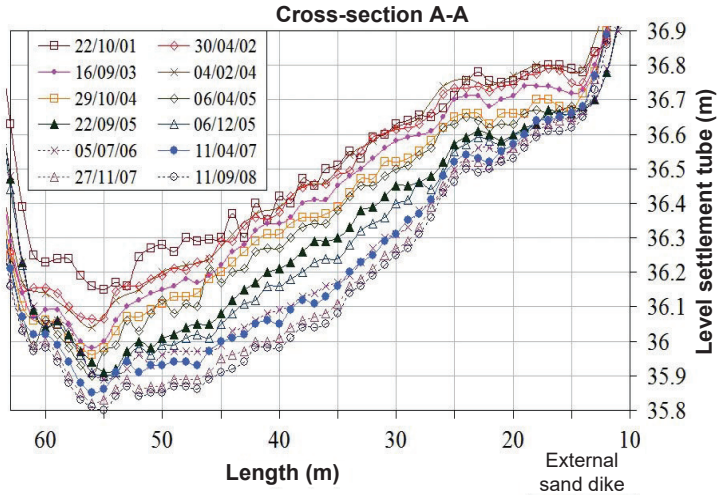

Figure 3.3: Settlement measurements under trial embankment 2 from 2002 till 2008, at section A-A [Yonatan et al., 2009]

Numerical modelling of trial embankment

A finite element analysis using the finite element program Plaxis was conducted in order to simulate the sludge behaviour. Different material models (Soft Soil Creep, Hardening Soil and Mohr-Coulomb) and different input parameters were compared. Using back-calculations the best parameter set and most suitable material model were determined. The HS (Hardening Soil) as well as the SSC (Soft Soil Creep) model both yielded good results for simulating the settlements and water pressure evolution, with parameters obtained from simple one-dimensional consolidation tests. The more complex consolidated undrained triaxial compression tests delivered no better simulation of the sludge behaviour regarding settlements and pore water pressures.

3.3 Literature references

In this section, some literature references regarding test embankments, slope failure tests and back-analyses of soft soils are outlined. The overall similarity is the presence of soft soils in the slope or embankment.

3.3.1 Performance of a test embankment constructed on an organic clayey silt deposit, Rowe et al. [2001]

Introduction

The instrumentation and field performance of a full scale test embankment constructed on a soft compressible organic clayey silt is discussed. The research was conducted in the framework of the widening of a two lane Trans-Canada highway between Moncton in New Brunswick and Amherst in Nova Scotia [Rowe et al., 1995]. Along the road, several sections of the terrain needed to be elevated which involved the construction of 2 – 4 m high embankments on the soft compressible soil. To gain better insight in the behaviour of the subsoil, a test embankment was constructed. The test embankment was equipped with a variety of instrumentation in order to monitor pore pressures, settlement, heave and lateral displacements.

Embankment construction

The construction of the embankment was performed in four stages, gradually increasing the height to around 7.25 m. The plan view and cross-section of the embankment are shown in Figure 3.4.

The fill material used to create the embankment had an average unit weight of 19.6 kN/m^3. Direct shear test on samples of the fill material indicated a cohesion and angle of friction of 17.5 kPa and 38°, and 10 kPa and 34° respectively for the peak strength and residual strength.

The test embankment was divided in two sections. The 25 m long first half of the embankment was reinforced with geotextile whereas the 25 m second half was not reinforced. The instrumentation consisted of piezometers, settlement plates, settlement augers, heave plates, inclinometer casings and total pressure cells and strain gauges on the geotextile.

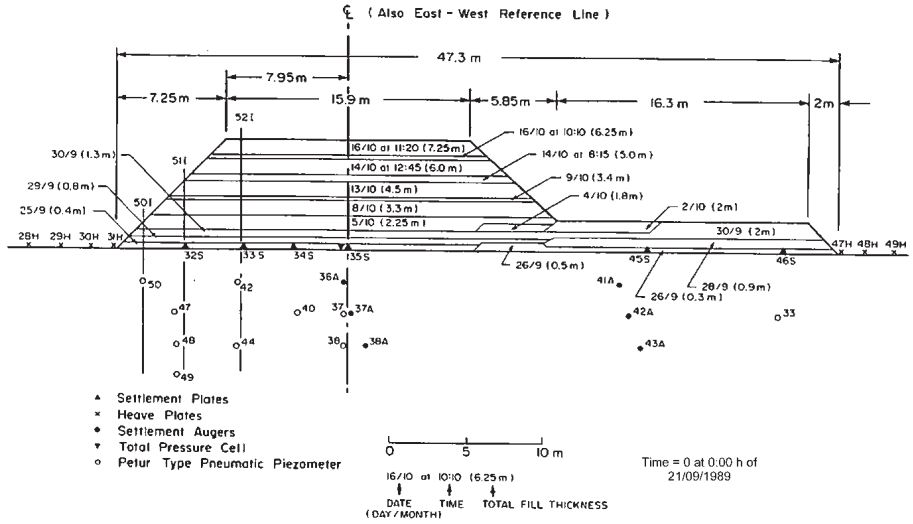

Figure 3.4: Cross section of embankment with layout of instrumentation and sequence of construction [Rowe et al., 2001]

The test embankment was situated in an area of intertidal salt marsh deposit [Rampton and Paradis, 1981]. The subsoil mainly consisted of clayey silt with some organics, fibres and occasional sand lenses. Undrained shear strength from vane shear tests carried out in the subsoil varied between 20 and 80 kPa.

Results of instrumentation

The embankment was constructed at a high elevation pace in order to stimulate slope failure. A very rapid pore pressure build-up was established, according to the piezometers installed, as the fill was raised. Measurement of horizontal displacements using inclinometers indicated significant displacement and even blocking of the measurement at a certain depth was noticed. The blockages potentially indicate the position of a failure surface. Furthermore, settlements on top of the embankment and heave below the slope were measured.

The gathered data from the monitoring of settlement, pore water pressure and deformations were compared with 2D analysis, available at the time. A substantial difference was found between the actual constructed embankment and the theoretical maximum height according to a 2D calculation.

3.3.2 Failure of a trial embankment on peat in Booneschans, the Netherlands, Zwaneburg et al. [2012]

Introduction

The Netherlands is by its low-lying ground level continuously threatened by water. In the prevention of dike failures in the Netherlands, a five-yearly review of all the dikes of primary flood defences is established by law. Changes in safety norms, elevation of sea levels, erosion or evolving understanding and knowledge of the behaviour of flood defences necessitates this periodic review.

The IJkdijk (calibration dike) was a test dike for the viability of modern sensor technology for the assessment of the actual dike strength. The trial embankment was built on an underlying peat layer, and loaded till failure. Several monitoring sensors were implemented to gather data of displacements, pore pressure, ...

The objective was to enable the development of an early warning system for dike stability. Furthermore, the influence of the embankment on a peat layer is investigated.

Test set-up

A full-scale trial embankment was built, with 6 m height and 100 m length. The embankment consisted of a sand core with a clay cover as shown in Figure 3.5. This setup is typical for dikes constructed since the 1960s in the Netherlands.

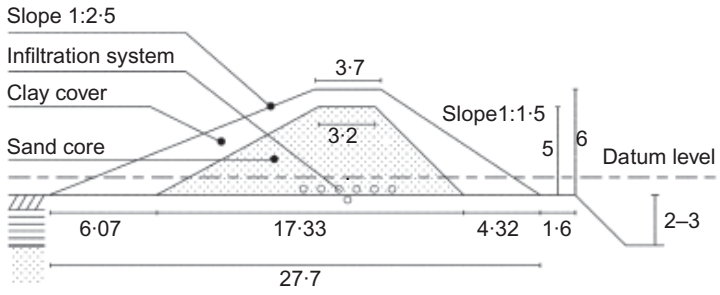

Figure 3.5: Cross section of embankment with layout of instrumentation and sequence of construction [Zwanenburg et al., 2012]

The test consisted of five stages:

Stage 1: Raising water level to 3 m above ground level (behind dike)
Stage 2: Excavation to 1 m below ground level (1 m ditch)
Stage 3: Complete excavation of soft soil layers (3 m ditch)
Stage 4: Raising water level in sand core to 2/3 sand core height
Stage 5: Filling sand core completely and filling containers on top

Subsoil properties

Cone penetration tests were conducted and borehole tests were made to investigate the subsoil. A typical profile at the test location is given in Figure 3.6.

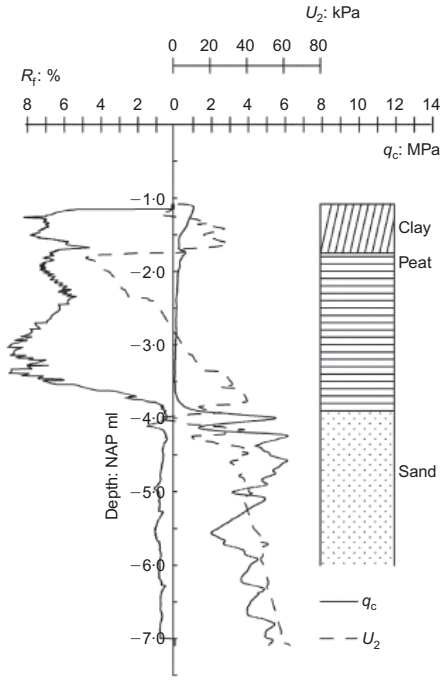

Figure 3.6: Typical subsoil profile at test location [Zwanenburg et al., 2012]

The profile indicates a clay layer at the top, followed by Holocene peat. Below the peat layer Pleistocene aeolian fine sand is found. The thickness of the peat layer is approximately 3.0 m at the centre of the embankment, decreasing to 1.5 m to the north and 2.0 m to the south.

Pre-consolidation stresses were derived from constant rate of strain tests (CRS). Accounting to the hydraulic pressure below the phreatic level, the pre-consolidation stresses range from 22 to 38 kN/m^2, with an over-consolidation ratio (OCR) of 2.5 to 4.0. In the peat layer an increase in pre-consolidation stress with depth was found, with an OCR of 1.8 – 1.9. The results of the CRS, however, show a significant scatter.

Results

During the fifth stage of the test, filling the core and the container on top of the dike with water, failure occurred near the middle of the trial embankment. A schematic cross-section of the failure zone of the embankment is given in Figure 3.7. The failure occurred by a downward movement of a wedge of dike material into the underlying peat. Next a section of the peat translated horizontally towards the ditch.

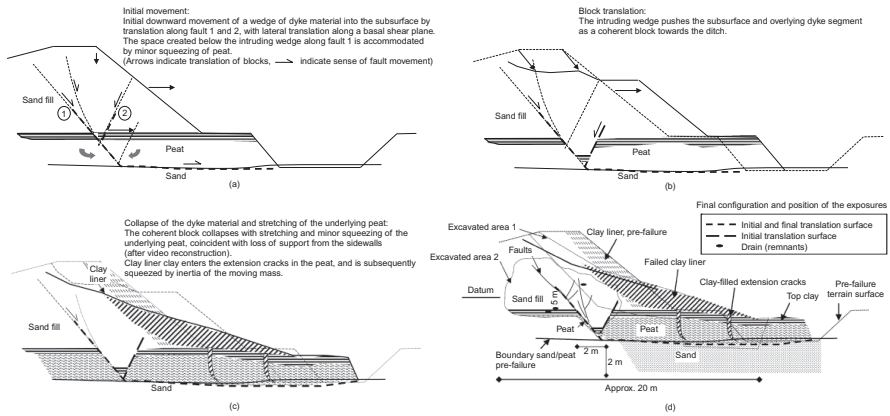

Figure 3.7: Illustration of failure mechanism at IJkdike failure [Zwanenburg et al., 2012]

Laboratory and field tests

An elaborate testing program consisting among others of 22 single-stage triaxial compression tests was conducted. The soil samples were both isotropically and anisotropically consolidated to a stress corresponding to the initial stress and to the final stress (after construction of the test embankment).

A large difference in undrained shear strength ratio ($S = s_u/\sigma_{vy,peak}$) for triaxial tests and direct simple shear tests was found: S= 0.61 for triaxial compression and S= 0.46 for DSS. The strong anisotropy may be explained by the fibrous nature of the peat.

Cone penetration tests were used to interpret the strength of the subsoil before and after the test. Based on experience, the authors used a bearing factor (N_{kt}) of 12.6. For the cone type used, the a factor (net area factor of CPT) was a= 0.86. CPT tests before construction and after construction were executed and the CPT profiles were compared with laboratory results. Particularly the DSS (direct simple shear) test indicated a good correspondence with the measurements from the CPT.

Pore water pressure transducers were used to monitor the hydraulic head during the construction of the dike and during the different stages of the failure test. Whereas the pore water pressure gradually increased during 4 stages of the test, a sudden decrease indicated the moment of failure of the trial embankment.

Stability analysis

A limit state equilibrium analysis is used to calculate the stability of the trial embankment. From the findings during the failure test it was concluded that the failure did not merely consist of a single continuous failure zone. The sliding plane can be divided in an active zone, a direct shear zone and a passive zone, corresponding respectively to triaxial compression, direct simple shear and triaxial extension [Ladd, 1969].

Different values for undrained shear strength were found from field and laboratory measurements. Hence, various cases were assessed and compared.

- Case 1 (s_u from TC with preconstruction σ'_{vc}) and 3 (s_u from DSS with preconstruction σ'_{vc}) underestimated the stability and predicted failure in stage 3.
- Case 2 (s_u from TC with FEM calculation for σ'_{vc}) overestimated the stability and predicted a FS > 1 after the final stage of the test.
- It was found that case 4 (s_u from DSS with FEM calculation for σ'_{vc}) and case 5 (s_u from field testing) correspond to the trial embankment stability test.

Sensitivity analyses were carried out to evaluate the influence of the variation of four parameters on the calculated safety factor. These four parameters were the undrained shear strength of the clay cover ($s_{u,clay\ cover}$), the effective angle of friction of the sand (ϕ'_{sand}), the volume weight of the sand (γ'_{sand}), and the active horizontal earth pressure coefficient for the peat layer (λ_a).

3.3.3 Effective Stress Finite Element Stability Analysis of an Old Railway Embankment on Soft Clay, Juho Mansikkamäki [2015]

Introduction

A considerable part of the Finnish railways lies on soft soil (embankments). To evaluate the safety of these embankments or elevations, total stress analyses with undrained shear strength are conducted. The objective of the study was to evaluate the capability of commercial isotropic finite element material model for performing effective stress stability analyses of soft clays. Furthermore, advanced finite element models are used to simulate the effects of anisotropy in the soil. The study is based on a back analysis of the Perniö failure test which was conducted on an old railway embankment in Perniö (Finland) in 2009.

Test set-up

A small railway embankment was built on a clayey soil. The embankments had a height of 0.6 m and a length of 60 m. A 2 m deep ditch was excavated at a horizontal distance of 14.5 m of the embankment. A steel framework was used to simulate a railway car with bogie carriages. On the carriages shipping containers were placed which were gradually filled with sand.

The monitoring program consisted of pore pressure gauges, earth pressure gauges, inclinometer tubes, total station monitoring of several prisms, settlement tubes and slip surface measuring pipes. A view on the test setup is given in Figure 3.8.

Subsoil properties

A soil investigation program was conducted to determine the subsoil parameters. The investigation program consisted of Swedish weight soundings, field vane shear tests and piezocone penetration tests (before and after failure). Besides in situ test, samples were taken for a range of laboratory tests.

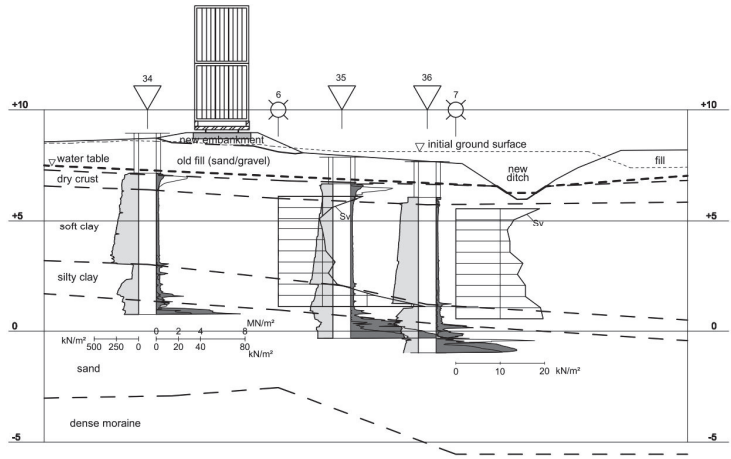

Figure 3.8: Cross section of test setup [Mansikkamäki, 2015]

The top layer (1.5 m) was an old embankment fill that consisted of sand and gravel. Underneath, a dry crust layer was found with a thickness of 0.6 – 0.9 m. A soft clay layer, 3.5 to 4.5 m thick is present beneath the dry crust. Deeper laying soil were a silty clay (1.5 m), a sand layer and dense moraine. Soil layers were slightly inclined towards the ditch.

Stability analysis

The Modified Cam Clay-model and Soft Soil (creep) are isotropic models suitable for soft soils but they cannot analyse anisotropic soil behaviour. The S-CLAY1 model [Wheeler et al., 2003] and the extension S-CLAY1S [Karstunen et al., 2005] are anisotropic models with elastoplastic behaviour. Hence, the S-CLAY1S model was utilised to simulate the failure test.

Based on inclinometer results, the shape of the failure surface below the embankment is estimated. Despite using different material models, the failure surface in the models deviated slightly. The results of the evaluation of the calculated failure loads with different calculation methods and material models are shown in Figure 3.9. The dashed line gives the actual failure load.

It can be concluded that some methods result in very conservative results. Furthermore, the field vane tests (FVT) often tends to underestimate the shear strength in soft clay. The material models S-CLAY1S and Soft Soil M-fit show good agreement with the field test. The EVP-SCLAY1S model predicted the displacement and excess pore pressures very well.

The Hardening soil model slightly overestimated the failure load at fast loading rate. Other models tend to overestimate the failure load. The shortcomings of these models are at the base of the discrepancy.

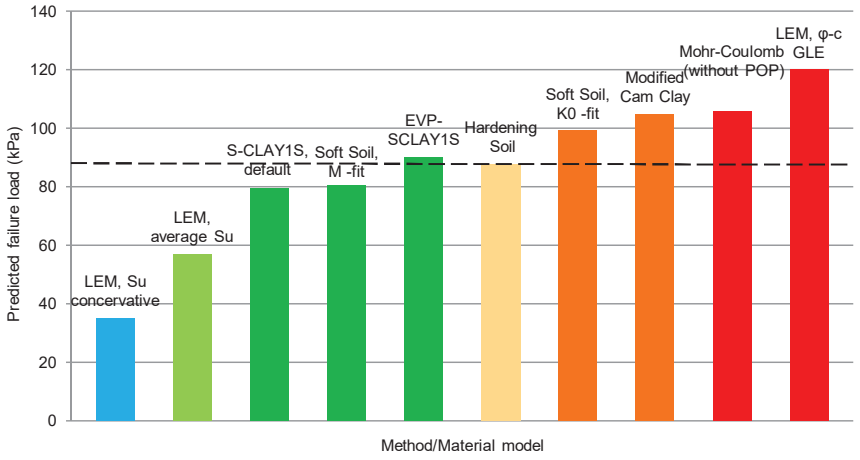

Figure 3.9: Predicted failure load with different calculation methods [Mansikkamäki, 2015]

3.4 Conclusions

In this paragraph some documented test embankments were reviewed. The objectives, dimensions and instrumentation are described. Furthermore the encountered problems are discussed.

The documented trial embankments are executed on natural soft soils such as clay and peat. However, the sludge material in the present study is not a natural but an artificial material originating from chemical processing. A significant difference in microstructure exist between the CaF_2 sludge and clays. Whereas the industrial sludge consists of microscopic spherical particles of a singular composition in the order of magnitude of a few µm, clays are composed of various minerals with layered packing in which water is trapped by physical and capillary actions. These minerals and stacking influence the physical behaviour of clays. By the fineness of the CaF_2 sludge, the water is also trapped by physical attractions. Water movement in the sludge must be forced by pressure increase (hydraulic gradient or drying), similar to clayey material.

In this study, the sludge behaviour is based on material models and correlations which apply to clays, because of the lack of data and experience on this specific sludge material. It should be kept in mind, however, that deviant behaviour is possible, given the intrinsic differences in microscopic composition between clays and sludge. Therefore, executing trial embankments is a useful way to evaluate the assumptions and extrapolations of (empirical) parameters from tests on clays.

Simulations, solely based on in situ and/or laboratory tests, have the tendency to over- or underestimate the actual shear strength of soft soil embankments. Without performing in situ tests, such as trial embankments, the choice of the most suitable material model and calculation method can be difficult. All material models have their own specific features and all have advantages and disadvantages. Some allow accurate simulation of the soil behaviour but can show discrepancy in shear strength, whereas others may account for anisotropy but don't estimate the pore pressure very well. The investigated trial embankments presented previously, learn that the choice of material model is important and may influence the results significantly.

Not all can be known or measured when performing a trial embankment, regardless of the extensiveness of instrumentation implemented. Local disturbances or other unknown phenomena may occur in the soil. Hence, there will always be a margin of error. As learned from the literature survey, the methods for characterisation of soft soils (peat, soft clay, ...) are of importance and may influence the final results of a stability analysis.

In the current study, attention will be paid to the impact of stress state anisotropy in the different in situ and laboratory tests. A suggestion for taking into account anisotropy is evaluated. Classic finite element material models don't allow the implementation of stress state anisotropy in undrained analysis. An advanced material model will be used and compared to classic material models.

Chapter 4

Undrained soil behaviour

4.1 Introduction

Analyses of soil behaviour are commonly executed in a drained configuration when regarding to shear strength. However, calculating with the undrained shear strengths will result in a better similarity to the actual soil behaviour when dealing with low permeable soft soils. The essence of undrained soil behaviour consist of the generation of pore water pressures when shear strains occur and the soil deforms. The excess pore water pressures generated, have an important influence on the shear resistance of the soil since they reduce the effective stresses and hereby reducing the shear strength.

The theoretical background on undrained soil behaviour and undrained analysis is already well known for decades and has been studied by many researchers ([Schofield and Wroth, 1968]; [Ladd and Foott, 1974]; [Mesri, 1975]; [Ladd, 1991]; [Mayne, 1980]; ...). Undrained analyses were though seldom applied for calculations of geotechnical structures since hardly any performant models were available in finite element programs. Recent developments of new material models improved the accuracy of undrained soil behaviour analysis.

In this chapter, an insight is given in the theoretical background of undrained soil behaviour. The advantages, disadvantages and specific issues when considering undrained soil behaviour are discussed. Furthermore, several material models available in the finite element program Plaxis, and specifically designed for undrained soil behaviour, are described in this chapter.

4.2 Drained vs undrained analysis

When a load is applied on a soil, the soil compresses by reducing the volume of the air or water filled voids. As a result the effective stress (σ') on the soil particles increases. If, however, the water in the soil pores cannot dissipate, the load is carried by the entrapped water, resulting in an excess pore water pressure (Δu). This is considered undrained soil behaviour. Drained and undrained soil conditions are dependent on the rate of which changes in load (loading or unloading) occur, compared to the capability of the soil to dissipate excess pore pressure (permeability). The relation between total stress (σ), effective stress (σ') and pore pressure (u) is given in equation (4.1). The situation of undrained loading is given in equation (4.2).

$$\Delta\sigma' = \Delta\sigma - \Delta u \tag{4.1}$$

$$\Delta\sigma' = 0;\ \Delta\sigma = \Delta u \tag{4.2}$$

Most sands and gravels have a high permeability, which allows for excess pore water pressures to dissipate quite fast. If a load is applied very quickly, even commonly presumed permeable soils can show undrained soil behaviour. In soils with a low permeability such as clay and silt, seepage of water progresses slowly. Depending on the permeability and thickness of the layer, consolidation can take seconds, days or even centuries. In case of undrained behaviour, the pore water is trapped in the pores. Due to the incompressibility of pore water, no volumetric deformation can therefore occur.

Drained or undrained behaviour is defined by the speed of the loading and the permeability of the soil. A high rate of loading compared to a low permeability is considered as undrained loading. A method to distinguish drained or undrained behaviour was suggested by Vermeer & Maier [Vermeer and Meier, 1998], based on the following equation (4.3).

$$T = \frac{k \cdot E_{oed}}{\gamma_w \cdot D^2} \cdot t \tag{4.3}$$

For a dimensionless time factor smaller than 0.10, undrained conditions can be presumed. $T < 0.10$ corresponds to a degree of consolidation lower than 10%. When the dimensionless time factor is greater than 0.40, drained conditions can be presumed. $T > 0.40$ corresponds to a degree of consolidation greater than 70%. Both drained and undrained behaviour need to be considered for T in between 0.10 and 0.40.

The permeability and oedometer modulus are the soil dependent parameters in equation (4.3). Therefore not only the permeability but also the compressibility influences the consolidation process. As commonly expected, a low permeable soil takes longer to consolidate since the pore water experiences more resistance in soil such as clay due to the fine pores. The presence of the oedometer modulus in the counter of the fraction indicates that a highly compressible soil (low oedometer modulus) has a longer consolidation time compared to a stiffer soil with high oedometer modulus.

The degree of consolidation (U) and the dimensionless time factor (T) vary with the depth as given in Figure 4.1 for dissipation of excess pore pressure possible at top and bottom.

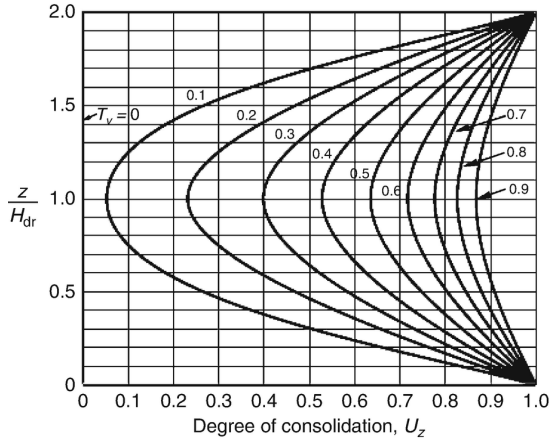

Figure 4.1: Degree of consolidation [Taylor, 1948]

For construction of levees with sandy material, a drained analysis will be suitable since the seepage of pore water will occur rapidly. For low permeable soils (clay, peat, sludge, ...), an excavation of a building pit or the construction of a levee can result into (positive or negative) excess pore water pressures.

Due to the low permeability and/or fast loading, excess pore water pressure cannot dissipate fast enough. As given in equation (4.2), at undrained loading, the change in total stress (load) will result into an equal change in pore pressure. The effective stress remains constant. Whereas the shear resistance in drained analysis is dependent on the effective stress, the undrained shear resistance is dependent on the (effective) stress history. The stress history of a soil is described in the over-consolidation ratio (OCR) as the ratio of the pre-consolidation stress (σ'_p) over the current overburden stress (σ'_{v0}). In the following paragraphs undrained shear resistance is explained more detailed.

When shear stresses are applied on a soil and deformations occur, pore water pressure is generated in undrained soil behaviour. The increase in pore pressure can lead to a reduction of the effective stresses and, therefore, reducing the shear strength.

For example, when a slope failure occurs in normally consolidated soil, shear stresses increase in the slope resulting in shear deformations. Pore water pressures are generated ($\Delta u > 0$) because of the deformations. Since no external forces are applied, the total stresses are constant ($\Delta\sigma = 0$) and therefore the effective stresses are reduced ($\Delta\sigma' < 0$). The difference between drained and undrained behaviour is presented in Figure 4.2. The shear strength (τ) of a soil is determined by the effective stress. The shear strength determined by either drained or undrained soil behaviour can differ significantly.

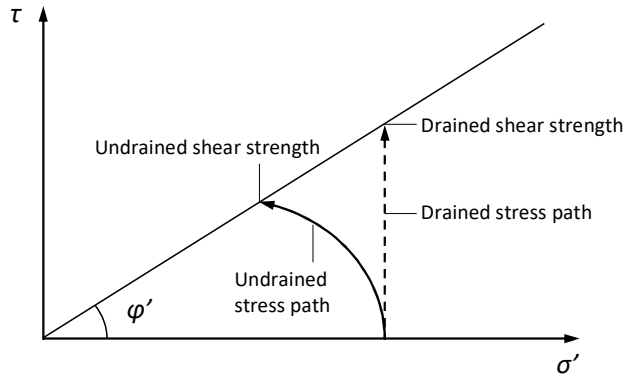

Figure 4.2: Drained and undrained stress paths

4.3 Critical state soil mechanics

4.3.1 CSSM theory

The critical state soil mechanics or CSSM is an effective stress framework by Schofield and Wroth [Schofield and Wroth, 1968] to give insight into the mechanical behaviour of shear strength and consolidation of soils. It defines that all soils fail at the critical state. Moreover, the critical state line (CSL) is a unique relationship between shear stress, the normal effective stress and the void ratio, as shown in Figure 4.3.

The CSSM method states that a continuously sheared granular material (such as soil) will flow as a frictional fluid. This state is called the critical state. Furthermore, in this critical state, the soil continues to distort with a constant mean effective stress, deviatoric stress and void ratio. The critical states correspond to shear strains in the order of 10% to 40%, depending on the material.

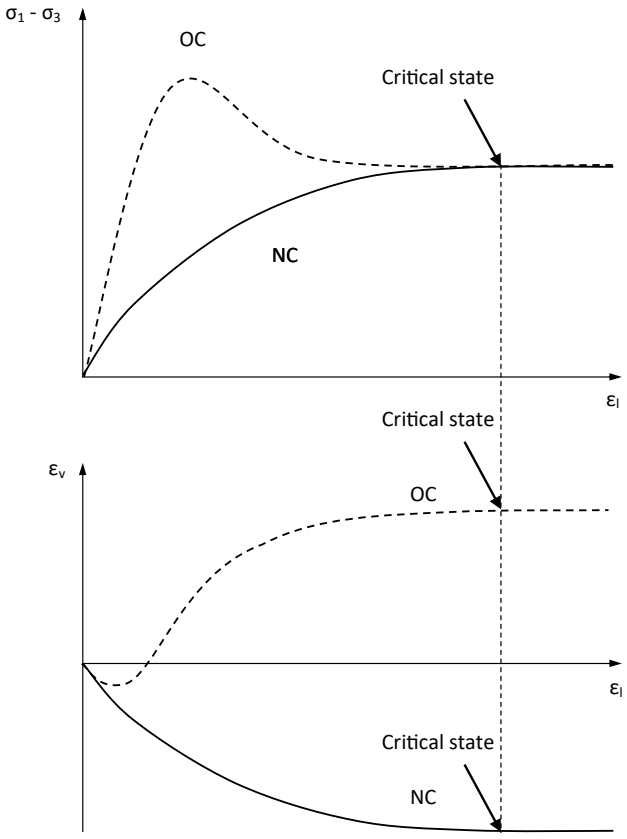

Figure 4.3: Definition of critical state

Due to the complex and diverse initial soil conditions, predictions in soil behaviour at yield are difficult. Hence, the CSSM theory starts from the ultimate fully remoulded condition that might occur at large deformations at which the soil flows as a frictional fluid. It than predicts the required change from an initial state to the ultimate state.

The critical state is determined by equations (4.4) and (4.5).

$$q = M \cdot p \tag{4.4}$$

$$\nu = \Gamma - \lambda \cdot \ln p \tag{4.5}$$

The first equation is represented in the upper graph of Figure 4.4 and defines the required deviatoric stress (q) to overcome the friction resistance, which is determined by the frictional constant (M) and the effective pressure (p).

In the second equation, the relation between the specific volume (ν) and the effective pressure is given. The constant Γ presents a specific volume of a point on the critical state line at a certain pressure. The gradient of the compression line is presented by λ (Figure 4.4, lower graph). The equation states that the specific volume decreases as the logarithm of the effective pressure increases.

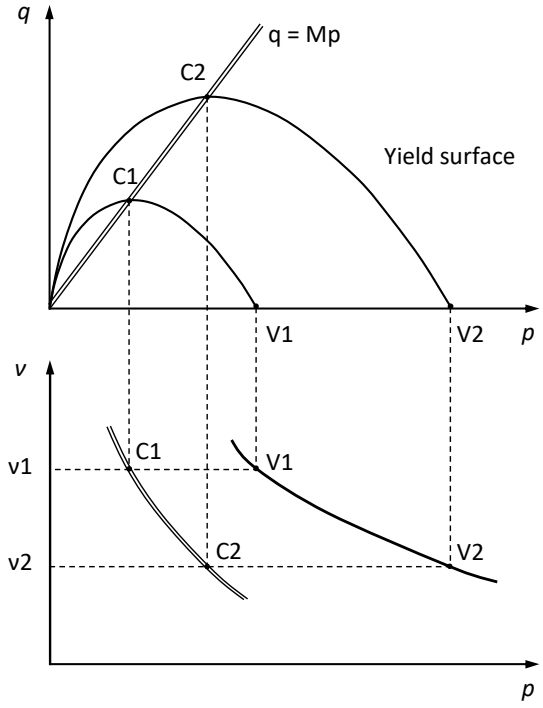

Figure 4.4: Graphic presentation of the critical state soil mechanic principle

In Figure 4.5, the family of yield curves is given, which generates a closed surface in three dimensions (p, ν, q). All possible stable states are enclosed by this stable-state boundary surface.

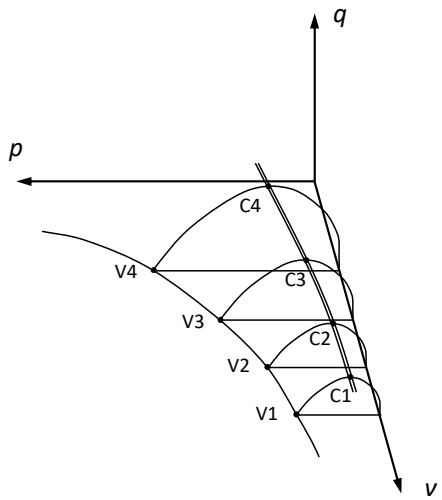

Figure 4.5: Three dimensional presentation of CSSM with the upper half of the state boundary surface. Different yield surfaces at various volume states are represented.

4.3.2 Shear strength in CSSM

When considering the shear resistance of the soil in the Critical State Soil Mechanics framework, the shear strength at critical state is given by equation (4.6).

$$t = s' \cdot \sin \phi'_{CS} \tag{4.6}$$

In the concept of the critical state the existence of cohesion is the consequence of over-consolidation, as presented in Figure 4.6. This over-consolidation results in a higher shear resistance, which is represented as a peak strength compared to the ultimate or critical state shear strength (see Figure 4.3). Whereas the shear resistance in drained analysis is dependent on the effective stress, the undrained shear resistance is dependent on the (effective) stress history.

A soil is considered over-consolidated when the pre-consolidation stress (due to previous loading) is higher than the current vertical effective stress. The stress history of a soil is described in the over-consolidation ratio (OCR) as the ratio of the pre-consolidation stress (σ'_p) over the overburden stress (σ'_{v0}).

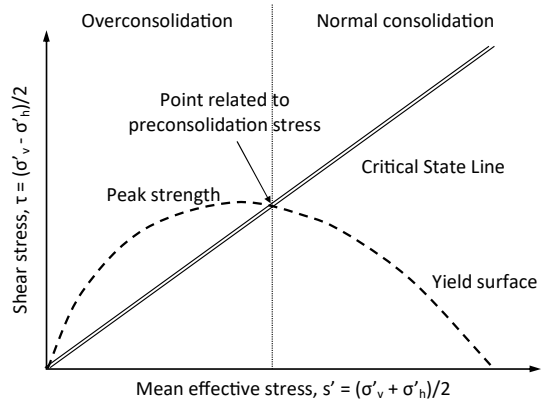

Figure 4.6: Shear strength in the Critical State Soil Mechanics framework

With the curves from one-dimensional consolidation tests (oedometer tests) and Mohr circles from (triaxial or direct) shear tests, the behaviour of soil in undrained and drained behaviour can be described using the CSSM theory. The void ratio (e) versus the logarithm of the effective stress (σ'_v) is obtained from one-dimensional consolidation tests. Mohr circles, obtained from triaxial tests or direct shear tests, give the relation between the effective stress and the shear stress. Four basic stress paths can be distinguished for drained and undrained behaviour of over-consolidated or normally consolidated soils. All the stress paths end on the critical state line. The slope of the critical state line in the $e - \log \sigma'$ diagram is equal to the slope of the normal consolidation line.

The four basic stress paths of soil during drained normal consolidation, undrained normal consolidation, undrained over-consolidation and drained over-consolidation are presented in Figure 4.7. The simplified stress paths are described as followed:

1. Drained, normal consolidation

   The current overburden stress is equal to the pre-consolidation stress ($OCR = 1$). With the increase in total vertical stress no excess pore water pressures are created, so the effective stress does not change. The volume changes in the soil are contractive till the ultimate state is reached. The maximum shear stress equals $\tau_{max} = \sigma' \cdot \tan \phi'$.

2. Undrained, normal consolidation

   The current overburden stress is equal to the pre-consolidation stress ($OCR = 1$). There are no volume changes with increase in total vertical stress. Positive excess pore water pressures occur.

The effective stress decreases until the critical state line is reached. The maximum shear stress equals $\tau_{max} = s_{u,NC}$. The undrained shear strength is lower for undrained compared to drained failure.

3. Undrained, over-consolidation

   The current overburden stress is lower than the pre-consolidation stress ($OCR > 1$). There are no volume changes with increase in total vertical stress. Negative excess pore water pressures occur. The effective stress increases until the yield surface is reached. The maximum shear stress equals $\tau_{max} = s_{u,OC}$.

4. Drained, over-consolidation

   The current overburden stress is lower than the pre-consolidation stress ($OCR > 1$). There are no excess pore water pressures created with the increase in total vertical stress. Thus the effective stress doesn't change. The volume changes are negative (dilatancy) till the yield surface is reached. The maximum shear stress equals $\tau_{max} = c + \sigma' \cdot \tan \phi'$.

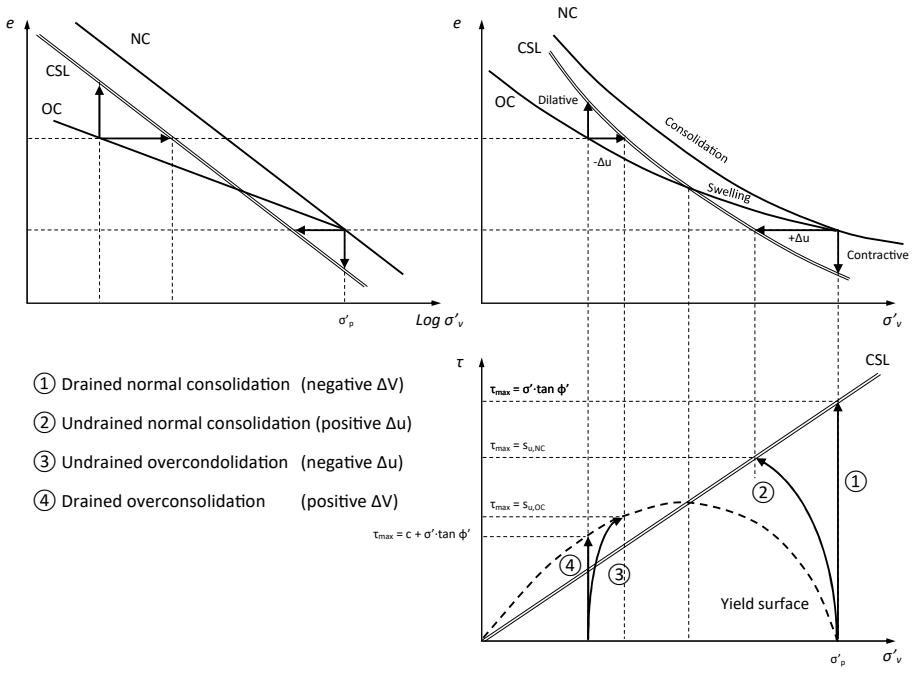

Figure 4.7: Soil behaviour in CSSM for four common stress paths

4.4 SHANSEP

4.4.1 General

The undrained shear strength is strongly dependent on the stress history and (current) stress conditions of the soil. In situ (shear) tests are mostly performed under the in situ stress configuration. Results of shear strength in laboratory tests can be affected by sample disturbance due to drilling, sampling, drying, ..., at which the initial stresses may change. The SHANSEP technique [Ladd and Foott, 1974] was developed in an attempt to minimize these effects of sample disturbance on laboratory results. SHANSEP stand for Stress History And Normalized Soil Engineering Properties and coheres with the Critical State Soil Mechanics method. By re-consolidating soil samples to the stress state, which corresponds to the stress state at the sample location, potential disturbances are restored and the initial stress conditions are reset.

Figure 4.8 illustrates a hypothetical disturbance of soil samples from drilling till preparation for laboratory testing. The undisturbed, initial stress state, is located at point 1 and is determined by a K_0 stress state. The dashed curved line from point 1 to A represents the actual stress path in a perfect undrained triaxial compression test. However, due to several manipulations of the soil sample the initial stress conditions can be lost. When performing an undrained unconsolidated triaxial compression test (UUC), the results will have no resemblance to the soil shear strength at the sample location.

The undrained shear strength can be defined based on the CSSM and SHANSEP method as followed [Ladd, 1991]:

$$s_u = \sigma'_{vi} \cdot S \cdot OCR^m \tag{4.7}$$

$$OCR = \frac{\sigma'_{vc}}{\sigma'_{vi}} \tag{4.8}$$

The normally consolidated shear strength ratio (S) is the ratio between undrained shear strength (s_u) over the in situ vertical effective stress (σ'_{vi}) at normal consolidation ($OCR = 1$).

The undrained shear strength of soils depends on the type of soil, the water content, the stress history and the stress path during loading. The stress history, denoted by the over-consolidation ratio (OCR), and stress path are not commonly considered in classic analysis. However, their influence on the undrained shear strength is substantial.

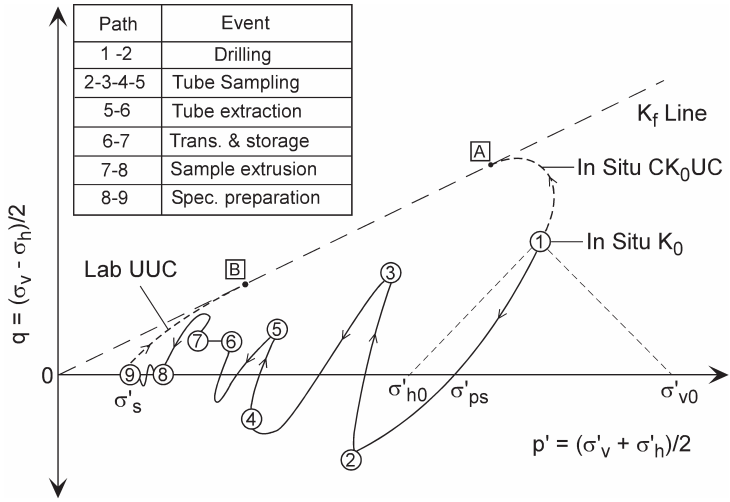

Figure 4.8: Hypothetical stress path during tube sampling and specimen preparation of centreline element of low OCR clay (after [Ladd and Lambe, 1963], [Baligh et al., 1987]), [Ladd and Degroot, 2003]

Throughout the history, there are several well-known cases were construction failure was triggered by erroneous assumed (un)drained stress paths. For example, the Nicoll Highway collapse in Singapore in 2004 [Magnus et al., 2005] was the result of incorrectly assumed soil behaviour and stress paths. This led to an overestimation of the shear strength and failure of the soil and construction.

4.4.2 SHANSEP test procedure

With the SHANSEP approach, the stress conditions during the laboratory tests are monitored carefully to evaluate the stress path during undrained shear. The SHANSEP procedure, for estimation of the in situ undrained properties, involve the following procedure suggested by [Ladd and Foott, 1974] and [Ladd et al., 1977]:

1. Determination of the initial stress history

   The pre-consolidation stress (σ'_p) can be derived from one-dimension consolidation testing (oedometer test) or with CRS-tests (constant rate of strain test) on undisturbed soil samples.

As presented in Figure 4.9, the pre-consolidation stress (σ'_p) is found near the tipping point between the first straight section (recompression) and the second, steeper, straight section (virgin compression).

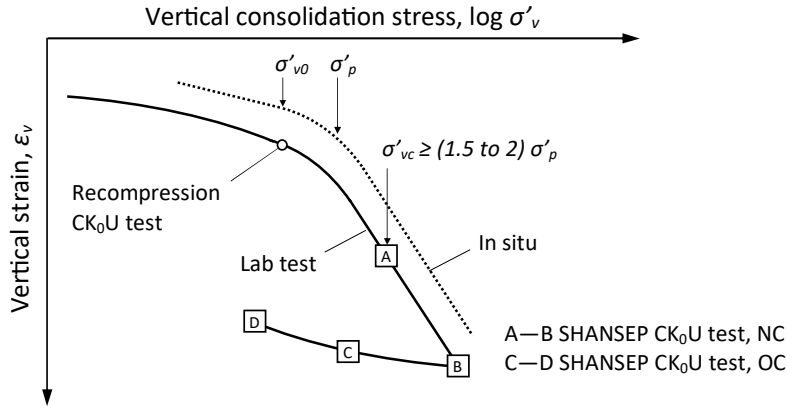

Figure 4.9: SHANSEP-method for re-consolidation of soil samples, after [Ladd et al., 1977]

2. Performing CK_0U tests

Triaxial or direct simple shear (DSS) tests are to be performed on soil samples at consolidation pressures greater than 1.5 to 2 times the found pre-consolidation stress (σ'_p). CK_0U tests are K_0 anisotropically consolidated (C), undrained (U) tests, where the soil samples are consolidated at a different vertical and horizontal stress. K_0 is the ratio of the effective horizontal stress (σ'_h) to the effective vertical stress (σ'_v).

Jaky [Jaky, 1944] suggested a value of K_0, based on the effective friction angle, (eq. 4.9 and 4.10).

$$\sigma'_h = \sigma'_v \cdot K_0 \tag{4.9}$$

$$K_0 = 1 - \sin\phi' \tag{4.10}$$

The anisotropic stress state, imposed in the laboratory tests, more closely resembles the actual stress state in the field. As a result, the followed stress paths till failure will lead to an accurate prediction of the in-situ shear strength. Besides normally anisotropically consolidated undrained shear tests (Figure 4.9, points A and B), also over-consolidated shear tests are to be performed at varying over-consolidation ratio's (Figure 4.9, points C and D).

Initially the test samples are K_0 consolidated at effective stress higher than the pre-consolidation pressure determined in step 1. Then the samples are reconsolidated at a lower effective stress, whereupon the (triaxial or direct) shear test is executed. The over-consolidated shear tests are performed at varying OCR.

3. Plotting the results of undrained shear ratio (s_u/σ'_{v0}) versus log over-consolidation ratio

   When plotting the normalised shear ratios ($S = s_u/\sigma'_{v0}$) versus the over-consolidation ratios (OCR), the result is a concave upward curve as shown in Figure 4.10. The curve corresponds to equation (4.7). The values of S and m can be obtained from plotted results.

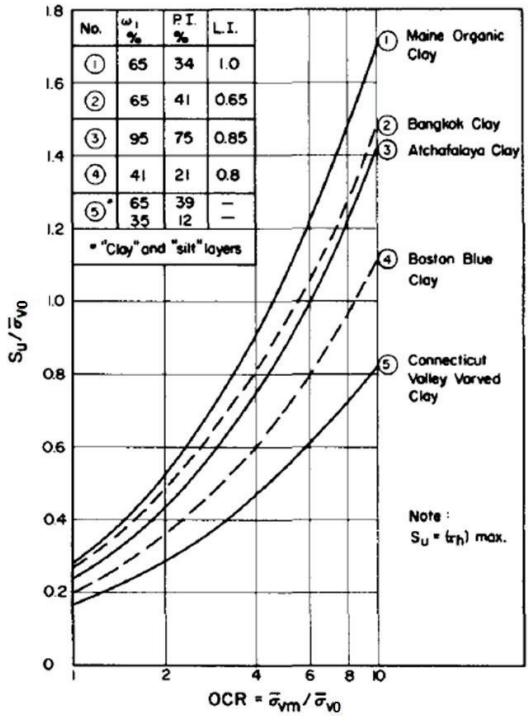

Figure 4.10: Variation of s_u/σ'_{v0} over OCR for five different clays [Ladd and Foott, 1974]

4. Calculation of s_u profiles

   The determined parameters (S and m) can be used in equation (4.7), to calculate s_u profiles based on the stress history.

4.4.3 Discussion

The Stress History And Normalized Engineering Properties (SHANSEP) method [Ladd and Foott, 1974] has the advantage of minimizing sample disturbance by re-consolidating specimens to a higher consolidation stress. The initial stress conditions are reset, avoiding unwanted over-consolidated soil tests. Nevertheless, the test procedure requires difficult and costly anisotropic triaxial testing (CK_0U). Common triaxial tests perform an isotropic consolidation ($\sigma'_h = \sigma'_v$), followed by a loading phase. The deviatoric stress is increased (increase in vertical stress and/or decrease in cell pressure) until failure occurs.

To perform CK_0U (Consolidated at K_0, Undrained) triaxial tests, the isotropic consolidation phase has to be followed by an anisotropic consolidation phase with a limited increase of the vertical load ($\sigma'_h = K_0 \cdot \sigma'_v$). After the second consolidation, the deviatoric stress can be increased. This procedure requires a longer consolidation time (two consolidation phases) and for testing at OCR > 1, an additional re-consolidation phase is required.

Besides the complex and therefore costly testing procedure, one should consider whether the additional information or higher accuracy will be in proportion to a cost reduction or efficiency benefit in the construction projects.

4.5 Anisotropy

4.5.1 General

The effect of anisotropy on the shear strength in clays has been studied by several authors e.g. [Bjerrum, 1973], [Ladd and Foott, 1974], [Ladd et al., 1977], [Jamiolkowski et al., 1985], [Nakase, 1983]. There are two types of anisotropy which can occur. The first type is caused by particle orientation and the geological formation of soil. During deposition of soils, particle shape has an influence on the orientation preference. This leads mostly to a horizontal direction of depositions.

The second type of anisotropy is a stress induced anisotropy. Here, the direction of the applied major principle stress deviates from the vertical (gravitational) direction. Furthermore, the strength and stiffness changes with the orientation of the major principal stress to the vertical direction. Figure 4.11 illustrates the orientation of the major principle stress along a slope. The stress state changes from an active state to a passive state along the shear plane.

In the active zone the vertical stress is larger than the horizontal stress, meaning the major principle stress acts more vertical. This stress state is comparable to the stress state in a triaxial compression test. The orientation of the major principle stress is horizontal in the passive zone, corresponding to a triaxial extension test. Between active and passive, the stress state is similar to the stress state in a direct simple shear (DSS) test.

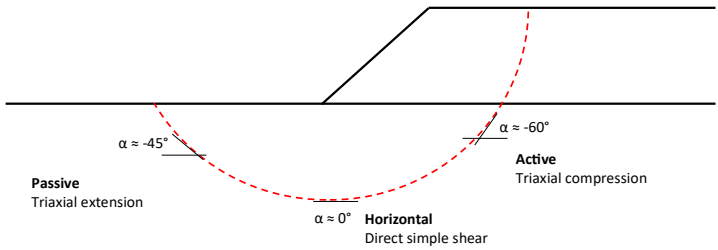

Figure 4.11: Orientation of major principle stress along a circular shear plane

Stress-strain curves of K_0 consolidated undrained triaxial compression and extension tests, are presented in Figure 4.12. The dashed line represents the K_0 consolidation (eq. (4.9) and (4.10)). The stress paths for triaxial compression (TC) and triaxial extension (TE) tests both end on the ϕ'_{CS}-line (critical state line), which is identical on the positive and negative side. However, both stress paths differ, resulting into a different stress state at failure. The stress-strain curves illustrate the significant larger strain at failure for triaxial extension compared to triaxial compression. Therefore, not only shear strength but also stiffness change with the orientation of the major principle stress.

The difference in strain has an important influence on the total shear resistance of a slope when strain compatibility is at issue. Further information about strain compatibility is given in §4.7.2.

A correlation exists between the plasticity index and the anisotropic behaviour of plastic soils ([Bjerrum, 1973], [Ladd et al., 1977], [Nakase, 1983], [Jamiolkowski et al., 1985], among others). In Figure 4.13 the peak undrained shear strength ratios ($S = s_u/\sigma'_{vc}$) are compared with the plasticity index (I_p) for triaxial compression (TC), direct simple shear (DSS) and triaxial extension (TE) tests.

The results of the tests show significant scatter, however, some trends are noted. The triaxial extension tests have the lowest shear ratio, which increases with the plasticity index (I_p). The DSS test exhibit a similar behaviour with a slightly higher ratio. A constant (average) undrained shear strength ratio was determined with the triaxial compression tests at various plasticity index.

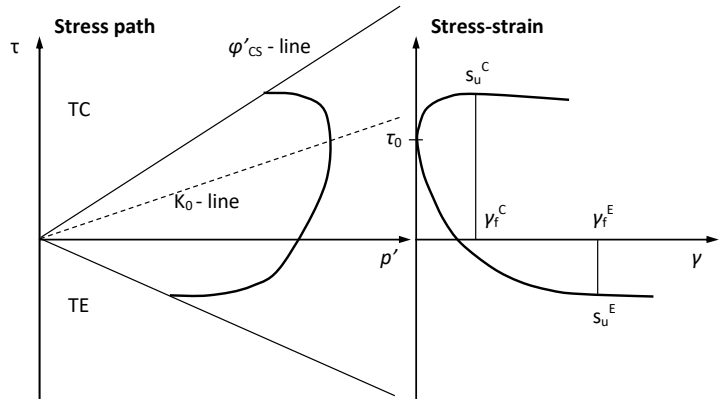

Figure 4.12: Typical stress paths and stress-strain curves for triaxial compression and extension tests with definition of stress/strain quantities

It can be noticed from Figure 4.13 that low plastic soils exhibit a more pronounced anisotropic behaviour. At a plasticity index of around 10%, the strength ratio of TE can be nearly half the strength ratio of TC.

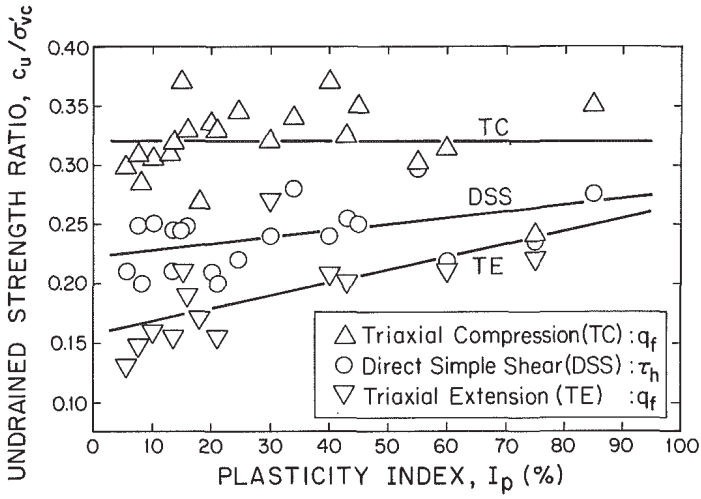

Figure 4.13: Undrained strength anisotropy from CK_0U tests on normally consolidated clays and silts (data from [Lefebvre et al., 1983]; [Vaid and Campanella, 1974]; and various MIT and NGI Reports) [Ladd, 1991]

In common undrained analyses the undrained shear strength is denoted as the average laboratory shear strength ($s_{u,Lab}$) from triaxial compression, direct simple shear and triaxial extension tests, equation (4.11).

$$s_{u,Lab} = \frac{s_{u,TC} + s_{u,DSS} + s_{u,TE}}{3} \tag{4.11}$$

This laboratory shear strength is often considered as a fairly representative value for the average shear strength in excavation, embankments and bearing capacity of footings [Bjerrum, 1972]. For simple cases the average laboratory shear strength can be sufficient to perform an adequate stability analysis. In more complex situations or when a higher accuracy is required, a more advance method, considering the anisotropic behaviour, can be necessary.

4.6 Material models

4.6.1 Introduction

The Plaxis finite element program was used in the analyses of the sludge embankments. Several material models are available from a simple linear elastic – perfectly plastic Mohr-Coulomb (MC) model to more advanced models such as the hardening soil (HS) model. Most finite element models determine the shear strength based on the effective stresses, which are influenced by the pore water pressure. The permeability of the geological structure determines whether drained or undrained behaviour is at issue. The finite element models described below are soil models, which are specially designed for undrained behaviour. Here the undrained shear strength is not a result of the effective stress but is an input parameter.

The SHANSEP MC, the NGI-ADP and the combined NGI-ADP SHANSEP models are described in the following paragraphs. Furthermore, the implications of using common material models such as the Mohr-Coulomb and Hardening Soil with undrained analyses is discussed.

Various material models, available in the finite element program Plaxis, allow the simulation of undrained situations to be analysed using undrained method A, B or C. Method A is an analysis in terms of effective stresses with effective strength parameters c, ϕ' and ψ' and effective stiffness parameters E'_{50} and ν'.

Method B is an analysis in terms of effective stresses with undrained strength parameters $c = s_u$, $\phi = 0$ and $\psi = 0$ and effective stiffness parameters E'_{50} and ν'.

Method C is an analysis in terms of total stresses with total strength parameters $c = s_u$, $\phi = 0$ and $\psi = 0$ and undrained stiffness parameters E_u and ν_u. Not all methods are available in the different material models.

4.6.2 SHANSEP MC

The SHANSEP MC model (Stress History and Normalized Soil Engineering Properties, Mohr Coulomb) is based on the linear elastic perfectly plastic Mohr-Coulomb model. Adaptations are made, which allows changes in the undrained shear strength to be simulated. The undrained shear strength is based on the effective stress state of the soil with additional parameters to incorporate stress history. The undrained shear strength is estimated according to equation (4.12).

$$s_u = \alpha \cdot \sigma'_1 \left(\frac{\sigma'_{1,max}}{\sigma'_1} \right)^m = \alpha \cdot \sigma'_1 \left(OCR \right)^m \tag{4.12}$$

The SHANSEP MC model behaves as a normal MC model until undrained soil behaviour is activated. Then the undrained shear strength is calculated based on the effect stresses and stress history.

Five additional parameters are added to the MC model to make the SHANSEP MC model (table 4.1).

α	Coefficient for normally consolidated shear strength ratio	[–]
m	Power	[–]
G/s_u	Shear modulus over undrained shear strength ratio	[–]
$s_{u,min}$	Minimum undrained shear strength	$[kPa]$
OCR_{min}	Minimum over-consolidation ratio	[–]

Table 4.1: Additional parameters in the SHANSEP MC material model

Advantages and disadvantages

The analysis in Plaxis with the SHANSEP concept is an improvement of the MC Undrained (B) calculations. Hence, an analysis in terms of effective stresses is performed but with undrained strength parameters for cohesion ($c = s_u$), friction angle ($\phi = 0$) and dilatancy angle ($\psi = 0$). The stiffness parameters are, however, effective parameters (E'_{50}, ν'). The Mohr-Coulomb criterion is reduced to the Tresca criterion [Tresca, 1868].

An undrained analysis in MC undrained A leads to an overestimation of the undrained shear strength and an underestimation of the excess pore pressure (Figure 4.14(b)). If the drainage type is set to undrained (B) (Figure 4.14(c)), the undrained shear strength will be limited to a predefined value. Any variation of the undrained shear strength due to change in effective stress during consolidation phases, can however not be taken into account.

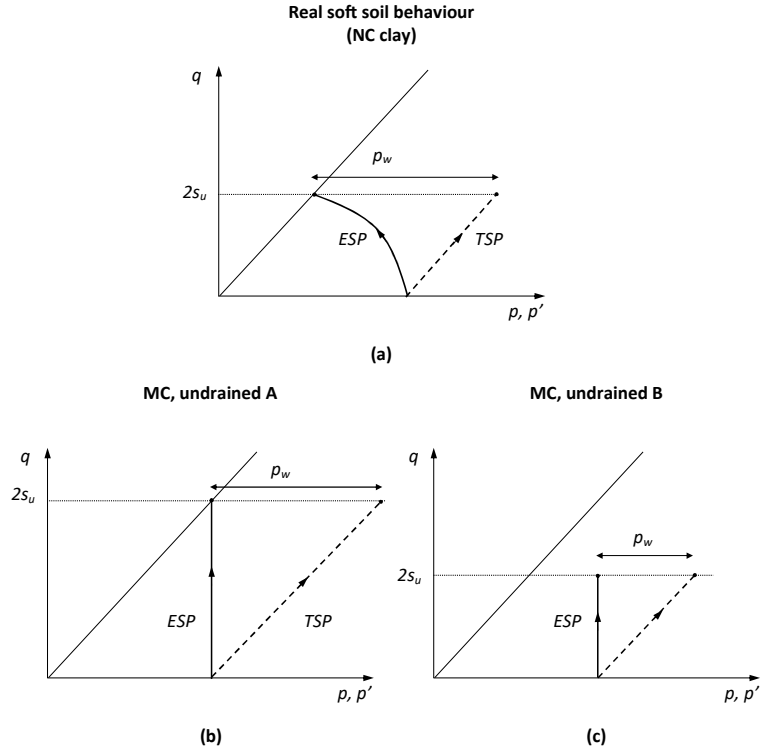

Figure 4.14: Effective and total stress paths of real soft soil behaviour and for Mohr-Coulomb Undrained A and B model

The main advantages of the SHANSEP MC model is the ability to give a more realistic value of the undrained shear strength compared to the traditional MC model. Furthermore, over-consolidation (stress history) can be accounted for in the simulation of the undrained shear strength as presented in Figure 4.15.

Because the undrained shear strength is stress dependent, it automatically takes into account the increase in shear strength with depth into account. With the parameter G/s_u the shear stiffness depends on the undrained shear strength, which will also increase with depth.

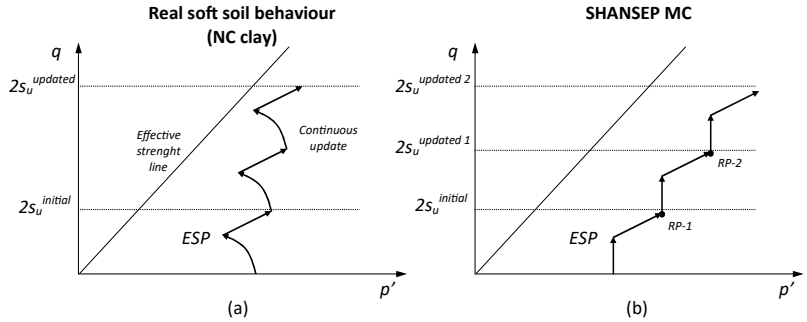

Figure 4.15: Effective stress paths of real soft soil and SHANSEP MC model

The use of the SHANSEP MC model should be limited to ultimate limit state situations. Simulating deformations is possible with the SHANSEP MC model but may lead to incorrect results due to the underestimation of pore water pressures and the resulting volume changes. Furthermore, there is no continuous update of the undrained shear strength (and shear stiffness) during consolidation phases. The undrained shear strength is only updated after each phase.

4.6.3 NGI-ADP

The stress state of soils is generally anisotropic, with a higher vertical stress compared to the horizontal stress. This consequently results in anisotropic shear properties. Common finite element models don't take account for anisotropic behaviour in undrained shear strength analyses. An average shear strength ($s_{u,ave}$ or $s_{u,Lab}$) is often used, where $s_{u,ave}$ is the average of triaxial compression, direct simple shear and triaxial compression tests (eq. 4.11).

The NGI-ADP model (Norwegian Geotechnical Institute – Active, Direct simple shear, Passive; [Andresen and Jostad, 1999], [Andresen, 2002], [Grimstad et al., 2012]) is an advanced undrained shear strength material model, designed for applying anisotropic soil properties and post-peak softening in saturated clays. The shear strength in the material model is defined in three stress states: active (A), direct simple shear (D) and passive (P).

The developed undrained shear strength depends on the followed stress path. Furthermore, the NGI-ADP material model considers the non-linear stiffness. The stiffness is described by plastic hardening, based on the ratio of initial elastic shear stiffness (unloading/reloading shear modulus G_{ur}) over the undrained active shear strength (s_u^A). Given the increase in shear strength with the effective stress, the stiffness also depends on the stress level.

The NGI-ADP model is based on the Tresca's yield criterion approximation after [Billington, 1988], which presents the isotropic undrained shear strength. This results in a hexagonal prism in three-dimensional principal total stress space, described by the following equation (eq. 4.13).

$$\sqrt{J_2} \cdot \cos\theta - \kappa \cdot s_u = 0 \tag{4.13}$$

The equation presents the relation between the second deviatoric stress invariant (J_2) and the Lode angle (θ) with the hardening parameter (κ) and the isotropic undrained shear strength (s_u).

The sharp corners of the hexagonal Tresca yield surface may lead to numerical difficulties, therefore the Tresca criterion in the NGI-ADP model is modified to circumvent possible problems at the corners by using von Mises plastic potential function [Von Mises, 1913]. There is no development of plastic volume strains because the yield and plastic potential functions are independent of the mean stress. By maintaining a Poisson's ratio close to 0.5, a restriction of approximately zero elastic volume strain is obtained.

Equation (4.14) defines the yield criterion for the NGI-ADP model in plane strain.

$$\sqrt{\left(\frac{\sigma'_{yy} - \sigma'_{xx}}{2} - (1-\kappa)\cdot\tau_0 - \kappa \cdot \frac{s_u^A - s_u^P}{2}\right)^2 + \left(\tau_{xy} \cdot \frac{s_u^A + s_u^P}{2 \cdot s_u^{DSS}}\right)^2} - \kappa \cdot \frac{s_u^A + s_u^P}{2} = 0 \tag{4.14}$$

As illustrated in Figure 4.16, the NGI-ADP model uses elliptical interpolation between failure strain in compression, direct simple shear and extension.

The NGI-ADP material model is defined in the finite element program Plaxis by parameters presented in table 4.2 (Material Models Manual, [Brinkgreve and Ragi Manoj, 2019]).

Advantages and disadvantages

The NGI-ADP model offers a total stress model for clays in undrained (C), based on total stress parameters (stiffness and strength). Different strengths with various stress paths can be taken into account allowing anisotropic behaviour to be modelled.

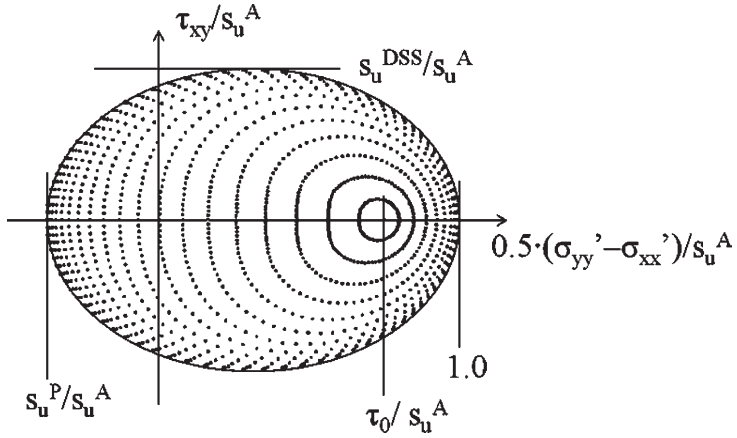

Figure 4.16: Typical deviatoric plane strain plot of equal shear strength contours for NGI-ADP model [Grimstad et al., 2012]

Stiffness parameters		
G_{ur}/s_u^A	Ratio unloading/reloading shear modulus over (plane strain) active shear strength	$[-]$
γ_f^C	Shear strain at failure in triaxial compression	[%]
γ_f^E	Shear strain at failure in triaxial extension	[%]
γ_f^{DSS}	Shear strain at failure in direct simple shear	[%]
Strength parameters		
$s_{u,ref}^A$	Reference (plane strain) active shear strength	$\left[kN/m^2\right]$
$s_u^{C,TX}/s_u^A$	Ratio of triaxial compressive shear strength over (plane strain) active shear strength (default = 0.99)	$[-]$
y	Reference depth	$[m]$
$s_{u,inc}^A$	Increase of shear strength with depth	$\left[kN/m^2/m\right]$
s_u^A/s_u^P	Ratio of (plane strain) passive shear strength over (plane strain) active shear strength	$[-]$
τ_0/s_u^A	Initial mobilization (default = 0.7)	$[-]$
s_u^{DSS}/s_u^A	Ratio of direct simple shear strength over (plane strain) active shear strength	$[-]$
Advanced parameters		
ν'	Poisson's ratio	$[-]$

Table 4.2: Specific parameters in the NGI-ADP material model

A non-linear stress-strain behaviour of soil is implemented by a hardening formulation. Softening of the soil is not possible. Because the analysis is based on the total stresses, no information is available about the pore pressure. Therefore, no consolidation phases can be taken into account.

4.6.4 SHANSEP NGI-ADP

A new material model was developed by Plaxis in 2018, combining the SHANSEP (Stress History and Normalized Soil Engineering Properties) with the NGI-ADP model (Norwegian Geotechnical Institute – Active, Direct simple shear, Passive). The new model is based on the NGI-ADP model to simulate anisotropic undrained soil behaviour. The SHANSEP method is added to allow undrained shear strength to be changed and stress history to be defined.

The undrained shear strength s_u, is estimated as followed (eq. 4.15 and 4.16):

$$s_u = \alpha \cdot \sigma'_1 \cdot OCR^m \tag{4.15}$$

$$OCR = \frac{\sigma'_{1,max}}{\sigma'_1} \tag{4.16}$$

Besides the NGI-ADP model parameters, presented in Table 4.2, five additional SHANSEP parameters are added, presented in Table 4.3.

α	Coefficient for normally consolidated shear strength ratio	$[-]$
m	Power	$[-]$
$s_{u,min}$	Minimum undrained shear strength	$\left[kN/m^2\right]$
OCR_{min}	Minimum over-consolidation ratio	$[-]$
POP_{min}	Minimum pre-overburden pressure	$\left[kN/m^2\right]$

Table 4.3: Additional SHANSEP parameters in the SHANSEP NGI-ADP material model

The parameter α is quite similar to the parameter S. The difference is in the definition of the effective stress. Parameter S is defined as the ratio of undrained shear strength (s_u) over vertical effective stress (σ'_v). With parameter α the vertical effective stress is changed to the major principal effective stress (σ'_1). In horizontal soil layering both parameters would result in the same value. On soil slopes, the major principal effective stress is not aligned vertical but is rotated, resulting in a difference between the major principal effective stress and the vertical effective stress.

Parameter m is the strength increase exponent as described in §4.4. A minimum shear strength is added to prevent very small stiffness (G) at limited depths where the effective stress is close to zero.

The parameters OCR_{min} and POP_{min} determine the initial stress state. The pre-overburden pressure is calculated, based on these parameters.

Advantages and disadvantages

Unlike the NGI-ADP model, the SHANSEP NGI-ADP model allows the undrained shear strength to be updated with consolidation phases. Variations in undrained shear strengths of soils as a consequence of load history (pre-overburden pressure) can be implemented.

The combination of the SHANSEP method and the NGI-ADP method makes the developed model better suitable for ultimate as well as serviceability limit state calculations. A principle of the SHANSEP NGI-ADP model is presented in Figure 4.17.

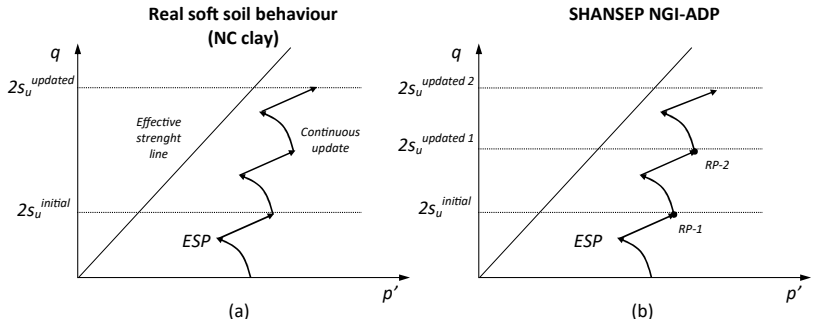

Figure 4.17: Effective stress paths of real soft soil behaviour and for SHANSEP NGI-ADP model

4.7 Other shear phenomena

4.7.1 Peak shear

As a result of the anisotropic behaviour of soils, the strain required to reach peak shear strength, varies with the failure mode. Figure 4.18 illustrates the shear strain at plain strain compression (PSC), plain strain extension (PSE) and direct simple shear (DSS) tests.

Where peak strength is reached at small shear strains in compression tests (active zone), extension tests (passive zone) requires large deformations to reach an ultimate shear strength. At these large deformations the peak strength in compression tests is already reduced due to softening. Consequently, at a slope failure, the strains in the active zone can be beyond its peak strength and there is a significant drop in shear resistance, before the horizontal and passive zone are fully mobilized.

Hence, the average shear strength mobilized along the shear surface of an elevation will be less than the average of the peak strengths from compression, DSS and extension tests, assuming equal section of active, DSS and passive zone occur at the failure plane.

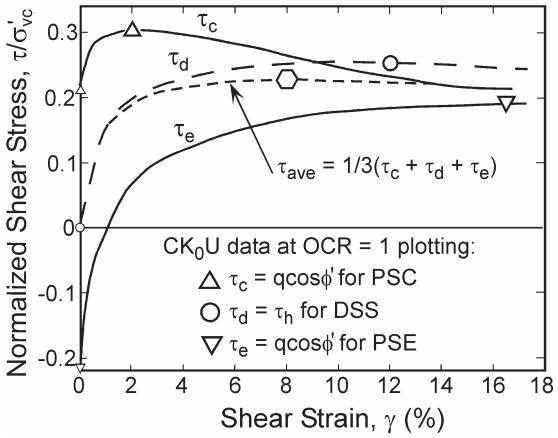

Figure 4.18: Normalized stress-strain data of clay for PSC, DSS and PSE (after [Koutsoftas and Ladd, 1985]), [Ladd and Degroot, 2003]

4.7.2 Strain compatibility

If equal strains along the shear surface are assumed, the magnitude of the strain at which the maximum shear resistance along the shear surface is obtained, can be determined. This strain compatibility can be derived from the analysis of the strain – normalized shear stress curves from triaxial compression, DSS and triaxial extension tests.

An ideal choice for strain compatibility should also consider the contributions of the different zones (A, D, P) along the shear surface. This method is, however, complex. In reality, the strains along the shear plane will vary.

Figure 4.19 illustrates the correlation between deformations and shear stresses in time of an excavated slope [Duncan et al., 2014]. Point A is influenced by the excavation immediately and reaches peak shear strength first. As the ground rebounds, displacements increase and respectively points B (t_2) and C (t_3) reach peak whereas points A (t_2) and B (t_3) reduce in strength (softening). As a result, progressive failure occurs.

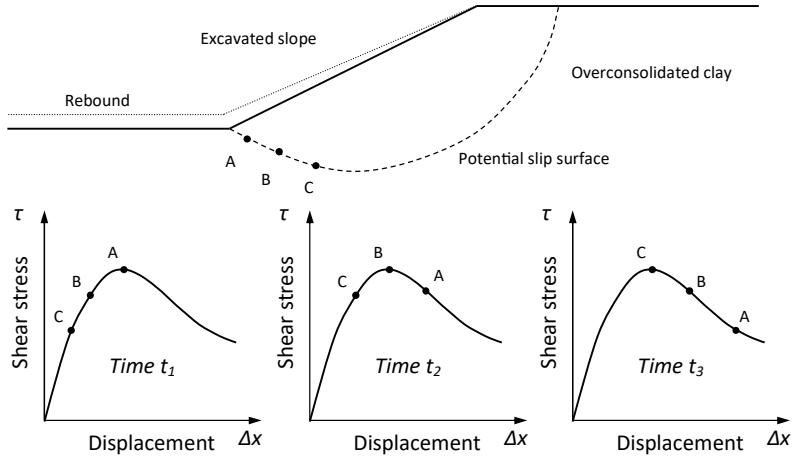

Figure 4.19: Mechanism of progressive failure on an excavated slope in overconsolidated clay (after [Duncan et al., 2014])

When assumed large deformations may occur, the ultimate strength at large strains can be used. At these large strains, peak strength has been reached and softening will have occurred. The ultimate strengths for TC, DSS and TE all lie on the critical state line and therefore can occur simultaneously, as illustrated in Figure 4.18 .

In the stability analysis of the embankments build with industrial sludge the deformations occurring during and after construction are of minor importance. The main objective is to realise a stable embankment. Any distortions can be re-profiled and adjusted when the capping layer is added. Hence, the analysis of the embankment is advised to take into account the strength at large strain (ultimate strength).

4.8 Conclusions

The low permeability of the CaF_2 sludge necessitates the use of undrained analysis for the elevation of embankments. Undrained soil behaviour requires a different approach and several other (undrained) shear strength phenomena are to be accounted for. In this chapter, the basic principles of undrained soil behaviour are explained.

The hydraulic conductivity and the loading pace are the main factors in distinguishing drained or undrained soil behaviour. The stress path of an undrained behaviour can deviate significantly from the drained stress path and can lead to a lower shear resistance. Hence, one should be aware of the discrepancy since it may lead to erroneous design, causing failure of the construction (dam, dike, foundation, ...). Care should be taken when choosing between a drained or undrained analysis.

The critical state soil mechanics is a useful way to define the failure of soil at the critical state. The CSSM defines the critical state surface in the p', q, ν space, creating a unique correlation between normal effective stress, shear stress and void ratio. All loading and unloading, drained or undrained stress paths can be described within this framework. The undrained shear behaviour is just one specific stress path, which can be described with the CSSM. Critical state models can be use to predict hardening and softening of soils and are mainly useful for modelling normally consolidated or lightly over-consolidated soft clays.

The application of the SHANSEP method on soil samples can lead to an increased accuracy of the measured parameters by reducing the influence of sample disturbance. By using anisotropic triaxial testing the initial stress conditions are reset avoiding unwanted over-consolidated soil tests. This method, using anisotropic (K_0) triaxial tests, however, requires specific equipment to measure minute volumetric changes and fluctuations in pore water pressure. Given the presence of pollution (such as heavy metals) in the CaF_2 sludge, there is a high risk of affecting the sensitive instrumentation of the anisotropic triaxial test setup. Hence, executing anisotropic testing of the industrial sludge at issue was not an option.

The anisotropic behaviour plays a vital role in the development of the shear plane given the different shear strength at compression, direct simple shear and extension failure. A correlation exists between the plasticity index an the anisotropic behaviour of plastic soils, where low plastic soils exhibit a more significant anisotropic behaviour then high plastic soils.

Various material models, which are specifically developed for the application of SHANSEP and anisotropic behaviour, are discussed. The SHANSEP MC, NGI-ADP and SHANSEP - NGI-ADP material models provide an alternative method for calculation of the undrained shear strength compared to classic material models. A downside of these models is the lack of an accurate estimation of pore water pressures and dissipation. Hence, no accurate deformation analyses are possible.

Chapter 5

Field investigation and test procedures

5.1 Introduction

The use of the industrial CaF_2 sludge as a construction material for creating embankments on existing sludge deposits, maximises the storage capacity of these deposits. Because of the origin of the industrial sludge (see chapters 1 and 2), the sludge can be regarded as a newly created waste material with soil-like properties. The determination of the geotechnical properties of this specific sludge is necessary to be able to perform further analyses and calculations.

The current investigated sludge is a combination of CaF_2 sludge and a, strongly varying, fraction of glauconite containing sand. Furthermore, the method of drying the sludge in dunes and trenches (see chapter 2) and stacking layer by layer, results in a variation of dryer and wetter layers. The created sludge embankment will, consequently, have heterogeneous properties. The characterisation of the material will focus on field investigations, accompanied by laboratory tests.

Because the sludge is characterised by a low permeability, the determination of drained parameters (ϕ', c, ...) is insufficient to estimate the short-term stability of embankments created with sludge. When elevating the sludge terrain, the material will behave undrained and therefore knowledge on the undrained soil parameters is vital.

In this chapter, different laboratory and in situ testing methods for characterisation of the industrial sludge are described. Their applicability in the specific situation of the CaF_2 sludge deposit is discussed and evaluated. Furthermore, the results of the executed tests are presented.

5.2 Field investigation and laboratory testing program

5.2.1 Borehole shear test

Geotechnical characteristics can be determined in a laboratory on samples taken on site. Due to several manipulations (sampling, extracting,...) and transportation of the test samples to the laboratory, soil parameters can be disrupted. Especially for soft wet sludge, losing information about the geotechnical parameters or surrounding phenomena in the soil is problematic. To overcome these problems, the applicability of in situ borehole shear tests (BST) [Handy, 1986] to measure the shear parameters (cohesion and friction angle) of the sludge was investigated. The BST-device is schematically presented in Figure 5.1.

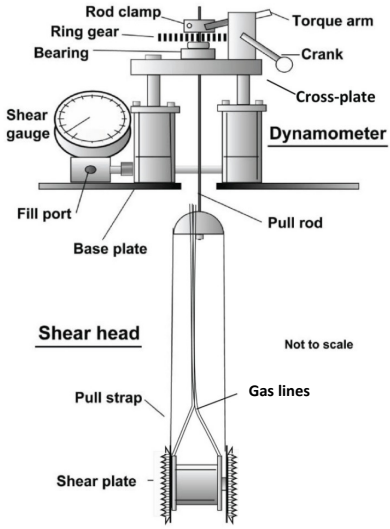

Figure 5.1: Components of borehole shear test device [Handy, 1986]

The borehole shear test is comparable to a direct shear test. It is, however, performed in a pre-drilled borehole, testing the walls of the hole. Sample disturbance is hereby reduced to disturbance caused by the drilling of the hole.

The maximum shear strength of the soil is repeatedly measured under increasing normal forces, as presented in Figure 5.2. The test comprises of two phases. In the first phase a shear head is lowered in a borehole to a certain depth. A normal force is applied by the shear head on the borehole walls. To allow the soil to consolidate, a waiting time of 5 to 15 minutes (depending on the permeability of the soil) between the first and second phase is recommended. After consolidation the shear head is slowly pulled upwards whilst measuring the resisting shear force. After the peak shear force is reached, the shear head is relieved of its shear force. The normal force is increased, and the test is repeated. The cohesion and friction angle are calculated from the graphical representation of shear strength to normal stress results.

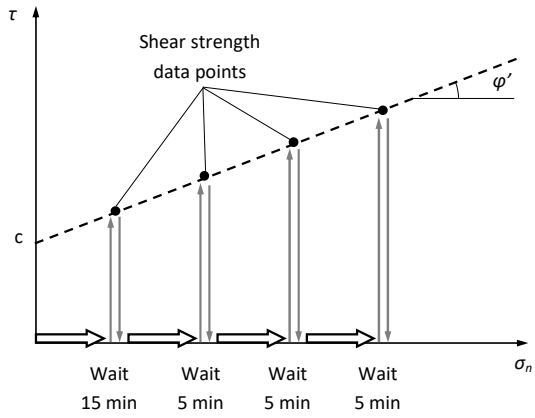

Figure 5.2: Stress path during various stages of the borehole shear test

Only the maximum shear resistance is measured with the BST, which is the peak shear resistance in over-consolidated soils and the maximum resistance in normally consolidated soils. The residual shear strength cannot be measured by continually increasing the shear displacement because new virgin soil will be mobilised with these additional displacements.

The borehole shear test is a consolidated, undrained (CU) test with a drained consolidation phase and an undrained shear phase. No pore water pressures are measured during consolidation or shearing phase.

In highly permeable soils, no significant deviation between the applied normal pressure and the effective stress during shearing is expected. Therefore, with BS-testing on sands, the effective friction angle (and cohesion) can be determined.

On low permeable soils, an insufficient consolidation period can lead to residual pore pressures present in the soil material. Furthermore, important excess pore water pressures can arise during shearing due to shear displacements. The normal stress, applied with the BST shear head, on the soil can therefore be higher or lower than the effective stress during shearing. However, because shearing occurs at the edge of the teeth of the BST, the drainage length of the shear plane is in the order of millimetres. This can result into a nearly instantaneous re-consolidation, depending on the permeability. The magnitude of the deviation of the effective stress can although not be measured or estimated.

The execution of borehole shear tests on low permeable soils will result in undrained parameters (friction angle and cohesion), which can approach drained parameters. By manually varying the consolidation time and the speed of shear displacement, the influence of the variation can be used to obtain an insight in the deviation from the drained soil parameters.

5.2.2 Piezocone penetration test

The cone penetration test (CPT) is a common in situ soil test generally used for the determination of the bearing capacity of the soil. The execution of a cone penetration test further allows for the determination of several soil parameters. There are numerous methods for analysing the CPT results such as bearing capacity theory ([Terzaghi, 1943]; [De Beer, 1977]), (cylindrical or spherical) cavity expansion theory ([Skempton, 1951]; [Vesić, 1975]), strain path theory [Teh, 1987] and analytical and numerical approaches [Ladanyi, 1967].

The methods suggested by Lunne [Lunne et al., 1997] are based on the theory of tip bearing capacity, which can be expressed as (5.1):

$$q_c = c \cdot N_c + D \cdot \gamma = c \cdot N_c + \sigma_v \tag{5.1}$$

These analyses are all based on the general formulation for determining the undrained shear strength, given in equation (5.2), which indicates a relation between the undrained shear strength and the cone resistance. In equation (5.1), N_c is the theoretical cone factor.

Later, empirical or semi-empirical correlations were established. To distinguish them from the theoretical correlation, an empirical cone factor N_k is denoted.

$$s_u = \frac{q_c - \sigma_{v0}}{N_k} \tag{5.2}$$

The determination of the cone factor is defined by empirical analyses. Many investigations have been conducted to define the cone factor for different soils. For example, a N_k (empirical cone factor) varying between 11 and 19 can be used for normally consolidated Scandinavian marine clays using field vane tests as reference [Lunne and Kleven, 1981]. In general, the empirical cone factor can vary between 5 and 30 depending on the soil type.

Due to the build-up of pore pressure behind the cone during penetration a more accurate approach, using cone penetration tests with pore pressure measurement, was developed. The pore pressure correction is especially important for soft clays, where the measured pore pressure can be significant [Rémai, 2013]. With the piezocone test (CPTu), the cone is equipped with a pore water pressure sensor, generally located in one of three locations (Figure 5.3): at the face of the cone (u_1), at the shoulder position (u_2) or behind the friction sleeve (u_3). The common method in Belgium is to determine the pore water pressure immediately behind the cone tip (location u_2) to measure the pressure during penetration.

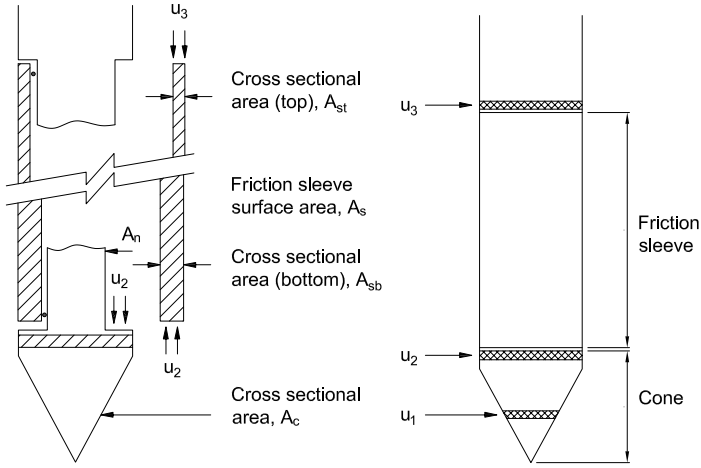

Figure 5.3: Positions for pore pressure measurements at piezocone

The actual cone tip resistance is denoted as followed:

$$q_t = q_c + u(1 - a) \tag{5.3}$$

As a result, equation (5.2) is reformed to the following formulation (eq. 5.4):

$$s_u = \frac{q_t - \sigma_{v0}}{N_{kt}} \tag{5.4}$$

Here, N_{kt} is the empirical cone factor related to q_t.

The correction of the cone resistance with pore pressure is important in soft clays where large excess pore pressure can arise during penetration of the cone and can significantly influence the measured cone resistance. Because the industrial sludge, investigated in the current study, has a similar behaviour to (soft) clay, the use of the corrected cone tip resistance is preferred.

There are other methods of determining the undrained shear strength by means of CPTu such as using the N_{ke} (empirical cone factor for effective cone resistance) or $N_{\Delta u}$ (empirical cone factor for excess pore water pressure). In the presented study these methods are however not considered.

5.2.3 Field vane test

General

The undrained shear strength of a soil can be estimated using the field vane shear apparatus. In situ field vane tests were performed according to [ASTM D2573 / D2573M-18,]. The vane apparatus used in the investigations is the Geonor H-70. A tapered vane was used, measuring 60 mm × 120 mm, with a range of 0 – 160 kPa.

The test procedure consists of hammering the vane in the soil to the desired depth. Next, a torque wrench is used to apply a shear load on the soil with the vane. The peak stress and residual stress are recorded based on the applied torque. The rod friction is subtracted from the total measured torque.

Field vane correction

A correction of the raw measured vane shear strengths is required for the further use of the results in stability analyses. Initially the correction factor suggested by [Bjerrum, 1973] was used, as also suggested in ASTM D2573.

Further analyses of a trial embankment, documented in chapter 6, indicate that different correction factors are to be used to account for anisotropic behaviour.

The correction factor suggested by Bjerrum, correlated to the plasticity index as illustrated in Figure 5.4, is used for the initial analysis.

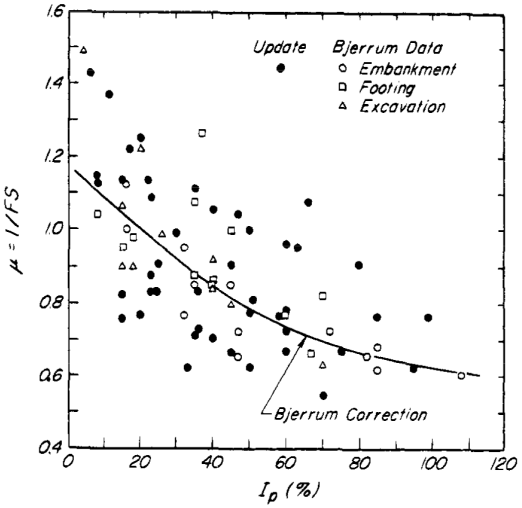

Figure 5.4: Bjerrum's field vane correction factor [Terzaghi et al., 1996]

5.2.4 Triaxial testing

Isotropically consolidated undrained (CIU) triaxial compression tests were performed with conventional triaxial cells according to [ASTM D4767-11, 2011]. With the triaxial compression tests, the specimens are first consolidated isotropically at a certain pressure until excess pore water pressure is dissipated. With isotropic consolidation the horizontal and vertical stresses are equal. Next, the vertical stress is increased (deviatoric stress) without further dissipation of pore water pressure, until failure occurs.

Less common is the use of anisotropic triaxial compression and extension tests (CAU). Anisotropic tests better approach the actual stress state of soil in situ. Compared to the isotropic triaxial tests, an additional anisotropic consolidation phase is required. Estimations of the undrained shear strength from isotropically consolidated undrained triaxial compression tests can result in an unsafe design [Ladd and Degroot, 2003].

The consolidation at $K = 1 = \sigma'_h/\sigma'_v$ (isotropic), leads to a low water content, which increases the undrained shear strength. Consolidation of the soil specimen at K_0 ($\approx 1 - \sin\phi'$) is recommended to enable better quality determination of undrained shear strength. The method of anisotropic triaxial tests, however, requires specific equipment to measure minute volumetric changes and fluctuations in pore water pressure.

The execution time is significantly increased with the additional anisotropic consolidation stage resulting in a more costly test. Moreover, the sensitive instrumentation of the water pressure can be affected by the pollutions (heavy metals, ...) present in the CaF_2 sludge.

Considering the pros and cons of isotropic and anisotropic triaxial testing, the classic isotropic triaxial test was retained, bearing in mind that the results might overestimate the actual undrained shear strength.

The triaxial tests consist of single stage tests were each test is performed on a new specimen, whereas in multistage test the samples are subjected to several failure stages. Influences of previous shearing are no issue at single stage tests, hence, a higher accuracy is achieved.

At the sludge deposit, no limitations are set regarding deformations of the sludge embankment, only the shear strength is of importance. Deformations of the slope will be levelled out during the final capping of the deposit. Therefore, the strengths at large strains i.e. the ultimate strength, are at issue. Peak strengths are not accounted for because these higher strengths may result in progressive failure as explained in §4.7.1. At large strains, the shear strengths (ultimate strength) along the entire failure plane are mobilized.

5.2.5 One-dimensional consolidation test

One-dimensional consolidation tests are performed using an oedometer cell to determine the compressibility of soil by incrementally applying a load on a soil sample. The one-dimensional consolidation tests are executed according to [ASTM D2435 / D2435M-11, 2011].

The test consists of measuring the vertical deformation of a soil sample under an increasing load. Based on the results, the compression parameters, among others, can be determined. Figure 5.5 plots the (log) vertical stress – strain distribution for a one-dimensional consolidation test, linked to triaxial test results. The first part of the plot represents recompression, the second part is virgin compression. Near the transition zone the pre-consolidation (σ'_p) or yield stress can be found.

The pre-consolidation stress corresponds to the loading history of the soil and indicates the border between normal consolidation and over-consolidation. It represents the maximum stress at which the soil is consolidated and is a key factor in the magnitude of the undrained shear strength. From the pre-consolidation stress, the over-consolidation ratio (OCR) can be defined.

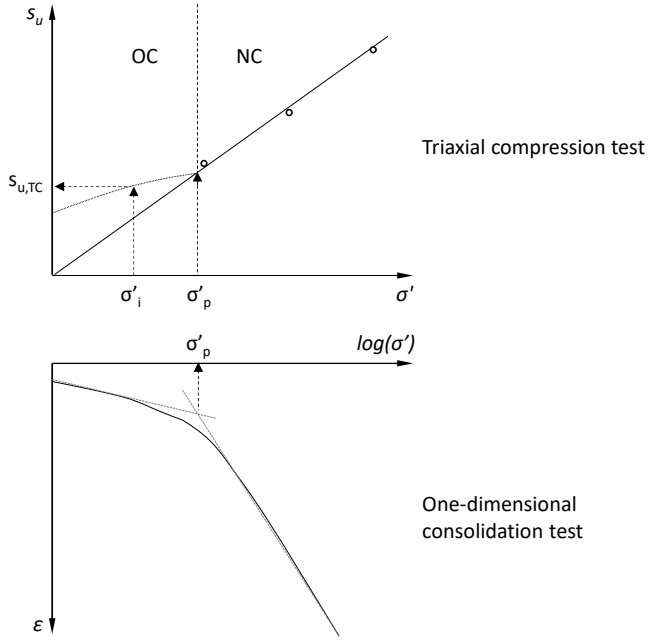

Figure 5.5: Principle compression curve from one-dimensional compression test and triaxial test

Numerous methods are proposed for estimating the pre-consolidation stress using the one-dimensional consolidation test such as the graphical method [Casagrande, 1936] or the strain energy method [Becker et al., 1987]. In the present doctoral research the strain energy method was used.

The sludge embankment is built in layers with compaction by the movements of earth-moving equipment. Additionally, intermediate drying periods allowed the sludge to dry by sun and wind. As a result, the embankment will contain layers of highly compacted sludge with a low water content, constructed in dry periods. On the other hand, sludge deposited in wetter periods will contain a higher water content and will be less compacted. This difference in compaction will correspond to a difference in yield stress.

5.3 Results of field investigation and laboratory testing program

5.3.1 BST results

In situ measurements of the shear parameters by means of Borehole Shear Test were carried out on several locations at multiple depths. The results of the BST on sludge deposits Veldhoven (V) and Kepkensberg (K) are given in Table 5.1. Sludge deposit Kepkensberg is a similar deposit as Veldhoven, however at Veldhoven the test are executed in filter cakes whereas the tests at Kepkensberg are executed on in situ consolidated sludge. At the locations on Kepkensberg the water content was determined. Samples were taken while digging the boreholes for borehole shear testing.

The (initial) water content could be correlated to the pre-consolidation pressure, determined with one-dimensional consolidation tests. However, the accuracy of the relation between water content (i.e. void ratio) and pre-consolidation pressure, is very low. Yet, the water content can give an insight in the consolidation of the sludge. A water content near the shrinkage limit of around 60% [Craeynest and Suys, 2010] usually corresponds to a relatively dry and well consolidated sludge. Sludge layers with a water content of 100% or more, can be considered unconsolidated. Nevertheless, with the analysis of the BST results, no correlation was found with the water content, as expected.

With the BST, the sludge is consolidated during the different stages of the test. The initial soil condition is therefore overruled, and the measured shear strength correspond to the applied normal stress. When the applied normal stress is lower than the effective stress in the soil, over-consolidation can influence the shear stress results.

The sludge at the deposit sites Veldhoven and Kepkensberg can differ in chemical composition due to changes in the production process throughout the years. Nevertheless, no significant difference in friction angle or cohesion is observed.

The average angle of friction is 33.5° with a spread of 3.7°, which corresponds to a coefficient of variation of 0.11 (= 3.7/33.5). The average cohesion is 8.0 kPa, with a spread of 3.9 kPa, which corresponds to a coefficient of variation of 0.48 (= 3.9/8.0). The accuracy of the determination of the angle of friction with the BST is acceptable. However, the results of the cohesion exhibit a large spread. A reliable estimation of the cohesion can't be obtained with the current BST results. It is therefore advisable not to use the cohesion results of BST test in further analysis of slope stability.

Location	Depth [m]	ϕ'_{BST} [°]	c_{BST} [kPa]	w [%]
V - S3 A.1	-1.00	32.5	6.9	-
V - S3 B.1	-0.75	35.7	7.7	-
V - S3 B.2	-1.25	34.8	11.8	-
V - S3 B.3	-2.00	35.5	1.6	-
V - S3 C.1	-0.75	36.0	1.5	-
V - S3 C.2	-2.00	29.0	3.4	-
V - S3 D.1	-1.00	38.1	4.9	-
V - S3 D.2	-2.00	31.4	11.9	-
V - S3 E.1	-1.20	34.9	10.4	-
V - Average		**34.6 ± 2.6**	**7.2 ± 4.0**	
K - A	-1.00	37.5	4.8	73%
K - B	-1.00	37.5	7.8	66%
K - C	-2.00	32.4	12.0	55%
K - D	-1.20	38.2	8.8	82%
K - E	-4.50	33.8	3.5	121%
K - F.1	-0.50	34.0	7.7	85%
K - F.2	-1.50	34.0	4.5	87%
K - F.3	-2.50	31.3	9.3	119%
K - F.4	-3.60	27.3	8.7	127%
K - G.1	-1.00	28.7	16.6	103%
K - G.2	-1.50	23.4	14.7	75%
K – H.1	-1.50	33.7	6.9	-
K – H.2	-2.00	32.0	7.8	-
K - Average		**32.6 ± 4.2**	**8.7 ± 3.8**	

Table 5.1: Results of borehole shear tests at deposits Veldhoven and Kepkensberg

5.3.2 CPTu results

General

At Veldhoven S3-3, piezocone penetration tests (CPTu) and field vane tests were conducted every 50 m along the edge of the elevation on the sludge deposit. The locations of the tests are given in Figure 5.6. The detailed results are added in appendix A.

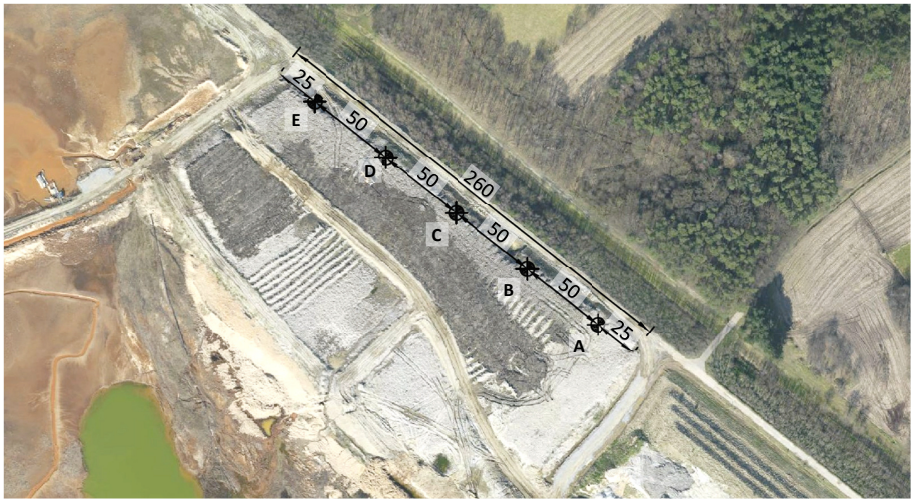

Figure 5.6: Areal view on sludge deposit Veldhoven, section S3-3 [Geopunt Vlaanderen, 13/05/2015]

The recently constructed sludge embankment has a length of 260 m and a width of 120 to 150 m. The sludge embankment protrudes 7 to 8 m above the surrounding sand dike as presented in Figure 7.2.

Along the embankment, five test locations (A, B, C, D and E) were spaced 50 m apart. On all locations field vane tests and cone penetration tests were performed. On three locations (A, C and E) samples were taken for oedometer and triaxial testing.

CPTu profile

The profile of the soil resistance was measured with cone penetration tests executed with a 20 ton track vehicle. With these piezocone measurements the corrected cone resistance can be calculated. An empirical cone factor is used to determine the undrained shear strength based on the corrected cone resistance.

The variation of the cone resistance with depth is given in Figure 5.7. The green zones are areas with potential high quantities of glauconite containing sand. These sands can be distinguished by a higher cone resistance (i.e. 1 – 2 MPa) compared to sludge and a limited disturbance in pore pressure, along with an increase of the friction ratio (R_f).

The yellow areas are sand layers, which can be distinguished by a significant increase in cone resistance, combined with a reduction in pore pressure.

The presence, thickness and position of these sandy layers are based on the results of the piezocone test. By performing bore samples, the position (and composition) of these layers can be determined with a higher accuracy. In the current situation it was considered that, based on the information of the CPTu tests, sufficient data could be gathered, therefore no bore samples were taken.

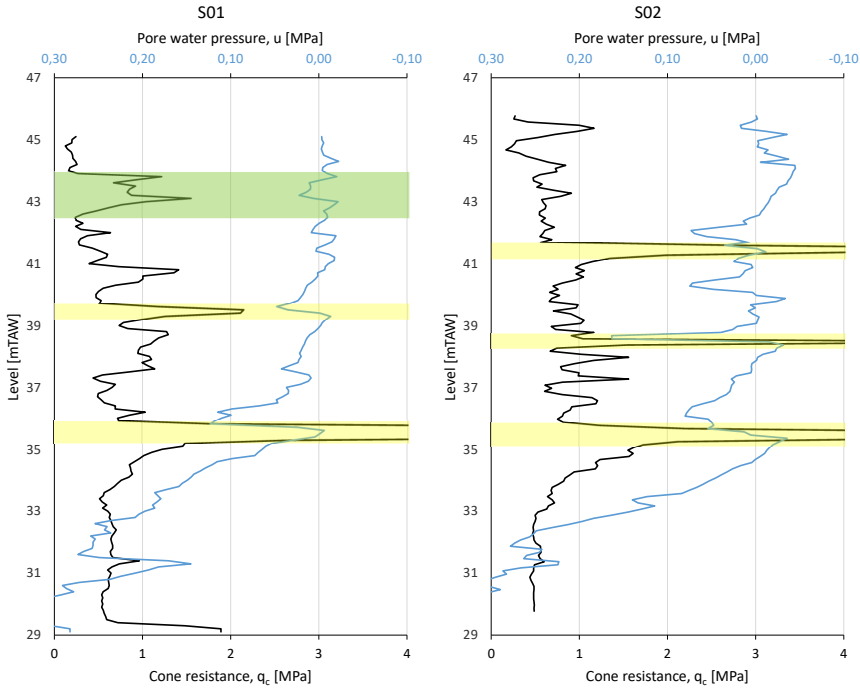

Figure 5.7: CPTu results for locations S01 and S02 with indication of sand or sandy layers (yellow) and glauconite containing sand (green). The profiles show the cone resistance and pore water pressure.

Starting from a level of 35.5 mTAW, an increase in pore water pressure was noticed with depth. This level corresponds to the global water level in the adjacent settling ponds on Veldhoven deposit at that time. High pore water pressures were measured in deeper laying layers with pressures up to 0.3 MPa and more. The high values of pore water pressure exceed the hydrostatic value and even the total stress expected at some levels, which is unrealistic. It can be presumed that, due to the low permeability of the sludge, significant excess pore water pressure arises when pushing the cone downwards during testing.

A more accurate estimation of the actual pore water pressures at these depths can be achieved by reducing the penetration speed, allowing the excess pore water pressures, due to the penetration, to dissipate. The steady state pore water pressure can then be measured.

Determination of OCR

The over-consolidation ratio (OCR) can be derived from the cone penetration test results, based on equation (5.5) [Ladd, 1991].

$$s_u = \sigma'_{vi} \cdot S \cdot OCR^m \tag{5.5}$$

When applying the shear strength ratio from triaxial testing ($S = 0.338$) and power from the one-dimensional consolidation tests ($m = 0.91$) in the above equation, a profile of the OCR can be estimated based on the s_u profile from the (converted) piezocone test. The vertical effective stress is to be estimated from the soil volume weight and the hydrostatic water level.

Vertical effective stress

An accurate determination of the effective stress in the sludge dike is hard to achieve. Because the embankment is elevated layer by layer, the consolidation ratio can vary from location to location. For the determination of the vertical effective stress, two methods are used and compared.

The first method of determining the vertical effective stress is by use of the (un)saturated volume weight. Starting from the top of the surrounding dikes (38 mTAW), a hydrostatic increase in pore water pressure (u_0) with depth is assumed. Because of the low permeability of the sludge, the supposed hydrostatic pressure can be an underestimation of the actual pore water pressure.

The second method is based on the measured pore water pressure with the piezocone penetration test (u_2). The difference between the total stress and the measured pore water pressure results in the effective stress. This method however, overestimated the pore water pressures because additional stresses are produced when penetrating the soil.

OCR profile

The over-consolidation profile at location A (S01) is shown in Figure 5.8. The methods, based on u_0 (hydrostatic profile) and based on u_2 (pore water pressure measurement in CPTu), correspond well for the upper half of the graph. The OCR differs at some locations, but the main profiles are similar.

A significant difference is noticed below a depth of 35 mTAW. Here, high pore water pressures were measured with the CPTu, resulting in a low effective stress and therefore high OCR. Below 33 mTAW pore water pressure even higher than the total stress were measured, resulting in unrealistic high over-consolidation ratio's. An OCR equal to 1 is therefore assumed below 35 mTAW. Table 5.2 presents a raw estimation of the OCR at the test location for different layers.

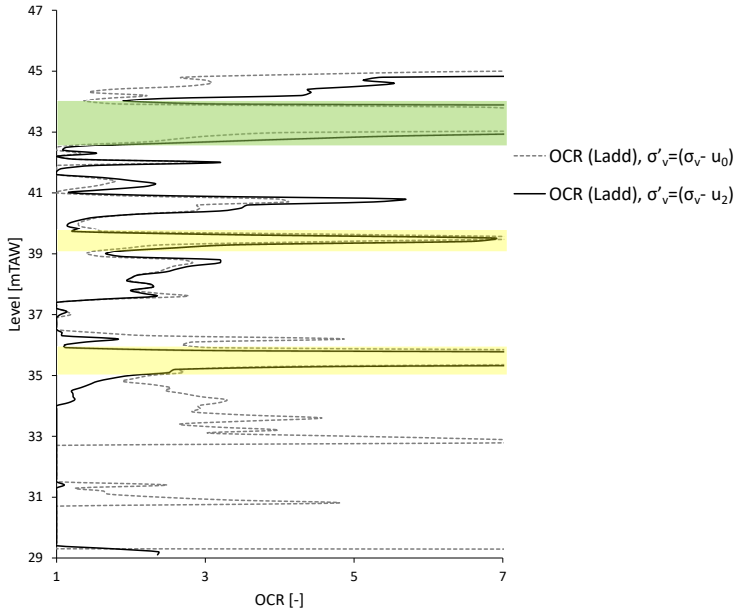

Figure 5.8: Profile of over-consolidation ratio based on CPTu results of S01, at location A (S01)

Depth	A/S01	B/S02	C/S03	D/S04	E/S05
46 - 40 mTAW	1 - 3	2 - 4	2 - 3	2 - 4	1 - 5
40 - 36 mTAW	1 - 2	1 - 2	1 - 2	1 - 2	2
36 - 29 mTAW	1	1	1	1	1

Table 5.2: Over-consolidation ratio for S01 to S05 (locations A to E)

The OCR-profile exhibits an irregular course. The high peak values are caused by the presence of sand layers (dirt roads, drainage layers, glauconite containing sand inclusions, ...), also indicated in Figure 5.7, S01. In the sandy layers, the method for determining the undrained shear strength, based on the net cone resistance and empirical cone factor, does not apply. Therefore, for these layers, no correct value of OCR can be determined, based on the calculated undrained shear strength.

Aside from the incorrect results of OCR in the sandy layers, the OCR can be estimated for the sludge layers. Above the level of the surrounding dike (38.4 mTAW), the sludge behaves mostly over-consolidated. The over-consolidation is caused by the natural air drying of the sludge. The used method of layered elevations with periods of intermediate drying results in a sludge with a higher undrained shear strength and apparent high OCR.

Below the level of the surrounding dike the sludge behaves less (over-) consolidated. The bottom of the deposit is sealed with a PVC foil to prevent pollution to penetrate the subsoil. This also prevents consolidation to taken place from below, increasing the drainage distance and therefore drainage time. The lower sludge layers are unconsolidated considering the low undrained shear strengths and high pore water pressures measured with the CPTu.

The accuracy of the determined over-consolidation ratio is affected by the transformation and measuring errors in the conversion of the cone test results to undrained shear strength values [Van Duinen, 2014]. Furthermore, the OCR is sensitive for the determination of in-situ effective stress. Hence, no reliable value of OCR can be achieved solely based on CPTu results. The CPTu tests must by accompanied by reliable data of volume weights (borehole samples) and determination of pore water pressure at various depths.

5.3.3 Field vane test results

Field vane tests were executed on site using the Geonor H-70 apparatus with a tapered vane of 60 mm × 120 mm. The procedure is described in §5.2.3. The vane was hammered in the soil up to a depth of 5 m. Due to the presence of stone inclusions in de soil, the intended depth was not reached at all test locations. The tests were commonly spaced vertically every 0.5 m to avoid interference between two tests. The results of the maximum (or peak) and remoulded shear strength are presented in Figure 5.9. The undrained shear strengths are the uncorrected raw data from the field vane tests. At each test location, samples were taken at various depths with an auger to determine the plasticity index and subsequently the correction factor (μ_B).

The measured undrained peak shear resistance ($s_{u,FV}$) varies between 5 kPa and 116 kPa, with an average of 60 kPa. The results of the field vane tests are added in appendix B. The sludge has a sensitivity (S_t) ranging from around 2 to 10, with an average of 4.4. Hence, the sludge corresponds to a medium (2 - 4) to extra sensitive (8 – 16) clay [Skempton and Northey, 1952]. No clear increase in shear resistance with depth can be observed.

The test results indicate a large scatter in shear strength, which can be the consequence of the method of storing and treating the industrial sludge as explained in chapter 2. Layers of poorly and well consolidated or dried material are encountered randomly.

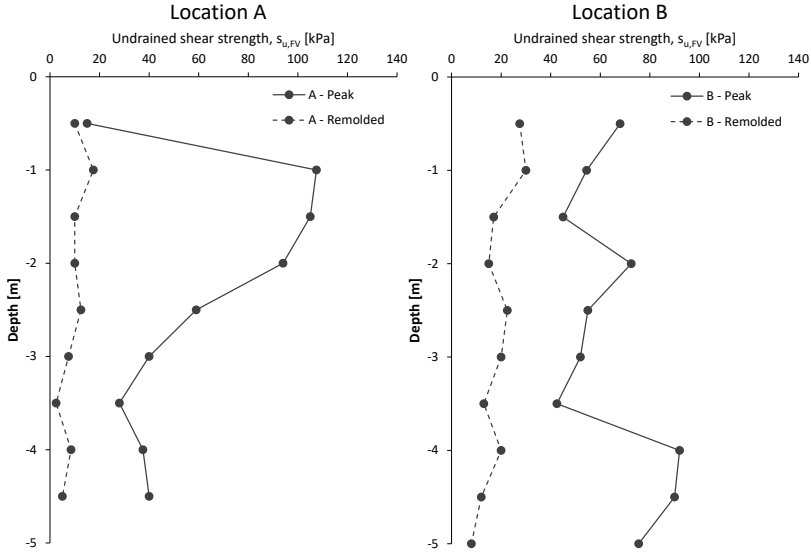

Figure 5.9: Field vane test results at locations A and B on sludge deposit Veldhoven S3-3

The plasticity index (I_p) was determined [ASTM D4318-17e1, 2017] at each field vane test location, on samples taken at various depths up to 4 m. Due to the presence of stones in the sludge elevation, the drilling of holes for sampling was often obstructed. In Table 5.3 the results of the plasticity index for all the test location are presented.

Depth	A	B	C	D	E
-1.0 m	25.1%	22.3%	31.5%	22.0%	30.6%
-2.0 m	24.2%	(6.9%)*	43.8%	19.6%	38.8%
-3.0 m	/	37.6%	36.3%	23.5%	30.3%
-4.0 m	/	37.8%	/	/	/
Average	24.6%	32.6%	37.2%	21.7%	33.2%

Table 5.3: Plasticity index for test locations A to E on deposit Veldhoven S3

The details of the water content, liquid limit, plastic limit and plasticity index are given for location B in Figure 5.10. The extreme low plasticity index at location B -2 m was due to local sand inclusions. The value was not considered in the calculation of the average values. At location A and D, a low plasticity was noted, ranging from 19.6 to 25.1%. During sampling it was noticed that mainly at location A, large concentrations of glauconite sand were present in de top layers, which influenced the results. For further analysis of the test results, a constant value for the plasticity index is assumed. In reality the plasticity index will vary with a high or low presence of sand in the sludge layers.

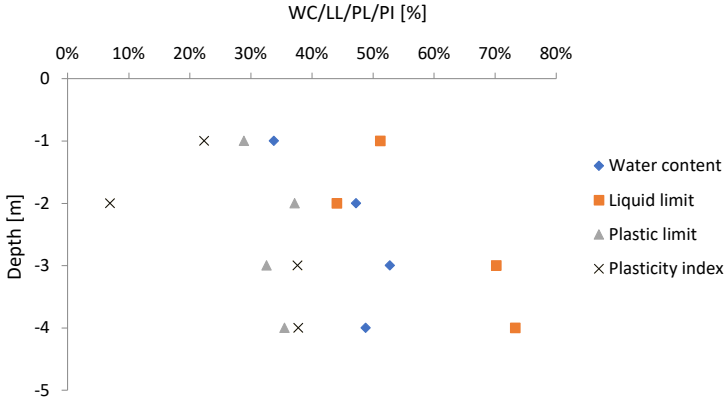

Figure 5.10: Results of borehole samples from location B

The average plasticity index was 30.2% ± 7.6%. Previous tests of the plasticity index on the sludge indicated a higher plasticity [Tennekoon, 2007], which is probably due to a lower content of sand particles in sludge of the lower sections of the embankment. The upper part of the elevation contains industrial CaF_2 sludge, mixed with glauconite sand. A plasticity index of 40% was assumed to be representative for the sludge below the top of the surrounding sand dike, given the results of earlier research.

Field vane corrections are necessary to compensate, among others, disturbance, anisotropy, strain rate effect, ... The correction factor suggested by [Bjerrum, 1973], correlated to the plasticity index is used for the initial analysis. A plasticity index of 30.2% corresponds to a correction factor (μ_B) of 0.901.

5.3.4 Triaxial test results

On locations A, C and E (Figure 5.6), samples were taken for CIUC triaxial testing (Consolidated Isotropic Undrained triaxial Compression test). Additional samples for one-dimensional consolidation test were taken at the same locations. The results of one-dimensional consolidation tests are described in 5.3.5.

The samples from location C were used to perform anisotropic consolidated undrained triaxial compression test in the framework of the master thesis research of [Tielemans and Van Herck, 2017]. Due to the presence of pollution in the sludge, such as heavy metals, the risk of damaging (corrosion, ...) or contamination of the sensitive components in the more advanced anisotropic triaxial setup were too great.

Hence, efforts were made to perform anisotropic consolidation in a standard isotropic triaxial setup by introducing an additional consolidation step with a small deviatoric stress applied. The performed tests, however, failed, resulting in a loss of the soil samples.

The results of CIUC triaxial test are presented in Table 5.4. The triaxial tests were performed on naturally dried sludge samples taken at Veldhoven S3-3.

Sample	Depth $[m]$	γ_w $[kN/m^3]$	w [%]	σ'_v $[kPa]$	$s_{u,TC}$ $[kPa]$	S_{peak} $[-]$	S_{ult} $[-]$
A.1	-1	18.8	35.6	179.1	60.5	0.343	0.330
A.2	-1	18.6	31.7	193.3	70.3	0.364	0.361
A.3	-1	19.4	37.5	240.5	83.0	0.345	0.338
A.4	-1	18.6	44.9	312.9	105.4	0.337	0.337
E.1	-3	18.4	48.5	305.8	105.6	0.345	0.331
E.2	-3	17.8	48.0	172.5	58.0	0.343	0.310
E.3	-3	18.2	52.1	260.6	90.2	0.346	0.339
E.4	-3	18.0	53.5	389.8	132.3	0.339	0.343
E.5	-3	18.5	49.6	292.1	101.2	0.346	0.338

Table 5.4: Results of consolidated undrained triaxial compression tests

The undrained shear strength ratio can be obtained as a peak strength or as an ultimate strength. For peak strength the ratio is determined at maximum deviatoric stress (q). The ultimate strength (S_{ult}) was determined at the ultimate strain with a maximum of 15%. In order to reduce the effect of strain incompatibility, the ultimate strength will be considered in further analyses.

The soil samples taken at location A have a low water content of 31.7 to 44.9%. The water content at location E is higher, 48.0 to 53.5%. This may be attributed to the depth of the sampling. On the other hand, a higher quantity of glauconite containing sand was noticed at location A. Nevertheless, the difference in water content does not result in a discrepancy of the undrained shear strength ratio (S).

The undrained shear strength of the sludge, assuming critical state and SHANSEP are applied, is defined by equation (5.5) [Ladd, 1991]. Figure 5.11 plots values of undrained shear strength (s_u) versus vertical effective stress (σ'_v) in triaxial compression. A linear regression of the test results indicates a value of $S = s_u/\sigma'_v = 0.338$. The angle of friction at peak and ultimate resistance amounts respectively 31.9° ± 1.2° and 30.5° ± 2.0°, assuming a cohesion equal to zero.

The stress paths during isotropic consolidated undrained triaxial compression tests are shown in Figure 5.12. The stress paths all converge to the critical state line.

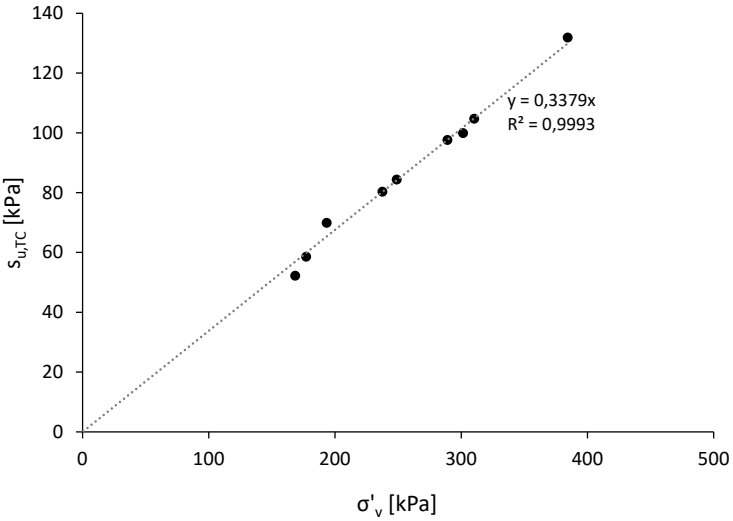

Figure 5.11: Graphical presentation of undrained shear strength ratio (S) from triaxial compression test

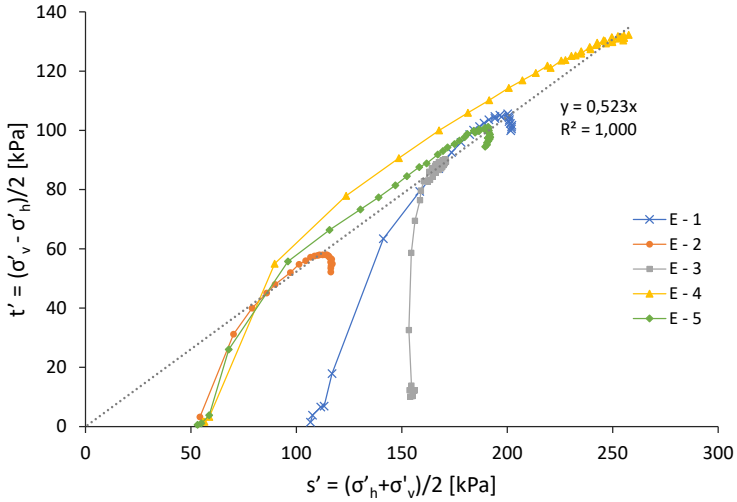

Figure 5.12: Detail of stress paths for consolidated undrained triaxial tests on samples E

5.3.5 One-dimensional consolidation test results

Samples were taken for location A, C and E at the same position of the triaxial tests. At location A, a pit was dug with a depth of 3 m. At this depth a high quantity of glauconite sand was found. This sand is not representative for the entire embankment. Hence, the samples were taken at a higher level.

The soil samples for laboratory tests (one-dimensional consolidation tests and triaxial compression tests) were taken by pushing in PVC tubes in the soft sludge (Figure 5.13). Oversize samples were taken which were trimmed in the laboratory. Hence, sample disturbance because of manipulations during sample taking was reduced.

The results of the one-dimensional consolidation tests are presented in Table 5.5. In the table the (wet) unit weight (γ), the water content (w), hydraulic conductivity (k), pre-consolidation stress (σ'_p), compressibility index (C_c), recompressibility index (C_r) and strength increase exponent (m) are given.

Based on the recompression steps in the one-dimensional consolidation test an average strength increase exponent (m) of 0.91 was assumed.



Figure 5.13: Sludge samples taken by pushing in PVC tubes

It should be noted that the determination of the pre-consolidation stress based on the results of one-dimensional consolidation test are subjective. Furthermore, when comparing different methods, for example the Casagrande method [Casagrande, 1936] and the strain energy method [Becker et al., 1987], different stresses may be found. To minimize the variation by using different methods for determination, the strain energy method was used.

Sample	Depth [m]	γ [kN/m^3]	w [%]	k [m/s]	σ'_p [kPa]	C_c [-]	C_r [-]	m [-]
A.1	-1	17.5	46.5	$4.7{\cdot}10^{-10}$	78	0.290	0.017	0.94
A.2	-1	17.7	46.2	$9.5{\cdot}10^{-10}$	79	0.259	0.017	0.93
C.1	-2.8	17.8	45.3	$6.8{\cdot}10^{-10}$	97	0.187	0.021	0.89
C.2	-2.8	17.3	51.4	$2.4{\cdot}10^{-10}$	110	0.220	/	/
C.3	-2.8	17.0	56.0	$2.7{\cdot}10^{-10}$	105	0.233	0.023	0.90
C.4	-2.8	17.6	44.5	$7.7{\cdot}10^{-10}$	104	0.202	0.017	0.90
E.1	-3	17.5	58.3	$4.7{\cdot}10^{-10}$	99	0.244	0.020	0.92
E.2	-3	17.9	47.6	$2.5{\cdot}10^{-10}$	122	0.207	0.016	0.92
E.3	-3	18.5	39.3	$1.3{\cdot}10^{-10}$	124	0.155	0.023	0.85

Table 5.5: Results of one-dimensional consolidation tests

5.4 Determination of cone factor from triaxial compression test and field vane test

The cone factor (N_{kt}) can be based on literature findings or can be determined by comparison with other shear tests. The majority of the studies show a cone factor between 5 and 20 ([Lunne et al., 1997]; [Karlsrud et al., 2005]; [Varathungarajan et al., 2009]), which can be influenced by over-consolidation, sensitivity and plasticity. At the investigated site, vane shear tests and triaxial compression tests were executed at the CPTu test locations. For the calibration of the cone penetration tests, the soil dependent cone factor can be determined as followed.

$$q_t = s_u \cdot N_{kt} + \sigma_{v0} \tag{5.6}$$

$$q_t = q_c + u_2(1 - a) \tag{5.7}$$

$$q_{net} = q_t - \sigma_{v0} \tag{5.8}$$

$$s_{u,CPTu} = \frac{q_{net}}{N_{kt}} \tag{5.9}$$

$$\text{Suppose: } s_{u,CPTu} = s_{u,TC} \text{ or } s_{u,FV} \tag{5.10}$$

$$N_{kt} = \frac{q_{net}}{s_{u,TC} \text{ or } s_{u,FV}} \tag{5.11}$$

A correction of pore water pressure is included by adding the pore water pressure (u_2), measured with the piezocone, to the cone resistance. The area ratio factor (a) depends on the type of cone used and discounted the pore water pressure in the gap behind the cone (5.3). A area ratio factor of 0.75 applies to the used CPTu device.

The correction of the total cone resistance (q_t) with the in situ vertical stress (σ_{v0}) is significant and depends on the weight of the soil. For the upper part (above 36 mTAW) and lower part (below 36 mTAW) of the sludge embankment, a soil volume weight of respectively 17.5 kN/m^3 and 16.5 kN/m^3 is applied.

5.4.1 Determination of cone factor with field vane test

The calculation of the cone factor for location A, based on field vane tests, is presented in Table 5.6. The CPTu measures the soil resistance every 2 cm, whereas the field vane tests are performed every 50 cm. Therefore, the corrected net cone resistance (q_{net}) is recalculated at 0.5 m interval with the average of the 0.5 m layer at the regarding depth of the field vane test.

The dataset of the piezocone penetration tests with the field vane test, $s_{u,FV} - q_{net}$ points, at locations A, B, C, D and E are illustrated in Figure 5.14. The details of the other locations are added in appendix C. The undrained shear strength from the field vane test are the uncorrected raw data.

Depth $[m]$	$s_{u,FV}$ $[kPa]$	q_{net} $[kPa]$	$N_{kt,FV}$ $[-]$	Average $N_{kt,FV}$ $[-]$	$s_{u,CPTu}$ $[kPa]$
-0.5	15.0	163	10.9		14.1
-1.0	107.5	188	(1.8)		16.3
-1.5	105.0	777	7.4		67.2
-2.0	94.0	997	10.6		86.3
-2.5	59.0	440	7.5	11.6	38.0
-3.0	40.0	297	7.4		25.6
-3.5	28.0	267	9.5		23.1
-4.0	37.5	445	11.9		38.5
-4.5	40.0	1022	25.6		88.4
-5.0	41.0	550	13.4		47.5

Table 5.6: Calculation of N_{kt} at location A, based on field vane test

The undrained shear strength from CPTu ($s_{u,CPTu}$) in Table 5.6 is calculated with the average N_{kt} from location A. For the final calculation of the undrained shear strength, a global cone factor will be used. The cone factors, calculated layer by layer, show variations between 1.7 up to 25.5. The individual values at the other locations (B, C, D and E) show a similar result. The purpose of this research is to determine the cone factor for the industrial sludge, however in some areas sand pockets or sand layers are present in the embankment. These anomalies can be recognised by a high net cone resistance and often a reduction in pore water pressure.

Although the field vane test and CPTu test were executed in close vicinity (less than 2 m apart), local deviations in the subsoil still occur. These deviations can be significant because the tested material, CaF_2 sludge, is not a natural soil but a waste material, which has been manipulated (excavated, transported, dumped, compacted, ...) several times. To calculate the average value of the cone factor for the industrial sludge, extreme values were excluded. Two types of erroneous measurements were noticed.

Firstly, measuring points from CPTu tests with a high net cone resistance indicate a sandy layer or inclusion rather than a sludge layer. This was often accompanied with a reduction of pore water pressure measured with the piezocone. Sand layers or sandy sludge layers contain more coarser material where excess pore water pressures can dissipate faster compared to mere sludge.

When sand pockets, enclosed by sludge, are penetrated by the piezocone, high cone resistance can be measured without a significant change in pore pressure. Based on experience on site, a net cone resistance of over 1500 kPa was set as a limit value for sand (or strong sandy) layers. Although sandy layers with a net cone resistance of less than 1500 kPa may occur, compacted sludge layer may have a higher cone resistance compared to soft sandy layers. Hence, to not exclude the results of dense sludge layers, the limit value of extreme values was set at q_{net} >1500 kPa.

Secondly, a large spread of the cone factor was noticed. This is due to deviations in the subsoil between the field vane test and CPTu test points. For example, a dense sludge lump can be present at the trajectory of the CPTu, whereas with the field vane test, executed at the same depth, only soft sludge was noticed. This therefore leads to a mismatch of the test results and an incorrect calculation of the cone factor. Cone factors lower than 5 and higher than 30 were considered extreme values and were not taken into account.

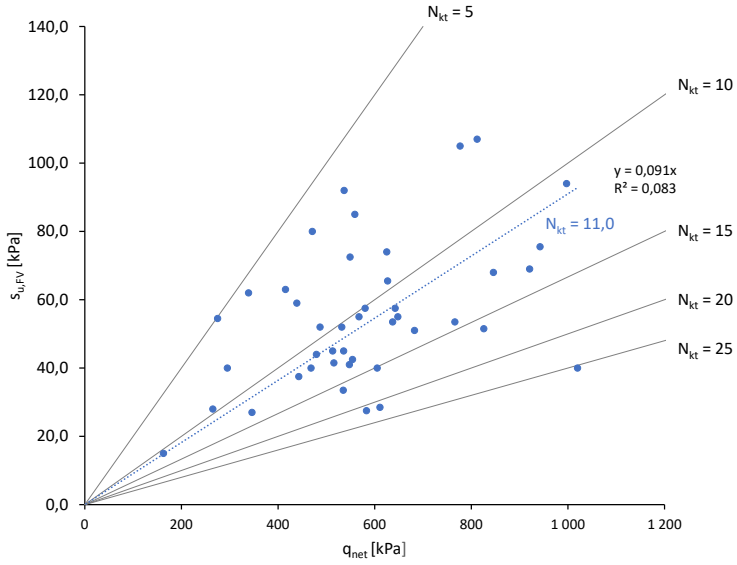

Figure 5.14: Graphical presentation of cone factor calculation from results of piezocone and field vane test

The dataset of the piezocone penetration tests with the field vane test, $s_{u,FV} - q_{net}$ points Figure 5.14, indicate significant spread with N_{kt} between 5.0 and 25.5.

Several methods for defining a suitable cone factor from the results are possible. Because the N_{kt} value is a denominator in the determination of the undrained shear resistance (eq. 5.12), defining a representative value using the average N_{kt} (as presented in Table 5.6) is not advised. In the current study the least square method is used as given in equation (5.13).

$$\frac{q_{net}}{N_{kt,FV}} = s_{u,FV} \tag{5.12}$$

$$\sum_{i=1}^{n} \left(\frac{q_{net,i}}{N_{kt,FV}} - s_{u,FV,i} \right)^2 \tag{5.13}$$

With linear regression a cone factor of 11.0 was found. It is to be noticed that the linear regression of the inverse ($s_{u,FV}/q_{net}$) was chosen. This cone factor will be denoted as $N_{kt,FV}$ since it refers to the conversion from q_{net} to $s_{u,FV}$.

When applying the corrected field vane data, with the Bjerrum correction factor based on the plasticity index, instead of the raw field vane data, an average cone factor of 12.3 can be found. This relates to the average undrained laboratory shear strength of triaxial compression, direct simple shear and triaxial extension test, also described as $s_{u,ave}$ or $s_{u,Lab}$ ($= (s_{u,TC} + s_{u,DSS} + s_{u,TE})/3$).

5.4.2 Determination of cone factor with triaxial tests

Apart from the determination of the cone factor with in situ field vane tests, the cone factor can also be obtained from triaxial test and one-dimensional compression test results. For the calibration the piezocone, the undrained shear strength is calculated at several points. From three test pits, samples were taken for one-dimensional consolidation tests. These will be the reference points for comparing the calculated undrained shear strength with the results of the piezocone test.

The undrained shear strength at the sample location was estimated, based on the Critical State Soil Mechanics (CSSM) [Schofield and Wroth, 1968] and the SHANSEP method [Ladd and Foott, 1974] (equations 4.7 and 4.8).

The results of the one-dimensional consolidation tests and triaxial tests on samples from location A, C and E, as presented above, are combined for the calculation of the undrained shear strength as given in Table 5.7.

The effective stress is based on the average unit weight of all the one-dimensional consolidation tests and triaxial tests. The average strength increases exponent (m) is 0.91.

There were no triaxial compression tests performed on samples from location C, hence no information was obtained on the undrained shear strength ratio. The average undrained shear strength ratio from locations A and E is presumed to be a representative value for location C.

Location	Depth [m]	OCR [-]	S_{ult} [-]	$s_{u,TC}$ [kPa]	q_{net} [kPa]	$N_{kt,TC}$ [kPa]
A	- 1.0	4.3 - 4.4	0.342	23.2 - 23.5	188	8.0
C	- 1.5	3.8 - 3.9	0.336	30.8 - 31.1	584	18.8
C	- 2.8	1.9 - 2.2	0.336	30.7 - 34.4	517	16.8 - 15.0
E	- 3.0	1.8 - 2.3	0.332	31.1 - 38.1	684	22.0 - 17.9

Table 5.7: Undrained shear strength based on triaxial tests and one-dimensional consolidation test

5.4.3 Comparison between triaxial and field vane test method

The cone factors determined at the various investigation points are presented in Table 5.8 The cone factor from the triaxial compression test and one-dimensional consolidation test method exhibits a large spread with cone factors between 8.0 and 22.0.

Location	I_p [%]	Average $N_{kt,FV}$ [-]	$N_{kt,TC}$ [kPa]
A	24.6	11.6 ± 5.7	8.0
B	32.6	10.0 ± 3.1	-
C	37.2	12.3 ± 4.4	15.0 - 18.8
D	21.7	13.5 ± 4.5	-
E	33.2	9.4 ± 2.6	17.9 - 22.0

Table 5.8: Cone factors from field vane test and triaxial compression test

Figure 5.15 presents the corrected CPTu values of location C with a cone factor of 11.0. The results of the field vane tests are added at the respective depth, along with the determined undrained shear strength from the triaxial compression and one-dimensional consolidation tests. The corrected CPTu results show a relatively good resemblance with the field vane tests, disregarding some extreme points. The dots of the triaxial tests indicate a slightly lower shear resistance. The corresponding cone factor is higher, which would result in a corrected CPTu profile shifted to the left.

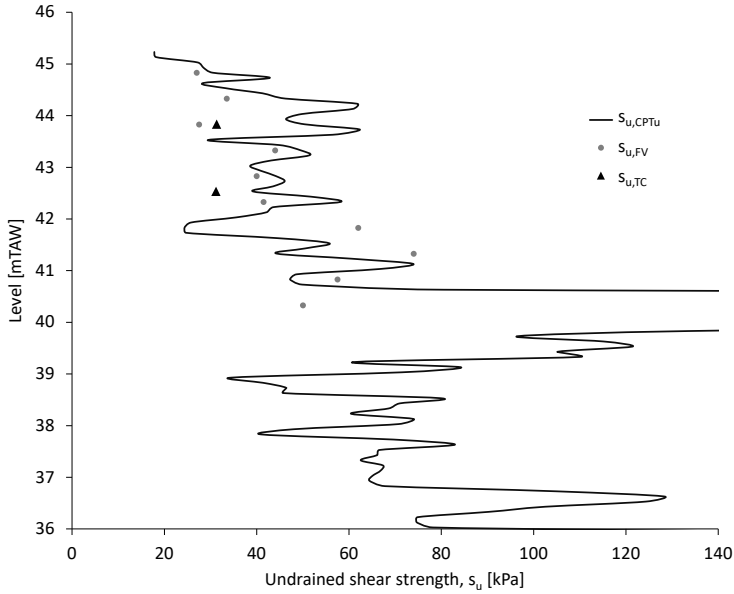

Figure 5.15: Comparison of undrained shear strength with a cone factor of 11.0 and field vane and triaxial compression test results

It should be noted that the elevation of the terrain above around 36 mTAW consists of a mixture of sludge and (glauconite containing) sand. Below the level of around 36 mTAW, a purer CaF_2 sludge is stored (filter cakes, ...). The soil characteristics (I_p, E_{50}, ...) can deviate, including the cone factor. Hence, the cone factor has more uncertainties regarding the sludge at the bottom half.

Determining the cone factor with the triaxial test method has some advantages and disadvantages, listed below.

- High quality data on the soil samples is obtained.
- The in situ effective vertical stress is estimated based on the soil volume weight, the position of the phreatic surface or estimations of the consolidation.
- The accuracy of the determination of the pre-consolidation stress at the one-dimensional consolidation test is limited to the chosen loading steps. An alternative method of determining the pre-consolidation stress is with constant rate of strain tests (CRS).

The CRS-test is a continuous test, which is deformation controlled (no loading steps) and therefore the tipping point between recompression and virgin compression can be distinguished more precise.

- Soil disturbance can occur while taking samples and/or when preparing the samples for testing.
- The number of test points with the triaxial compression test and one-dimensional consolidation test method is limited due to the time-consuming sample taking and costly laboratory tests. More data points are preferable but will result in a costly research program.

The cone factor determined with field vane tests also exhibits a certain spread, which can, partially, be attributed to the variation of the subsoil itself. The advantages and disadvantages of the field vane test method are listed below.

- A large set of data points can be obtained in a relatively short time span and at a low cost, which allows a better understanding of the spread. Furthermore, the larger dataset allows for a better comparison with the net cone resistance, resulting in a more accurate determination of the cone factor.
- The risk of sample/soil disturbance is limited because the soil is tested in situ. However, soil disturbance can occur when inserting the vane blades.
- The accuracy with the field vane test is lower compared to laboratory tests and the data acquired is limited to solely the undrained shear strength.
- Engineering judgement is required to distinguish erroneous measurement caused by disruptions in the subsoil.
- No information on over-consolidation can be obtained.

5.4.4 Comparison of cone factor with literature findings

The defined empirical cone factor is often correlated to the average laboratory undrained shear strength $s_{u,Lab} = (s_{u,TC} + s_{u,DSS} + s_{u,TE})/3$, where $s_{u,TC}$, $s_{u,DSS}$ and $s_{u,TE}$ are respectively the undrained shear strength from triaxial compression (TC), direct simple shear (DSS) and triaxial extension (TE) tests.

Several investigations have found a correlation of the cone factor with certain parameters such as plasticity index, over-consolidation ratio, ... Other works, however, did not find any correlation [La Rochelle et al., 1988]. Information from some related studies are presented in Table 5.9.

N_{kt}	Reference test	Correlation	Reference
7 - 19	Vane test	Increasing with OCR	[Almeida and Parry, 1983]
13 - 18.5	TC, TE, DSS	Increasing with plasticity index	[Aas et al., 1986]
10 - 18	Vane test	No relation with OCR or plasticity index	[La Rochelle et al., 1988]
8 - 29	TC	Increasing with OCR	[Rad and Lunne, 1988]
10 - 20	TC	Increasing with plasticity index	[Powell and Quarterman, 1988]
12 - 18	TC	/	[Senneset et al., 1982]
14 - 20	TC, TE, DSS	Increasing with liquid limit and correction for OCR	[Larsson and Mulabdic, 1991]

Table 5.9: Summary of literature data regarding the cone factor

A cone factor of 11.0 was derived from field vane tests on the industrial sludge. The analysis with one-dimensional consolidation tests and triaxial compression tests indicated a cone factor between 8.0 and 22.0 (average 15.9 ± 4.9).

Compared to literature data, the found cone factor is on the low side of the spectrum for vane tests as reference test. According to the classification of soils [Burmister, 1950], the industrial sludge at the investigated site corresponds to a highly plastic soil ($20\% < I_p < 40\%$) with a plasticity index of around 31%. The low value of the cone factor does not seem to correspond to the correlation with the plasticity index, according to some of the research mentioned in Table 5.9. However, in other researches no correlation with the plasticity index was found.

According to [Löfroth, 2008], the cone factor can be estimated from the liquid limit (w_L, Atterberg limits) of the soil. Based on the equations below, the active (triaxial compression), DSS (direct simple shear) and passive (triaxial extension) cone factors can be determined.

$$N_{kt}^{A} = 3.6 + 13.2 \cdot w_L \tag{5.14}$$

$$N_{kt}^{DSS} = 13.4 + 6.65 \cdot w_L \tag{5.15}$$

$$N_{kt}^{P} = 19.7 \tag{5.16}$$

A correlation between the plasticity index and the cone factor (N_{kt}) has been studied by [Karlsrud et al., 2005]. For respectively low sensitive clays ($S_t < 15$) and highly sensitive clays ($S_t > 15$), the best fit correlations are presented in equations (5.17) and (5.18).

$$N_{kt,CAUC} = 7.8 + 2.5 \cdot \log(OCR) + 0.082 \cdot I_p \qquad (S_t \leq 15) \tag{5.17}$$

$$N_{kt,CAUC} = 8.5 + 2.5 \cdot \log(OCR) \qquad (S_t \geq 15) \tag{5.18}$$

For the CaF_2 sludge, the empirical cone factor according to the methods by Löfroth and Karlsrud are presented in Table 5.10.

Reference test	Cone factor	Parameters CaF_2 sludge
[Löfroth, 2008]		
Triaxial compression test	$N_{kt}^{A} = 10.5$ - 13.3	$w_L = 63.2 \pm 10.6\%$
Direct simple shear	$N_{kt}^{DSS} = 16.9$ - 18.3	$w_L = 63.2 \pm 10.6\%$
Triaxial extension	$N_{kt}^{P} = 19.7$	$w_L = 63.2 \pm 10.6\%$
[Karlsrud et al., 2005]		
Anisotropic triaxial	$N_{kt,CAUC} = 9.7$ - 10.9	$I_p = 30.2 \pm 7.6\%$
compression test	$(S_t \leq 15)$	$OCR = 1$
Anisotropic triaxial	$N_{kt,CAUC} = 10.8$ - 12.1	$I_p = 30.2 \pm 7.6\%$
compression test	$(S_t \leq 15)$	$OCR = 3$

Table 5.10: Cone factor for CaF_2 sludge according to methods by [Löfroth, 2008] and [Karlsrud et al., 2005]

When comparing the derived cone factor on the industrial sludge with the empirical equations by Löfroth and Karlsrud, a discrepancy can be found. The triaxial compression tests on the sludge indicated a higher cone factor ($N_{kt,TC}$) of 15.9 ± 4.9 whereas Löfroth and Karlsrud indicate a lower $N_{kt,TC}$.

The cone factor from the field vane test ($N_{kt,FV} = 11.0$) can be compared to the average of the triaxial compression, direct simple shear and triaxial extension tests. The average of N_{kt} by Löfroth for TC, DSS and TE corresponds to a value of 15.7 to 17.1. The $N_{kt,FV}$ found from the in-situ tests are significantly lower than the empirical value, which would result in a higher undrained shear strength. It should be noted that the determined $N_{kt,FV}$ results in the uncorrected field vane shear strength whereas the literature data most likely will result in a corrected shear strength value. When using the correction factor by Bjerrum on the field vane data, the corrected cone factor will amount to 12.3. The low value of the cone factor, compared to literature data, will result in a higher undrained shear strength value.

5.5 Conclusions

Several field investigations and laboratory tests were conducted on the industrial sludge. Because the sludge is a combination of CaF_2 sludge and a varying fraction of glauconite sand, a large scatter in shear strength results was to be expected. Hence, the focus was on in situ tests, accompanied by laboratory tests for reference. Due to the low permeability ($\pm$ 1·10^{-9} m/s), the undrained shear strength of the sludge is important in the further analysis of sludge embankments in short term stability problems.

The borehole shear test (BST) allows for the determination of the cohesion and friction angle in boreholes on site. The BST indicate a friction angle of around 33.5° $\pm$ 3.7° and a cohesion of 8.0 kPa $\pm$ 3.9 kPa. The coefficient of variation for the cohesion is rather high. Hence, no reliable estimation of the cohesion can be obtained from the BST results. The found angle of friction with the BST approximates the results of isotropic consolidated triaxial compression tests (ϕ'_{peak} = 31.9°; ϕ'_{ult} = 30.5°). However, due to the lack of pore pressure measurements during the consolidation and shearing phase of the borehole shear test, no information can be gathered on the consolidations process and the occurring effective stresses. If the test is executed slow enough, drained parameters can be obtained, if not, the results will lie between fully drained and fully undrained. Because of this uncertainty no further use was made with the results of the BST.

It can be useful to perform borehole shear tests for a first estimation of the shear parameters (ϕ' and c). Furthermore, extrapolation of laboratory test results can be made possible by performing borehole shear tests, spread across a terrain, accompanied with laboratory tests (direct simple shear test, triaxial test, ...) for reference.

Piezocone penetration tests (CPTu) were executed for profiling the CaF_2 sludge deposits. Glauconite containing sand layers and other sandy layers (drainage layers, construction roads, ...) were identified in order to subtract these layers from the calculation of the undrained shear strength of the sludge. For determining the undrained shear strength for the CPTu results, an empirical cone factor is required. Literature data allows for an estimation of the cone factor based on some soil characteristics (plasticity index, liquid limit, over-consolidation ratio, ...). Discussion exists on the correlation of these characteristics with the cone factor. Therefore, reference tests (field vane tests and triaxial tests) were executed in the vicinity of CPTu in order to determine the cone factor.

A cone factor of 11.0 was derived from field vane test ($N_{kt,FV}$). With the $N_{kt,FV}$ the results of the piezocone tests are transformed to uncorrected field vane test results. Further corrections of the vane test results are required. With laboratory tests (triaxial compression tests and one-dimensional consolidation tests) an average cone factor of 15.9 ($N_{kt,TC}$) was found. The cone factor from field vane tests is on the low side, whereas $N_{kt,TC}$ corresponds to a slightly elevated value compared to literature data.

It should be noted that the cone factor from the triaxial compression test and one-dimensional consolidation test method has a significant spread, with results between 8.0 and 22.0. This is due to the complexity of the analysis of the laboratory tests and potential soil disturbance during sample taking and preparing. The field vane test is a rapid method for estimating the undrained shear strength of the industrial sludge. The easy setup and portable testing equipment allow for testing at locations, which can be difficult to reach with heavy machinery (steep slopes, soft soils, tree-covered areas, ...). Hard inclusions in the subsoil e.g. rocks, debris, roots, ..., can hinder the penetration of the vane, which was experienced on site. Field vane corrections are necessary to compensate, among others, disturbance, anisotropy, strain rate effect, ... Furthermore, the accuracy of the field vane test is lower compared to laboratory tests.

The values of shear strength measured with the field vane test indicate a significant scatter with values ranging from 6 to 135 kPa. The large scatter can be attributed to the sand inclusion and the intermediate drying of the material before levelling, resulting into stronger and weaker layers. By performing vane tests spread across a terrain, the variation of the parameters can be obtained. In this case the vane test was used to calibrate the piezocone test and to determine the cone factor.

Because of the large variation of undrained shear strength in the sludge deposit, obtaining a larger data set was considered more valuable than performing accurate laboratory tests on just a few samples.

Chapter 6

Full-scale slope failure test

6.1 Introduction

A slope failure can provide useful information on the failure mechanism of the particular soil. Back-calculations of (natural) slope failures are often performed in order to pinpoint the cause of effect. The knowledge on the soil behaviour can be improved and appropriate measures can be taken to avoid similar problems in the future.

Using back-calculations, the stability of the slope is analysed with different models and material properties. Because the failure of the slope has occurred, the factor of safety (FS) is considered to be unity (1.0). Any information on the shear strength parameters, pore water pressure conditions, ..., along with the knowledge that FS = 1.0, is used to determine the most suitable model, which can reproduce the slope failure.

However, there are limitations to the method of back-analysis of slope failure as stipulated by [Duncan et al., 2014] and [Deschamps and Yankey, 2006]:

- If progressive failure occurs, peak as well as residual shear strength are mobilized along the failure surface, whereas back-calculated values present an average shear strength.
- Soil softening may lead to a significant decrease in shear strength.
- The appropriate material model is important for the (back-)calculation of the shear strength.

- Plain strain conditions are assumed compared to an often three dimensional slope failure.
- Knowledge of the pore water pressure is difficult to obtain. Pre-failure or post failure piezometric data may be obtained. However, the actual pore water pressure at the failure zone is more complex due to, among others, shear induced pore pressure.

This chapter presents the construction, execution and back-calculation of a large scale slope failure test conducted on an embankment consisting of industrial sludge. To simulate the procedure of elevating the sludge deposit and the influence of self-consolidation of the sludge, a large scale test embankment was constructed. The objective of the full-scale test is to calibrate the embankment stability analysis procedure. The use of the vane shear tests, for a reliable estimation of the undrained shear strength of the sludge deposits and to assess scatter, is evaluated. The construction and instrumentation of the test embankment are presented below as well as the characterisation of the industrial sludge present in the test embankment. Finally, the results of the load test are discussed and a back-calculation is performed with the results of the slope failure test.

6.2 Geometry and construction of test embankment

A test embankment was constructed on top of the existing sludge deposit Veldhoven, section S3-3. The embankment, shown in Figure 6.1, measures 15 m by 60 m with a height of around 4 m. The bottom layer of the embankment consists of a one meter thick sand layer. On top of this layer, 3 m of sludge was piled up. The slope of the test embankment is inclined at an angle of 38.6° (1:1.25). The construction of the embankment took place within a period of about 2 months (September-October 2015). Figure 6.2 shows the cross section of the test embankment.

A similar method was used for constructing the test embankment as for elevating the entire deposit. The wet, solid sludge is firstly dumped in ridges (Figure 6.3). By doing so, the evaporation surface is increased to enhance drying by wind and sun, to reduce the water content of the sludge. The sludge is left to rest several days (depending on the weather conditions), after which the piles are levelled with a bulldozer. A sludge layer with a thickness of around 1.0 to 1.5 m is generally created. The test embankment consisted of two layers with a total thickness of around 3 m on top of a sand layer.



Figure 6.1: Test setup of large scale slope failure test

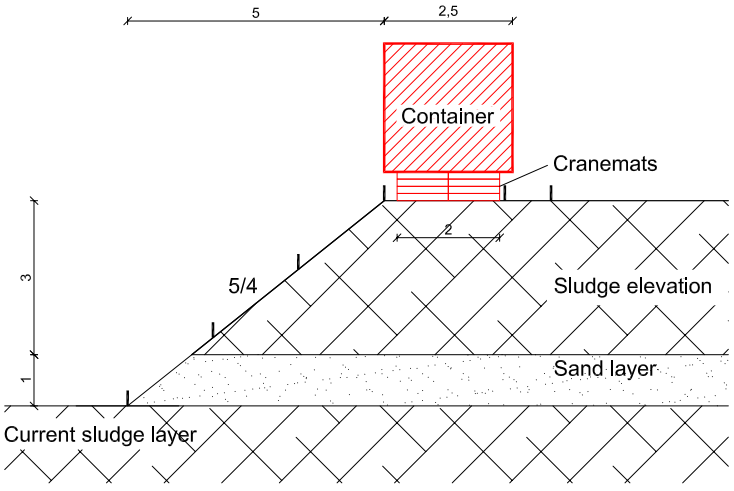

Figure 6.2: Cross-section of setup of large scale slope failure test



Figure 6.3: Sludge dumped in ridges during the construction of test embankment to enhance drying by wind and sun

To initiate slope failure, the embankment is loaded with three 40 m^3 containers, placed on top of a stack of crane mats, positioned near the edge of the slope. The crane mats, weighing around 1 ton each, are placed in two rows and stacked 4 elements high. The containers are gradually filled with water, until slope failure occurs. To calculate the ultimate load, the degree of filling in the containers is monitored during the test by using floats. The floats were attached to measuring poles protruding above the containers to allow measurement of the degree of filling from a safe distance. The deformations of the embankment are monitored by means of reference points on wooden posts, placed behind the containers and on the slope. The positions of these posts are recorded with a theodolite before the start of the test and after each loading step.

The following procedure steps were maintained during the slope failure test:

- Measuring monitoring points (baseline measurement)
- Increasing water level in containers by 20 to 30 cm
- Waiting period for consolidation of settlements (15 minutes)
- Measuring monitoring points
- Repeating increase of water level by 20 to 30 cm
- ...
- Failure of slope

6.3 Geotechnical characterisation

6.3.1 Field vane tests

The undrained shear strength of the freshly dumped and wheel compacted sludge was estimated with field vane tests, in accordance with [ASTM D2573 / D2573M-18,]. The vane tests were carried out at 6 locations on top of the test embankment, each time at 3 depths (-0.5 m, -1.5 m, -2.5 m), and at two sections of the slope (Figure 6.4). At each location, samples were taken to determine the plasticity index. The results of vane shear tests, carried out on the test embankment a few weeks after its construction, are shown in Figure 6.5.

Along the periphery of the entire deposit site, various tests (laboratory and in situ) are carried out every 50 m. Relative to the maximum height of the embankment of 9 m, the ratio of testing spacing over height is (50/9=) 5.6. The test embankment has a height of 3 m (sludge layer) and vane tests were performed about every 7 m, which results in a ratio of 2.3. The testing density on the test embankment is therefore more than twice as on the actual deposit site.

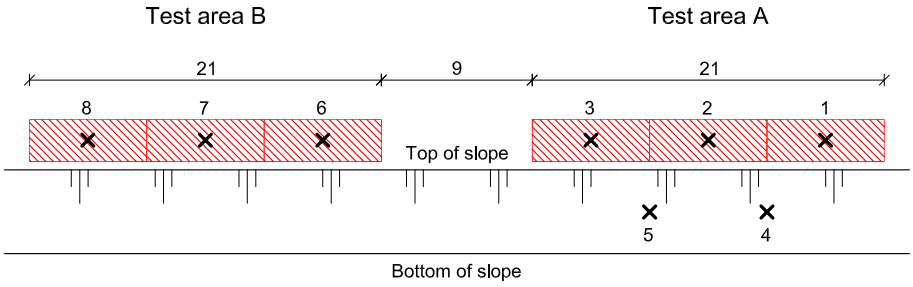

Figure 6.4: Location of field vane tests at areas A and B of the test embankment

The failure test of the embankment was intended to be split up in 2 phases with the first phase being carried out on the first 30 m of the test embankment (area A), shortly after completion of the embankment construction. The second phase was planned on the second half of the embankment (area B), about one year after construction. With these tests, the aim was to determine the actual shear resistance of unconsolidated (stage 1) and (partially) consolidated sludge (stage 2) at slope failure.

On area A, the average undrained shear resistance of the sludge is 9.7 kPa, with a standard deviation of 4.0 kPa and a coefficient of variation (COV) of 0.41.

On area B the mean value is 16.2 kPa, with a standard deviation of 12.0 kPa and a COV of 0.74. The results of the vane shear test indicate a (very) large spread, especially in area B. If the extreme values ($\geq$ 30 kPa), measured in area B, are excluded, the average value is 10.9 kPa, with a standard deviation of 5.8 kPa (COV = 0.54).

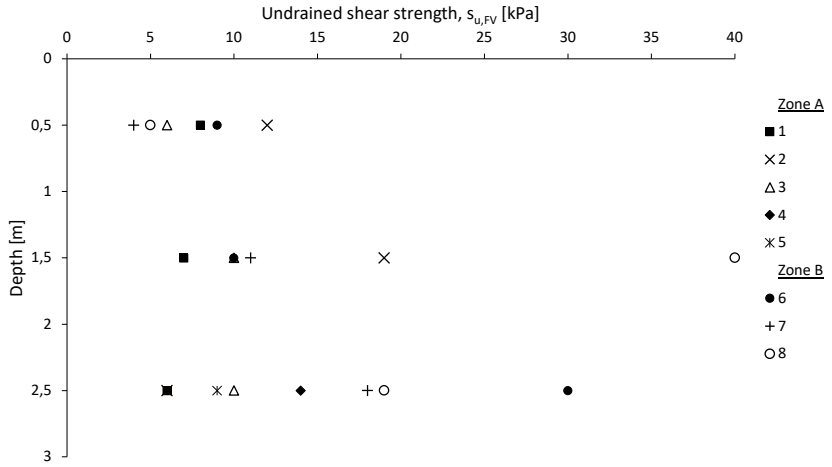

Figure 6.5: Undrained shear strength from vane shear test at test area A and B, at different depths

No correlation is observed between the shear strength and the depth. The exceptionally high resistance measured at a few locations may be due to local areas with denser compacted sludge or can be the result of local sand or stone inclusions. The large variations in the vane test results can be attributed to the manner of constructing the test embankment as well as due to the origin of the sludge, as described above. Hence, the lower accuracy of the vane shear test, compared to lab tests (triaxial tests, ...), is compensated by the larger numbers of data points acquired on the test site, allowing the variation to be mapped. Nevertheless, calibration tests are advised to quantify the uncertainty of the vane shear tests compared to laboratory tests.

According to ASTM D2573, a correction factor μ_B has to be used for correcting the raw results of the undrained shear strength determined with the vane apparatus. The correction factor developed by [Bjerrum, 1973], based on the plasticity index, is used in the initial analysis. The average plasticity index [ASTM D4318-17e1, 2017] of the sludge material of the test embankment is 33.9% ($\pm$ 3.0%), which results in a correction factor (μ_B) of 0.875 (Figure 5.4).

6.3.2 Unconsolidated undrained triaxial compression tests

At the test embankment, calibration tests were executed on two soil samples, which were subjected to unconsolidated undrained triaxial compression test (CUU) for determination of the undrained shear strength. At the extraction point of the samples, several field vane tests were executed for comparison of both test methods. The laboratory test on the samples and the vane test were done several weeks after the slope failure test.

The undrained shear strength in the UU-triaxial tests were 22.0 kPa and 24.0 kPa, respectively for samples 1 and 2. Five field vane tests near sample point 1 indicated an undrained shear strength ranging from 23.7 up to 41.0 kPa, with an average of 30.1 kPa and a standard deviation of 6.8. At sample point 2, the undrained shear strength from five field vane test ranged from 18.5 up to 30.0 kPa, with an average of 24.1 kPa and a standard deviation of 5.5 kPa. Even with tests in close vicinity of each other (only several tens of centimetres apart) the undrained shear strength, measured with the vane shear test, varies significantly. Based on the results of the calibration measurements no clear correlation between the tests methods could be observed. Therefore it was decided not to carry out additional laboratory tests as they are unlikely to provide more relevant information.

6.4 Results of the large scale slope failure test

During the slope failure test, the deformations of the embankment were monitored as described in §6.2. The results of the horizontal displacement are shown in Figure 6.6. A detailed visualisation of the horizontal deformations of the reference points of row c are presented in Figure 6.7. The displacement of the slope was measured with reflectors applied at the top of beacons, which protrude half a meter above the ground (slope) level. During the test, the beacons started tilting, due to the deformation of the soil. The influence of the tilt of the beacons was underestimated. To avoid erroneous measurements, the reflectors should have been placed as low as possible to the soil surface. The measured displacements are affected by the tilting and consequently don't represent the actual soil displacements but merely give an impression of the deformation.

Nearly no deformations were recorded during the first loading steps. Starting from an overload of approximately 23.4 kN/m^2 (step 5), the deformations increased systematically with the applied load. Gradually a bulge formed below container 1, as shown in Figure 6.8.

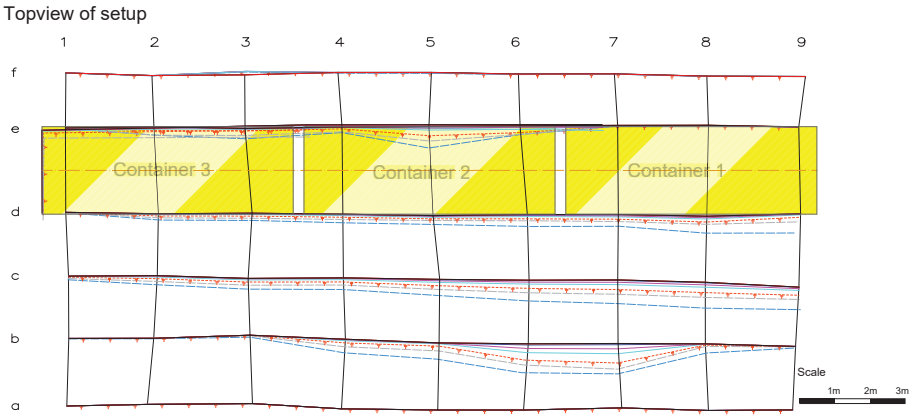

Figure 6.6: Grid of measuring points for horizontal deformations during slope failure test

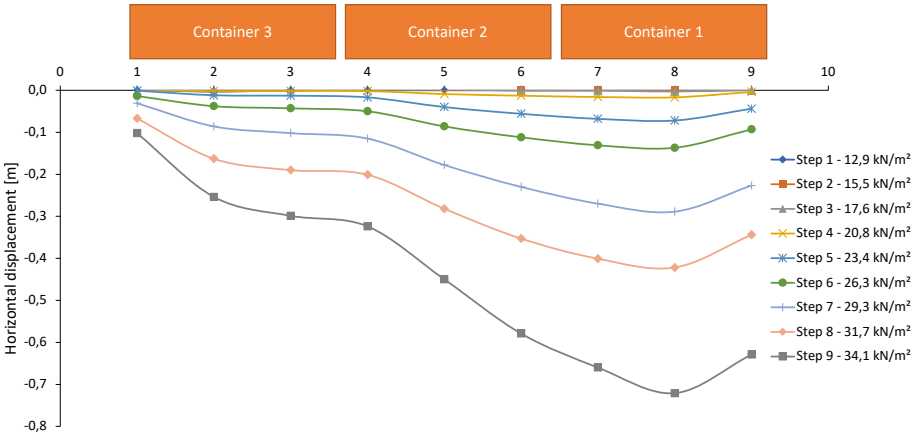

Figure 6.7: Horizontal displacements of measuring points at row C



Figure 6.8: Bulge formed below container 1, just above the interface between the sand layer and the sludge

With further increase of the surcharge, in step 9 (from 31.7 to 34.1 kN/m^2), large deformations were noticed, mainly at the zone under container 1. The deformations resulted in a tilting of the container causing the water to overflow. Increasing the surcharge became impossible. Furthermore, the deformations continued to increase under a constant load. A stable measurement of the reference points was no longer possible. Container 1 had to be retained with an excavator to prevent it from tipping over. The end of loading step 9 could not be reached.

The failure load was estimated at 33 kN/m^2, based on the water levels in the containers. The deformations at containers 2 and 3 were significantly smaller, but due to the large deformations at container 1, the test had to be terminated for safety reasons, and to avoid collapse and damaging of the containers. The displacements measured on the reference points on the containers are given in Figure 6.9 and Figure 6.10. Due to the large displacements of container 1, some reference points were no longer within reach of the theodolite at a certain load.

During the test large cracks appeared in the top surface of the embankment just behind the containers, shown in Figure 6.11. The bulge, formed in the slope just above the sand layer, initiated below container 1 but progressively spread along the entire length of the test area (Figure 6.8).

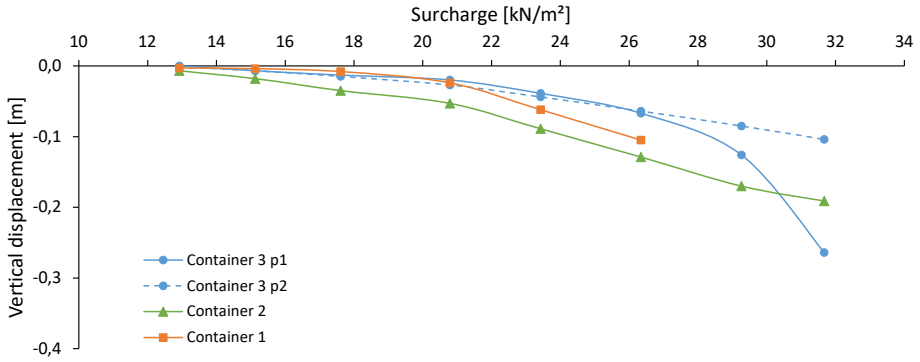

Figure 6.9: Vertical displacements of containers, monitored with two reference points on container 3 and one point on each of containers 1 and 2. After a surcharge of 26 kN/m^2 container 2 overshadowed the reference point on container 1

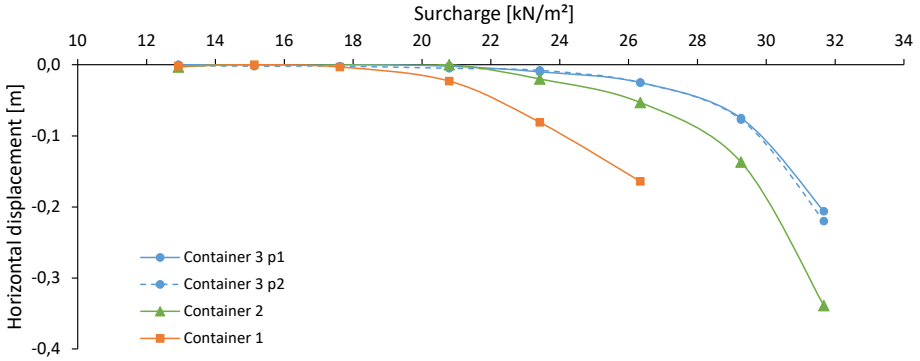

Figure 6.10: Horizontal displacements of containers, monitored with two reference points on container 3 and one point on each of containers 1 and 2. After a surcharge of 26 kN/m^2 container 2 overshadowed the reference point on container 1

The slope failure test indicates that the sludge embankment can exhibit large deformations before failure occurs. Furthermore, the results of the monitoring of the deformation indicate significant differential displacements. Although absolute values of deformations are influenced by the inclination of the measuring poles, it is still obvious that the deformations at container 1 are more than double of these at containers 2 and 3. Those differences may be caused by variations in sludge mechanical properties, most probably caused by different stacking and compaction actions at the end of the test embankment.



Figure 6.11: Open cracks adjacent to crane mats, after termination of test

6.5 Back-calculation of slope failure test

6.5.1 Correction factors

Correction factor are required to compare the actual slope failure with the back-calculation using finite element model (FEM) Plaxis. In the paragraphs below the corrections for 3D-effects, anisotropic behaviour and strain rate effect are assessed.

3D-effect

To estimate the ultimate surcharge on the embankment and the resulting average shear resistance of the sludge at failure, a 2D finite element model (Plaxis) was used. The test setup consisted of 3 containers placed on the edge of the embankment. Hence, only in the central area plain strain applies, as presumed in the 2D FEM. Edge effects will occur at the boundaries of the test setup. Azzouz [Azzouz et al., 1983] investigated the increase of the factor of safety (FS) with actual 3D failure modes and compared them with 2D calculations.

As a rule of thumb, the following equation can be applied to estimate the deviation of the factor of safety of a full plane strain situation compared to the actual 3D setup (eq. 6.1):

$$\frac{FS_{3D}}{FS_{2D}} = 1 + 0.7 \cdot \frac{D}{L} \tag{6.1}$$

For the test setup in the presented study, the depth (D) of the shear surface was assumed to be around 2 m and the length (L) of the test area was 20.5 m, resulting in a correction factor of 1.07 (FS_{3D}/FS_{2D}). The maximum surcharge in the 2D analysis is recalculated with the correction factor for the factor of safety. The accuracy of the calculated correction factor is limited, given the estimated position of the shear plane, which is based on visual observation. Its purpose is merely to give an idea of the order of magnitude of the deviation.

The equation above is based on empirical research with the use of the limit equilibrium method (e.g. Bishop's method of slices [Bishop, 1955]) for determining the factor of safety for the investigated slopes. The current method for determining the factor of safety relies on finite element method where commonly a phi-c reduction is used. Both methods may result in a different FS for the same geometry due to the variance in defining the FS. In the approximate framework the difference in FS between stress reduction method (as used in Plaxis calculation) and limit equilibrium method is disregarded. Furthermore, Plaxis [Plaxis, 2015] conducted a verification of the capabilities of the ultimate limit state of Plaxis for determining the factor of safety. The results of the stability analysis of an embankment were compared with Bishop's method of slices. For the presumed embankment the discrepancy of the FS was minute ($\approx 0.4\%$). The test embankment in the presented study is similar to the embankment in the verified simulation. Therefore, it was assumed that the calculated FS of the test embankment with the finite element analysis in Plaxis, will also have a limited discrepancy compared to a (Bishop) method of slices.

Anisotropic behaviour

The undrained shear strength depends on the orientation of the failure surface. This is due to the angle of the principle stress direction, which changes along the critical failure plane (Figure 6.12). The active, horizontal and passive part of a circular failure surface corresponds respectively to triaxial compression (TC), direct simple shear (DSS) and triaxial extension (TE) tests. In the investigated embankment, slope failure is triggered by applying an overload on the embankment crest near the edge of the slope. By doing so, the failure mode of the sludge in the embankment is predominantly compression.

At the bottom of the sludge layer (just above the sand layer), the failure mode can be between triaxial compression or DSS. A failure mode of triaxial extension is very unlikely to occur in this setup.

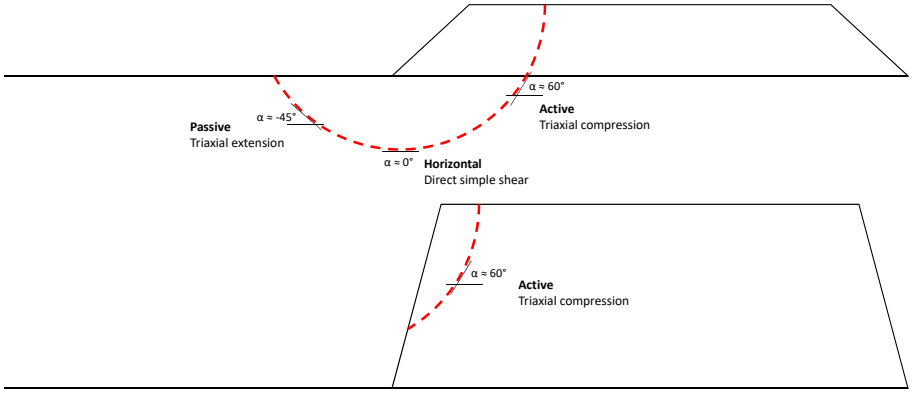

Figure 6.12: Relation between triaxial extension, direct simple shear and triaxial compression and orientation of failure surface for different shapes of embankments.

In Figure 6.13 the undrained shear strength ratio ($S = s_u/\sigma'_p$) is compared with the plasticity index (I_p) for triaxial compression (TC), direct simple shear (DSS) and triaxial extension (TE) tests [Ladd et al., 1977]. The correlation between undrained shear ratio and plasticity index for field vane tests by Skempton [Skempton, 1957] and Bjerrum [Terzaghi et al., 1996] is also added in Figure 6.13. Mayne & Mitchel [Mayne and Mitchell, 1988] conducted an extensive research on the relation between S and I_p for normally consolidated soils, which confirmed the relation as proposed by Skempton. It is to be noted that the individual results, whereupon the linear regressions in Figure 6.13 are based, exhibit a certain scatter. Due to the lack of data of the shear ratio for the industrial sludge, it is assumed that the behaviour of the sludge is similar to clay as presented Figure 6.13.

Conversion factors for the conversion of field vane test results to triaxial compression test results are available [Chandler, 1988]. In the current study, the use of the conversion factors in Figure 6.14 is proposed for the conversion of vane shear test results, based on the anisotropic shear ratio shown in Figure 6.13. Appropriate conversion factors are used, which depend on the plasticity index and the desired anisotropic state (active, DSS, passive). They represent the undrained shear strength ratio of the relevant anisotropic state to the undrained vane shear strength ratio.

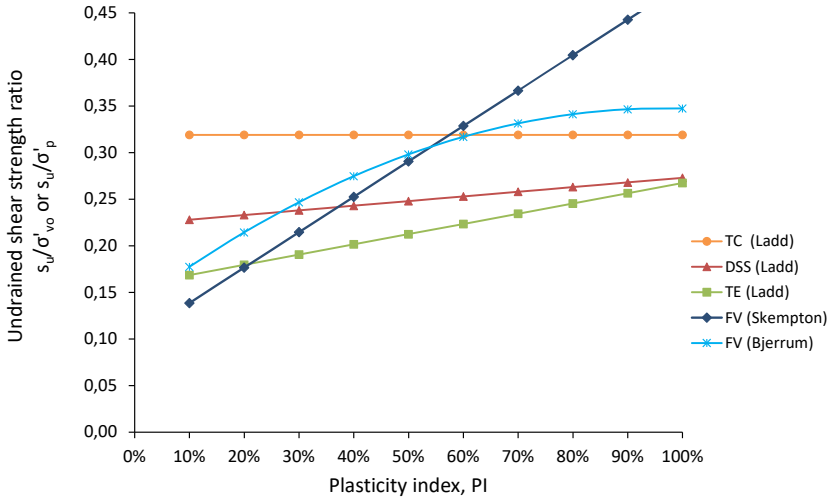

Figure 6.13: Influence of anisotropy on undrained shear strength of CK_0U tests on normally consolidated clay and loam [Ladd, 1991] (triaxial compression, direct simple shear and triaxial extension), supplemented with suggestion for the relation between s_u/σ'_p and I_p, based on the data from field vane test by Bjerrum [Terzaghi et al., 1996] and data from field vane test by [Skempton, 1957]

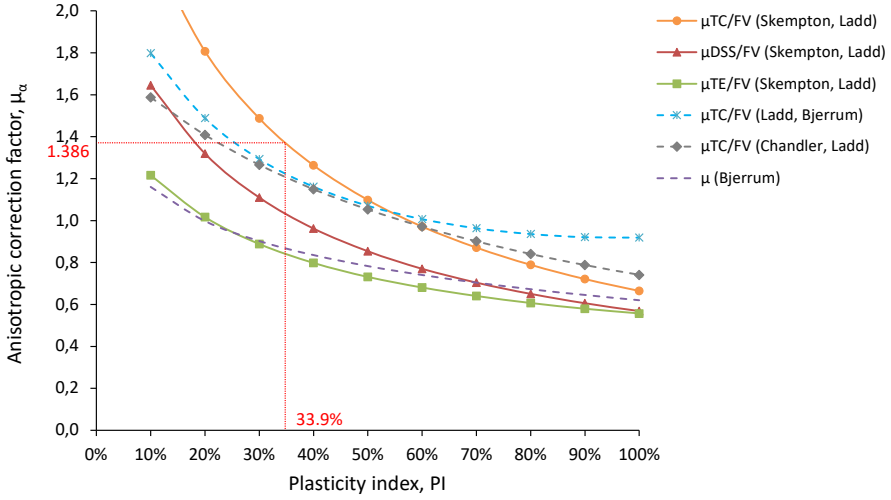

Figure 6.14: Anisotropic conversion factors for conversion of shear strength ratio of undrained shear resistance from field vane tests to triaxial compression, direct simple shear and triaxial extension. Example of anisotropic correction factor $\mu_{TC/FV}$ at a plasticity index of 33.9%.

An example for the anisotropic conversion factor μ_α is given in equation 6.2.

$$\mu_\alpha = \frac{S_\alpha}{S_\alpha} : \mu_{TC/FV} = \frac{S_\alpha}{S_\alpha} = \frac{S_{TC}}{S_{FV}} = \frac{s_{u,TC} \Big/ \sigma'_{v0}}{s_{u,FV} \Big/ \sigma'_{v0}} \tag{6.2}$$

The proposed (anisotropic) conversion factors are presented in Figure 6.14 by full lines. These conversion factors are to be used on the raw vane shear test results. The vane test correction factor such as suggested by Bjerrum (Figure 6.14, dashed lines), is also used in one of the back-analysis of the slope failure test, for comparison with the conversion factors in the suitable material models. It is assumed that by converting the raw vane shear test data to TC, DSS or TE results, any errors are adjusted by using the conversion factor, which depends on the plasticity index.

For a plasticity index of 33.9% (sludge embankment), the anisotropic conversion factor for field vane test to triaxial compression ($\mu_{TC/FV}$) amounts 1.386, indicated in Figure 6.14.

Strain rate effect

The rate at which failure occurs has an influence on the shear resistance of a material. Due to the viscosity of plastic soils, a higher shear resistance is encountered when the speed of loading is increased. For clayey and loamy soils with a plasticity index greater than 5%, the following correlation is suggested regarding the magnitude of the strain rate effect [Chandler, 1988]:

$$s_{u,t_f} \cdot \mu_R = s_{u,t_0} \tag{6.3}$$

$$\mu_R = 1.05 - b\,(I_p)^{0.5} \tag{6.4}$$

$$b = 0.015 + 0.0075 \cdot \log t_f \tag{6.5}$$

With the Bjerrum correction factors for field vane tests, the strain rate effects are taken into account by correcting the, fast, field vane test according to an assumed time to failure at real slope failures. According to ASTM D2573 a time to failure of around 10 000 minutes (7 days) is generally to be used for a long term failure. If the time to failure is assumed to be 10 000 minutes, the correction factor would be $\mu_{R,10\ 000} = 0.788$ ($I_p = 34\%$). In the large scale slope failure test a higher strain rate is imposed by the applied load increment. The large scale slope failure test took 6 hours, from the first loading step till failure. The corresponding correction factor is $\mu_{R,360} = 0.851$ ($I_p = 34\%$).

Besides the Bjerrum correction factor, an additional correction is therefore required in this case, to adjust the Bjerrum correction factor (which assumes long term failure). The additional correction will be $0.851/0.788 = 1.080$ ($\mu_{R'}$).

In the conversion of test results for undrained shear resistance measured by field vane tests to triaxial compression, direct shear or triaxial extension tests according to Figure 6.14, an additional correction, taking into account the strain rate effects, is not required. The time till failure in triaxial compression/extension tests and direct simple shear test, as well as the full-scale slope failure test, is in the same order of magnitude of several hours.

Bjerrum's correction factor μ_B [Bjerrum, 1972] is based on strengths back-calculated from actual failures in the field. The correction factor accounts for anisotropy, strain rate effects and probably also errors due to soil disturbance associated by vane insertion. In an attempt to break down the correction factor μ_B into the various aspects, anisotropic influence and the time effect were estimated by Bjerrum [Bjerrum, 1973]. The research was extended by Chandler to establish a correction factor for the strain rate effects at various plasticity index [Chandler, 1988]. The empirical correction factor μ_R is partially based on the same data as the correction factor μ_B. Consequently, the correction factor μ_R has an equal accuracy and degree of application. The application of the empirical correction factor μ_R doesn't diminish the credibility of the undrained shear strength values already corrected by the Bjerrum correction factor.

6.5.2 Material models

A two-dimensional finite element model (Plaxis) was used to carry out a back-calculation of the slope failure test. Taking into consideration the large variation in undrained shear strength of the sludge, a similar variation in (initial) pore water pressure is expected. Hence, using the effective strength parameters in undrained loading conditions after consolidation may lead to an erroneous effective stress path and accordingly erroneous undrained shear strength. Therefore, a direct input of the undrained shear strength in a total stress analysis is preferred.

As presented in Table 6.1, two different material models were applied for the sludge elevation. Firstly, a Mohr-Coulomb undrained (C) model was applied, where the results of the field vane test were used, corrected with the correction factors by Bjerrum and an additional stain rate correction factor.

The determination of the undrained shear strength is given in equations 6.6 and 6.7.

$$MC : s_u = \mu_B \cdot \mu_R \cdot s_{u,FV} \tag{6.6}$$

$$s_u = 0.875 \cdot 1.080 \cdot 9.73\ kPa = 9.19\ kPa \tag{6.7}$$

To take into account the anisotropic behaviour, a second simulation was carried out using the NGI-ADP (Norwegian Geotechnical Institute - Active, Direct simple shear, Passive) material model. The NGI-ADP model [Andresen and Jostad, 1999] is an advanced undrained shear strength model. The shear strength in the material model is defined in three stress states: active (A), direct simple shear (D) and passive (P). The active undrained shear strength was determined with an anisotropic conversion factor (μ_α) applied on the shear strength for the field vane test (eq. 6.8 and eq. 6.9).

$$NGI - ADP : s_u^A = \mu_\alpha \cdot s_{u,FV} \text{ with } \alpha\text{: TC/FV} \tag{6.8}$$

$$s_u^A = 1.386 \cdot 9.73\ kPa = 13.48\ kPa \tag{6.9}$$

A high angle of friction of 35° was adopted for the sand layer underneath the sludge elevation, along with assigning a small cohesion of 0.5 kPa. Because the analysis concerns a back-calculation of an occurred failure, the ultimate parameters are to be used, compared to the characteristic values of sand, as suggested in the applicable standards.

In the finite element program, Plaxis, a ratio of triaxial compression shear strength over active shear strength ($s_u^{C,TX}/s_u^A$) equal to 0.99 is suggested. The ratios of passive and direct simple shear strength over active shear strength (s_u^P/s_u^A and s_u^{DSS}/s_u^A) are derived from the graph in Figure 6.13 at a plasticity index of 33.9%. The relative proportions are used to define the ratios where $s_u^P = s_{u,TE}$ and $s_u^A = s_{u,TC}$.

Parameter	Symbol	Sludge elevation	Sludge elevation	Unit
General				
Material model	Model	NGI-ADP	MC	-
Type of material behaviour	Type	Undr. C	Undr. C	-
Unsaturated unit weight	γ_{unsat}	16	16	$\left[kN/m^3\right]$
Saturated unit weight	γ_{sat}	16	16	$\left[kN/m^3\right]$
Initial void ratio	e	1.4	1.4	-
Parameters				
Young's modulus	E	-	3600	$\left[kN/m^2\right]$
Poisson's ratio	ν	0.495	0.495	$[-]$
Cohesion	c	-	-	$\left[kN/m^2\right]$
Friction angle	ϕ'	-	-	$[^\circ]$
Undrained shear strength	s_u	-	9.2	$\left[kN/m^2\right]$
Ratio unloading/reloading shear modulus over active shear strength	G_{ur}/s_u^A	250	-	$[-]$
Reference active shear strength	$s_{u,ref}^A$	13.5	-	$\left[kN/m^2\right]$
Ratio of triaxial compression shear strength over active shear strength	$s_u^{C,TX}/s_u^A$	0.99	-	$[-]$
Ratio of passive shear strength over active shear strength	s_u^P/s_u^A	0.610	-	$[-]$
Ratio of direct simple shear strength over active shear strength	s_u^{DSS}/s_u^A	0.752	-	$[-]$

Table 6.1: Model input data for sludge elevation (Mohr-Coulomb and NGI-ADP)

6.5.3 Results of back-calculation

Figure 6.15 presents the results of the back-calculation of the undrained shear strength of the industrial sludge embankment with a crest load of 33 kN/m^2. The factor of safety is plotted against the (raw) vane shear strength. In the analysis the corrected and converted shear strengths are applied. The average vane shear strength from the field tests is indicated, as well as the average value plus and minus the standard deviation (SD). The factor of safety from the 2D finite element analysis is converted to the corresponding three dimensional factor of safety. In the MC model, first of all, the average shear strength (s_u) was implemented to calculate the corresponding FS. Second, the active undrained shear strength (s_u^A), as determined for the NGI-ADP model, was used in the MC model to compare these results with the NGI-ADP model. The decrease of the factor of safety (assuming the average s_u) with the increase of the crest load is presented in Figure 6.16.

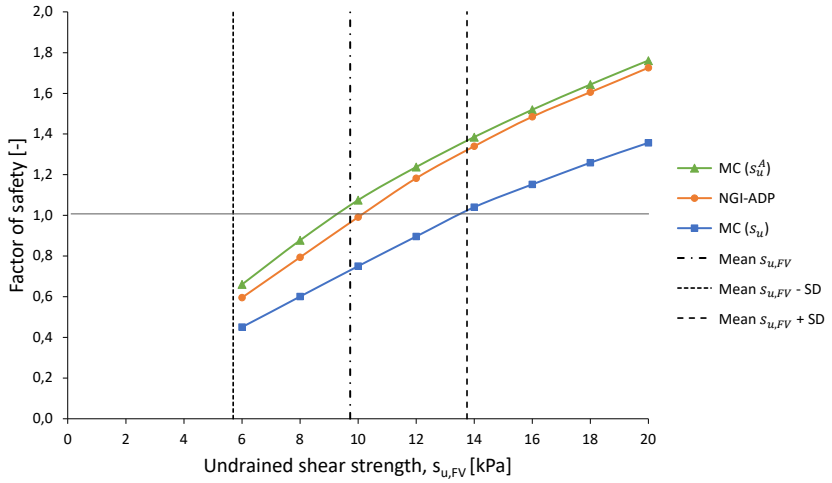

Figure 6.15: Calculated FS (3D) of the sludge embankment with a load of 33 kN/m^2 for a range of undrained (field vane) shear strength with MC and NGI–ADP material models

The Mohr-Coulomb model, with the use of the correction factors by Bjerrum for the undrained shear strength from vane shear tests, underestimates the stability of the sludge elevation. A factor of safety of only 0.73 was reached for the average undrained field vane shear strength in the MC model. This indicates that the test embankment should have collapsed at a lower crest load or, subsequently, that the shear resistance of the sludge is higher than assumed in the analysis.

When the active undrained shear strength (s_u^A) is used in the MC model, the achieved FS increases to 1.05, thus approximating the actual failure of the test embankment. In the MC (s_u^A) simulation, it is assumed that all the soil shears in active shear, resulting in a higher shear resistance. This assumption is however an overestimation given the critical slip surface illustrated in Figure 6.17, where a horizontal shear section occurs.

In the NGI-ADP material model the various anisotropic stress states are taken into account at the exact location. A FS of 0.96 is computed with the NGI-ADP model, hence corresponding well with the actual slope failure when using the average undrained field vane shear strength.

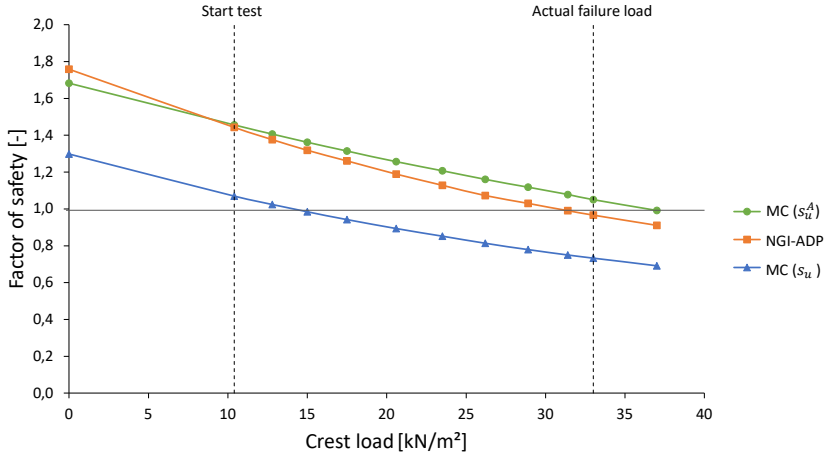

Figure 6.16: Calculated FS (3D) of the sludge embankment during the different steps of the slope failure test with MC and NGI–ADP material models

Both the NGI-ADP model as well as the MC (s_u^A) model give a reasonable representation of the factor of safety for the test setup at failure, if the average shear strength is assumed. Nevertheless, it is to be noted that the variability of the undrained vane shear strength, determined with the field vane, is significant. Furthermore, the factor of safety is highly sensitive to the undrained shear strength. The FS for NGI-ADP and MC (s_u^A) ranges from approximately 0.6 to 1.4 over one standard deviation (+ and -) from the mean value.

The large scatter of the vane shear test results is not a direct consequence of the chosen test method, but is mainly due to the variation of the material itself. The process of natural consolidation determines the undrained shear strength. By building the embankment with various layers of excavated sludge, which have been consolidated at different stress levels, the embankment is a mixture of high and low consolidated sludge.

Considering the relatively small scale of the (forced) slope failure test, it can be assumed that the slip surface will run through both strong and weak layers. Therefore, the average shear strength is used in the back analysis.

When performing stability checks on larger slopes, an appropriate method for taking into account the spread of the shear strength is to be used to determine the characteristic values. Due to the large spread of the results, applying a normal distribution will lead to a very low characteristic value. The choice of an appropriate method to quantify the distribution is further discussed in chapter 7.

A sensitivity analysis is performed to verify the influence of the variation of the plasticity index (33.9% ± 3.0%) on the factor of safety. In the Mohr-Coulomb analysis a variation of the I_p of ± 3.0% resulted in a nearly equal variation of ± 2.7% of the FS (range: $1.0 \leq FS \leq 1.5$). With the MC (s_u^A) and NGI-ADP analysis, the variation of the FS lies between +3.7% and −4.1%. The (small) unequal distribution is due to the curve of the correction factors given in Figure 6.14. As expected, a decrease in plasticity index will have a larger impact on the correction factor (μ_α) than an equal increase.

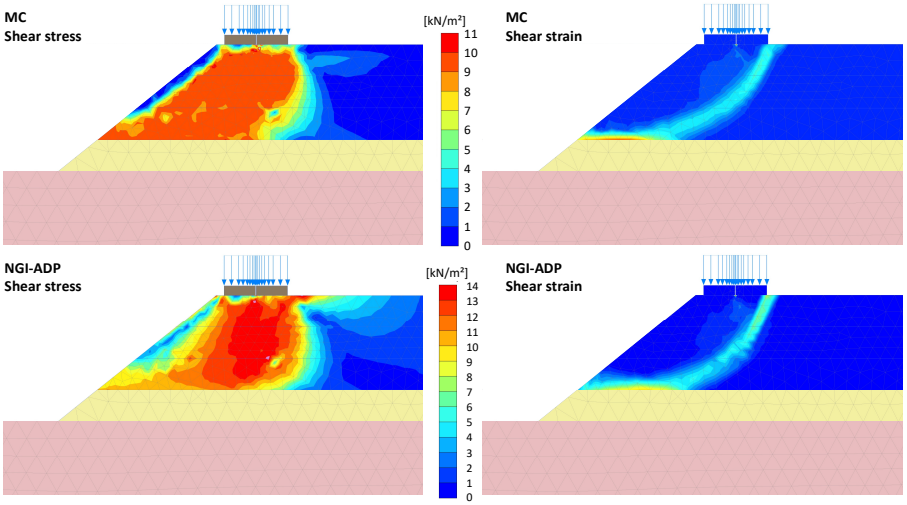

Figure 6.17: Shear stress and shear strain in elevation in the MC and NGI–ADP model at a crest load of 33 kN/m^2. The location of the maximum incremental deviatoric shear strain indicates the position of the shear plane.

The shear stresses at the failure load of the full-scale slope failure test (33 kN/m^2) for the MC and NGI-ADP material model are presented in Figure 6.17. The incremental deviatoric shear strains illustrates the position of the theoretical shear plane.

The results of the shear stress distribution in the soil indicates the difference between the Mohr-Coulomb (MC) model and the NGI-ADP model. In the analysis using the MC material model, the shear stress is nearly constant along the critical slip surface, indicated by the incremental deviatoric strain. No relation between the magnitude of the shear stress and the position on the slip surface is observed. The shear stress distribution in the NGI-ADP model fluctuates along the slip surface and reaches the highest stress level in the active zone ($30° \leq \alpha \leq 60°$). The horizontal section, near the sand layer, is smaller in the MC model compared to the NGI-ADP model, visualised by the incremental deviatoric strain in Figure 6.17. Subsequently the active section (below the crest load) in the NGI-ADP model is steeper, whereas in the MC model the curve is less steep and smooths out circular. The model results are in keeping with the expectation that the choice of material model not only influences the shear stresses but can also change the position of the slip surface.

6.5.4 Slope failure test after consolidation

The full-scale slope failure test consisted of two phases. The first phase was executed on one half of the test embankment, shortly after construction, as described above. In the second phase, the slope failure test was to be repeated one year later on the remaining part of the embankment (Zone B, Figure 6.4). The objective was to evaluate the influence of consolidation of the industrial sludge. After determining the vane shear resistance, at locations spread over the entire embankment in the context of the first testing phase, repeating measurements were conducted in zone B several months later. The results are presented in Figure 6.18.

Over a period of five months (winter and spring), the average undrained shear strength had roughly doubled from 16.2 kPa to 35.4 kPa (SD = 15.5 kPa; COV = 0.44). Ten months after the first vane shear test, the shear resistance had increased further up to around 250% of the initially measured values ($s_{u,FV,ave}$ = 40.9 kPa; SD = 18.2 kPa; COV = 0.44). Because of the strong increase of the undrained shear strength, the initial test setup at zone A could not be repeated because of the high loads required to trigger slope failure. The results of the vane shear tests indicate a significant increase in undrained shear strength.

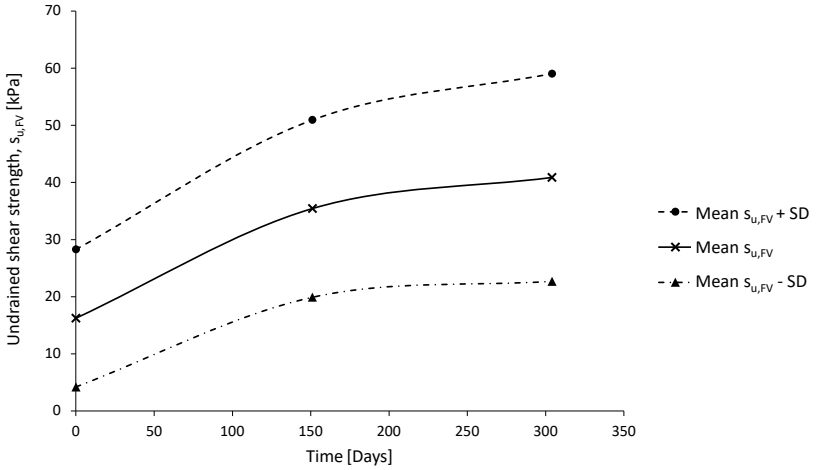

Figure 6.18: Average and SD of undrained shear strength from vane shear test at location B over a period of 10 months

It is unlikely that the consolidation of the sludge would result in a shear strength of around 40 kPa, if the internal stress can only be generated by its own weight. At the maximum depth the maximum effective stresses are too limited (σ'_{max} = 3 m × 16 kN/m^3 = 48 kN/m^2). The additional increase in shear strength will most likely be due to suction stresses, caused by dehydration of the sludge during the resting period. With the presence of the sandy drainage layer below the sludge layers, the phreatic surface is kept below this layer, resulting in an additional artificial effective stress (suction) in the sludge.

The suction stresses are, however, often only temporarily and caution should be maintained when taking sucking into account. Variations in phreatic level or precipitation may lead to a rapid decline of the artificial additional effective stresses caused by suction. Nevertheless, these additional effective stresses will have led to an over-consolidation of the sludge, which will have a positive influence on the sludge behaviour during further elevation.

6.6 Conclusions

A full-scale slope failure test was conducted on an embankment constructed with industrial CaF_2 sludge to determine the actual shear strength at failure. Field vane tests were used to estimate the undrained shear strength of the sludge.

The field vane test results exhibited a large spread, which will be mainly the consequence of the origin of the material (varying sludge-sand mixture), the initial (pre)consolidation and the various manipulations (excavation, dumping, spreading, ...) to which the material is subjected. The main advantage of the field vane test is the simplicity of the test allowing to obtain a large number of measurements. A reliable variation of the undrained shear strength can thus be determined. In combination with laboratory tests (triaxial tests, direct simple shear, ...) the accuracy of vane shear tests might be increased. However, a direct correlation between laboratory tests on soil samples and in situ tests near sampling location is hard to establish in this heterogeneous material.

To correct the undrained shear strength, measured in situ with the vane shear apparatus, to the actual shear strength in slope failure, the Bjerrum correction factor was used as well as an alternative method. The Bjerrum correction factor applies, among others, a correction for the anisotropy in which the field vane test is assumed to be equivalent to the average anisotropy of triaxial extension (passive), direct simple shear and triaxial compression (active) tests. In the presented case, this can be a conservative assumption. The alternative method consists of converting the vane shear strength to a more suitable anisotropic shear strength i.e. passive (triaxial extension), DSS (direct simple shear) or active (triaxial compression) shear strength. The current assumed conversion factors are solely based on literature findings. To reduce the uncertainty of these factors, performing and comparing several direct shear tests, triaxial tests and vane shear tests on the concerning material is needed.

A back-calculation of the slope failure test was made to compare the measured in situ shear strength with the theoretical shear stresses arising in a 2D model of the slope at failure. Two different approaches, Mohr-Coulomb and NGI-ADP, were used to determine the shear strength of the sludge in the finite element model (Plaxis), based on the average vane shear tests and to calculate the factor of safety at the critical failure load of the slope failure test. The analysis of the full-scale slope failure test based on the average corrected (Bjerrum) undrained shear strength from the vane shear test, using the Mohr-Coulomb material model, resulted in an underestimation of the actual shear strength. The anisotropic converted shear strength values were used in the NGI-ADP material model.

A second MC model was used, which included the s_u^A value (active undrained shear strength) instead of the corrected shear strength value. Both methods using the anisotropic values, approached the results of the slope failure test. The position of the shear plane, however, could not be verified and checked with the theoretical shear plane. For larger slopes it is advised to use the NGI-ADP model since the different anisotropic shear strength ratios (active, DSS and passive) are implemented in the model, whereas, in this example, the assumed main failure mechanism (active shear) was manually assigned in the adapted MC-model.

It should be noted that the back-calculations are based on the average values of the vane shear tests. The material variability was not accounted for. The sensitivity analysis indicates that the factor of safety is highly sensitive for variations of the undrained shear strength. It was assumed that, due to the rather small failure zone of the slope failure test, the average shear strength is representative for the shear resistance. Nevertheless, the significant spread leads to a high degree of uncertainty. For stability analysis of larger elevations, the spread of the material characteristics must be taken into account through an appropriate probabilistic design, based on an accordingly extended test program on the site.

Chapter 7

Stability analysis of a sludge embankment on Veldhoven deposit

7.1 Introduction

In basic engineering design, calculations are made based on information gathered on the material parameters. If possible, tests can be performed on the material to determine the required parameter for implementation in a model. If, however, the material is not available for testing, assumptions must be made based on literature data of similar materials.

To reduce the uncertainties on the assumptions made, additional testing, on the actual material, during the construction is always advised. Potential erroneous assumptions can be uncovered, and the initial design can be adapted.

In the present case, a design was made for an elevation of CaF_2 sludge on sludge deposit Veldhoven section S3-3. Initially, a hardening soil model was used for simulation of the staged construction of the embankment. The characteristics of saturated sludge, present at Veldhoven deposit, were implemented in the finite element analysis. The speed of elevation and the maximum height of the embankment were defined to ensure a safe embankment construction.

Not only sludge material was used during the construction work of the elevation, but also additional material, with different origin, had to be stored in the created embankment. Apart from CaF_2 sludge coming from clearance works at an old sludge deposit, also sandy material from the remediation of the subsoil of this deposit, had to be stored in the new embankment. Furthermore, the material properties (density, water content, pore volume, ...) of the sludge had to be estimated in advance. These properties varied significantly.

In situ tests at intermediate phases of the embankment were executed. Adaptations to the initial stability analysis were needed in order to assess the actual situation. In this chapter, the investigation of the soil properties and the numerical analyses of the built embankment are discussed.

7.2 Geometry

As illustrated in §1.2, the sludge deposit Veldhoven is divided in three main sections: S1, S2 and S3. Section S3 is further divided in subsections, as shown in Figure 1.2, and contains: a wet deposit (S3-1); an elevation of about 20 m above the deposit base, built with filter pressed sludge (S3-2); an elevation of about 16 m above the deposit base built with naturally dried sludge (S3-3) and a zone for a future percolate buffering reservoir (S3-4).

Initially, the entire section S3 was used as a wet sludge reservoir. Subsection S3-2 was reclaimed more than twenty years ago. During the last ten years, subsection S3-3 was converted into a dry sludge storage by gradually filling in the wet area with (naturally) dried sludge and filter pressed sludge (filter cakes). By gradually dumping in the sludge, the water and the wet sludge at the bottom are driven back and a dry terrain is created. Figure 7.1 gives a view of the gradual transformation from wet to dry deposit from 2007 till 2015.

Most of the sludge dumped below the water level consisted of filter pressed sludge. These filter cakes were obtained by filter pressing the sludge, hereby significantly reducing the water content (see chapter 2). The resulting filter cake clods are over-consolidated due to the filter pressing at 13 bars and do not tend to take up much water or soften when submerged under water.

Because of decreasing and ultimately shutting down of phosphate production, insufficient amounts of filter cakes were available on site to fill area S3-3 below the waterline, thus, also naturally dried sludge was dumped below the water level.



Figure 7.1: Aerial photo's of deposit Veldhoven, S3 [Geopunt Vlaanderen]

Earlier research, [Van Der Veken, 2002], indicated that (over)intensively naturally dried sludge tends to pulverize. When rehydrated, the structural integrity of the dried sludge lumps is lost and a silty mud is obtained. Hence, the use of naturally dried sludge results in more uncertainties about the constructed sludge foundation below the water level.

The new sludge embankment on S3-3 of Veldhoven deposit, measures 260 m long and 120 m to 150 m wide. The elevation height is about 7 m (± 45.8 mTAW) above the level of the surrounding (sand) dike (± 38.4 mTAW). The bottom of the sludge deposit and the nearby ground level lies 9 m lower (± 29.5 mTAW).

The profile of the elevation at location B, measured with GPS, is shown in Figure 7.2. At several locations, the profile of the slope was measured in detail. The positions of the profile measurement correspond to the location of the executed in-situ tests (chapter 5), as presented in Figure 5.6. The in-situ tests consists of vane shear and piezocone tests. Soil samples were taken at several locations for laboratory testing.

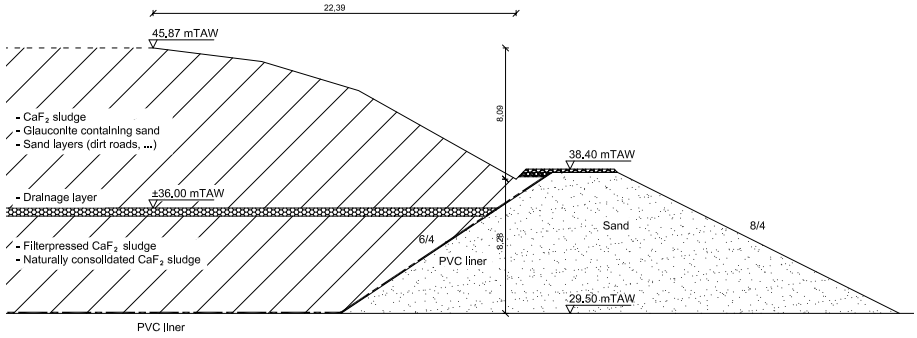

Figure 7.2: Profile of slope at elevation of sludge deposit Veldhoven, subsection S3-3, at location B

Deposit site S3 was constructed in 1987 with a surrounding sand dike with an elevation of about 9 m. The outer slope has an inclination of 8/4 (26.6°). The inner slope is steeper with an inclination of 6/4 (33.7°). The internal slope of the sand dikes and the bottom of deposit site Veldhoven S3 is sealed with an impermeable PVC liner with a thickness of 0.5 mm, foreseen to prevent seepage of pollutions in the subsoil. The watertight seal at the bottom of the deposit has a significant influence on the consolidation time of the stored sludge, because excess pore water can only dissipate at the top of the elevation and at the slope of the sludge embankment.

The elevated terrain consists of a combination of glauconite containing sand and CaF_2 sludge, which is naturally dried or filter pressed (filter cakes). The glauconite containing sand originated from the excavation of the Old Deposit (see chapter 1), a former CaF_2 sludge deposit site. The reconversion of this old site comprised the excavation of the CaF_2 sludge and the contaminated part of the subsoil (glauconite containing sand). Consequently, the sludge arrived at Veldhoven deposit as a mix of sludge with sand, of which the concentration varied from location to location.

A drainage layer was constructed below the crest of the surrounding dike, at a level of about 36 mTAW. Furthermore, local sand layers from site roads, used during the elevation works, may be present in the upper part of the embankment. The positions of these layers are not known and can occur discontinuously across the site at various levels.

7.3 Soil investigations

Because of the nature of the material used to build the elevation (excavated, reconsolidated sludge) and the method of handling the sludge (excavating, transporting, dumping, drying and spreading), a large spread in material parameters was expected. The execution of solely detailed laboratory tests on specific points may lead to erroneous expectations regarding the material parameters, without any insight in the variation of these parameters. Therefore, the research consisted of in situ vane tests and cone penetration tests to establish the variation of results, in combination with laboratory testing (triaxial tests and oedometer tests).

Piezocone penetration tests (CPTu) and field vane tests were conducted on lateral profiles every 50 m along the edge of the 260 m long elevation on sludge deposit Veldhoven S3-3. The combination of field vane tests, triaxial tests and one-dimensional consolidation tests resulted in the determination of a cone factor (chapter 5) for the industrial sludge, which allows the calculation of undrained shear strength from piezocone penetration profiles.

7.3.1 Anisotropic transformations for cone factor

The cone factor, determined in chapter 5, was based on field vane tests. Hence, the defined cone factor allows for the calculation of vane shear strength with the net cone resistance from piezocone penetration tests.

A conversion of the cone factor is required for determining the undrained shear strength profiles for other anisotropic stress states (active, DSS, passive). The conversions factors, illustrated in Figure 6.14 (based on Skempton and Ladd), are applied in the further analysis.

The transformation from cone factors for field vane test shear strength, $N_{kt,FV}$, to cone factors for triaxial compression or active shear strength ($N_{kt,TC}$) is given below.

$$s_{u,FV} = \frac{q_{net}}{N_{kt,FV}} \tag{7.1}$$

$$s_{u,FV} \cdot \mu_{TC/FV} = s_{u,TC} \tag{7.2}$$

$$s_{u,TC} = \frac{q_{net}}{N_{kt,FV}} \cdot \mu_{TC/FV} = \frac{q_{net}}{N_{kt,TC}} \tag{7.3}$$

$$N_{kt,TC} = \frac{N_{kt,FV}}{\mu_{TC/FV}} \tag{7.4}$$

It is assumed that the anisotropic conversion factor depends on the plasticity of the soil, as indicated in chapter 5.4. The upper part of the sludge elevation is characterized by an average plasticity index of 30.2% ± 7.6. For the lower part of the sludge (below 36 mTAW) a plasticity index of 40% is assumed, based on earlier research [Tennekoon, 2007].

Tables 7.1 and 7.2 give the conversion factors and cone factors for different anisotropic states at several plasticity indexes. The quantities $\mu_{Lab/FV}$ and $N_{kt,Lab}$ are respectively the conversion factor from field vane test shear strength to the average laboratory shear strength (average of triaxial compression, direct simple shear and triaxial extension) and the average cone factor derived from the inverse cone factors for triaxial compression , direct simple shear and triaxial extension (assuming: $\left(\frac{1}{N_{kt,TC}} + \frac{1}{N_{kt,DSS}} + \frac{1}{N_{kt,TE}}\right)/_3 = \frac{1}{N_{kt,Lab}}$).

Plasticity index	Anisotropic conversion factor			
I_p	$\mu_{TC/FV}$	$\mu_{DSS/FV}$	$\mu_{TE/FV}$	$\mu_{Lab/FV}$
20%	1.81	1.33	1.02	1.38
30%	1.48	1.11	0.89	1.16
40%	1.26	0.96	0.79	1.01

Table 7.1: Various anisotropic conversion factors at different plasticity indexes

Plasticity index	Cone factor				
I_p	$N_{kt,FV}$	$N_{kt,TC}$	$N_{kt,DSS}$	$N_{kt,TE}$	$N_{kt,Lab}$
20%	-	6.1	8.3	10.8	7.9
30%	11.0	7.4	9.9	12.4	9.5
40%	-	8.7	11.5	13.8	10.9

Table 7.2: Cone factors for various stress states at different plasticity indexes

7.3.2 Determining characteristic value of undrained shear strength

A detailed profile of the undrained active shear strength (s_u^A), assumed to be equal to the undrained shear strength from triaxial compression tests ($s_{u,TC}$), is obtained from the cone penetration tests with the cone factor $N_{kt,TC}$. To obtain the characteristic values, a standard deviation on a Gauss distribution is commonly used.

Because of the large spread between the different CPTu's, this method would not result in realistic values for further analysis of the slope stability. Hence, an alternative procedure is used for the interpretation of the soil investigation by using sample collections as suggested by the Dutch technical advisory commission for the flood defence [Technische adviescommissie voor de waterkeringen, 1989].

Figure 7.3 presents a theoretical fluctuation of a soil parameter and the correlation with two hypothetical mechanisms [Calle et al., 2008].

- For mechanism I, the mechanism scale is small compared to the fluctuation scale. Hence, the mechanism is sensitive for local values.
- For mechanism II, the mechanism scale is large compared to the fluctuation scale. For this mechanism, the average value within the scale of the mechanism is of importance, because local fluctuations are levelled out.

[Calle et al., 2008] stated that for slope failure analysis, the variation of shear strength along the vertical axis will be levelled out because correlation length of e.g. CPT tests is small (centimetres) in relation to the scale of the potential failure mechanism vertically (slope failure occurs at depth of several meters). In the horizontal axis (other CPT tests), the correlation length has commonly the same scale as the potential failure mechanism, hence, no averaging will be made.

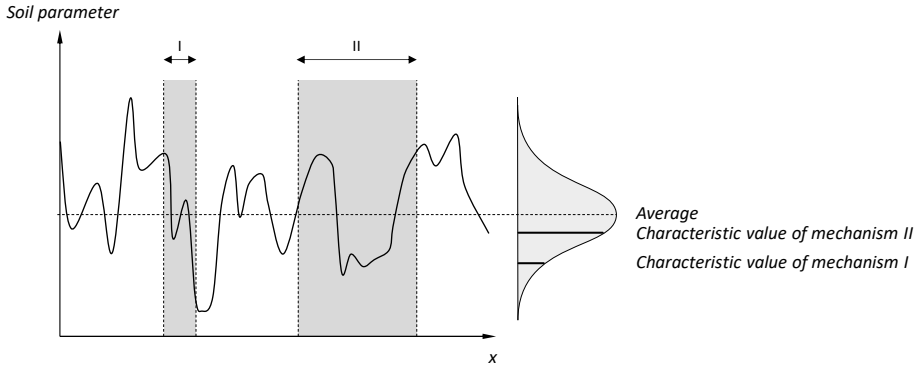

Figure 7.3: Schematic presentation of the characteristic value of two mechanisms with a different problem scale compared to the fluctuation scale (after [Calle et al., 2008])

Two types of soil investigations are distinguished: local and regional investigations. Local soil investigations consist of several tests performed at one location or one (homogeneous) site. The layer average, in analogy of the average of the mechanism, can be calculated as shown in equation (7.5) [Technische adviescommissie voor de waterkeringen, 1989], with standard deviation s.

$$s_{u,ave,char} = s_{u,ave} \pm t_{n-1}^{0.95} \cdot \frac{s}{\sqrt{n}} \tag{7.5}$$

Regional soil investigations on the other hand, comprise the determination of soil parameters on a large area. The results of the individual tests are used to compile a data collection. With the regional data collection, the spatial variation of the local averages is taken into account. The characteristic average value is calculated according to equation (7.6) [Technische adviescommissie voor de waterkeringen, 1989].

$$s_{u,ave,char} = s_{u,ave} \pm t_{0.95}^{n-1} \cdot s \cdot \sqrt{\Gamma^2 + \frac{1}{n}} \tag{7.6}$$

The spread reduction factor (Γ) averages the spread along the shear plane. Based on probabilistic stability analyses a value of Γ= 0.5 is suggested [Technische adviescommissie voor de waterkeringen, 1989]. It is assumed that the current test campaign (CPTu spaced every 50 m) can be interpreted as a regional soil investigation, because of the large spread in undrained shear strength. Hence, the second method (eq. 7.6) for calculating the characteristic average value will be applied for further analyses.

Figure 7.4 presents the characteristic undrained shear strength calculated per 0.5 m thick floating layer. Peak values were manually removed from the CPTu results. These peak values can be caused by anomalies in the subsoil (stones, debris, ...) or local sand layers (temporary construction road, ...), which may give a distorted picture of the undrained shear strength of the industrial sludge and its spread. Furthermore, the used methods for determining the undrained shear strength with the acquired cone factors are not applicable for sandy layers.

Further clustering of the results is necessary for implementation in a finite element analysis. For the sludge elevation (above 36 mTAW), two linear profiles were manually defined. For the sludge foundation (below 36 mTAW), several fixed values will be used.

For ease of notation, further reference to the active average characteristic undrained shear strength will be made as s_u^A instead of $s_{u,ave,char}^A$.

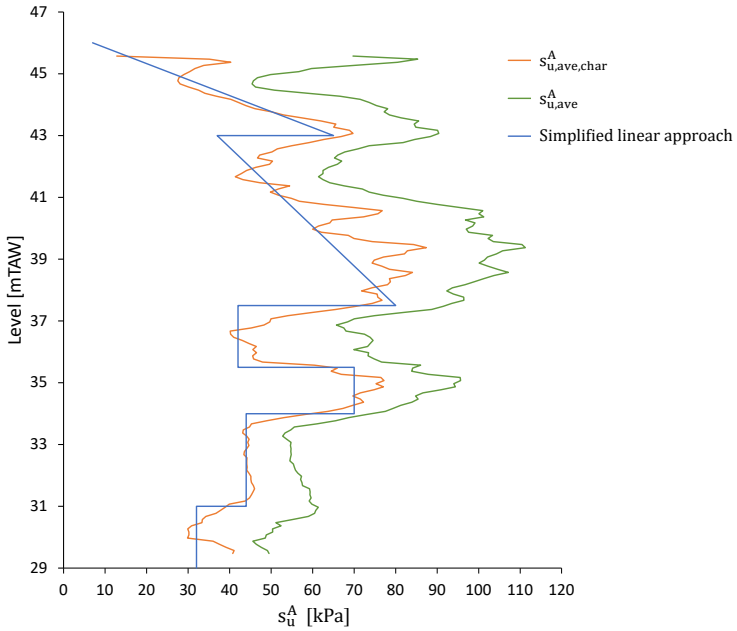

Figure 7.4: Result of active average undrained shear strength from CPTu S01 to S05 with $N_{kt,TC}$= 7.4 (above 36 mTAW) and $N_{kt,TC}$= 8.7 (below 36 mTAW), characteristic values and simplified linear approach for finite element analysis

7.4 Numerical analysis of embankment

7.4.1 Geometry

In the original design of the sludge embankment, a staged construction method was assumed to simulate the approximately yearly elevation of 1.5 to 3 m over the entire area of S3-3. Cone penetration tests, executed during an intermediate phase, indicated a significant variation of the shear strength of the sludge, whereas a more homogenous development of shear strength was expected. No staged construction model could account for the noticed variation of the cone resistance profile. An undrained analysis was chosen, where the results of the CPT were implemented. The undrained analysis is a snapshot of the stability at the moment of the soil investigations.

An intermediate evaluation of the sludge embankment was made to ensure the designed maximum height was to be reached safely. The elevation was constructed up to a height of about 45.8 mTAW, as shown in Figure 7.2, whereas the initial design height amounted 48.5 mTAW. The created model of the embankment is shown in Figure 7.5.

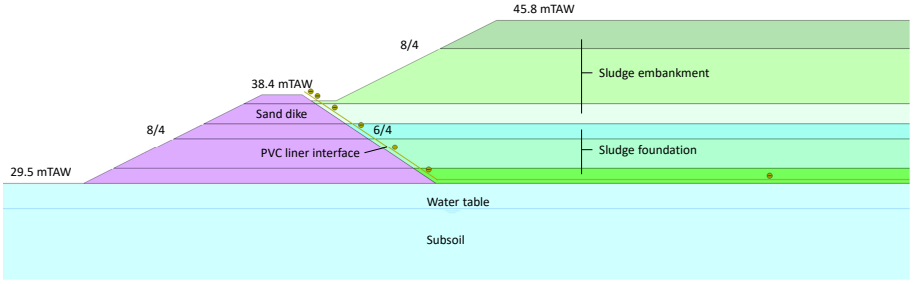

Figure 7.5: Finite element model of sludge embankment

The Plaxis finite element program (Version Plaxis CE 2020) is used in the stability analysis of the sludge embankment. Along the elevation on sub-deposit S3-3 the slope of the embankment was measured. An average slope of 8/4 (26.6°) was found. The bottom of the deposit and the inside of the surrounding sand dike is covered with a PVC geomembrane (thickness= 0.5 mm). The friction of the sludge-liner and liner-sand interface is unknown. It is expected that the sludge-liner interface will be the limiting interface. For thin smooth PVC geomembranes, a friction angle of 20.8° can be assumed [Bhatia and Kasturi, 1996], for a silty clay at 10% strain in shear tests. Considering the similarities in the behaviour between CaF_2 and clay, a similar interface friction is assumed.

In the undrained analyses, no angle of friction can be assigned to the interface between sludge and geomembrane. The interface strength must be defined as a ratio of the shear strength of the adjacent material (sludge). The angle of friction of the industrial sludge is about 30.5°, a ratio of 0.6 ($\approx \tan 20.8° / \tan 30.5°$) is used to simulate the reduction of the shear strength at the liner-sludge interface.

7.4.2 Material parameters

Different material models are used to evaluate the influence of the choice of material model on the stability analysis of the embankment. A hardening soil (HS) material model and a material model developed by the Norwegian Geotechnical Institute (NGI-ADP) are adopted. The corresponding parameters are given in tables 7.3 and 7.4.

The finite element program Plaxis, allows the users to define three types of undrained behaviour (A, B and C) in various material models. Method A corresponds to an analysis in terms of effective stresses, where effective strength parameters (c, ϕ', ψ') and effective stiffness parameters (E'_{50} and ν') are used.

Method B is also an analysis in terms of effective stresses with effective stiffness parameters as in method A. However, the strength parameters are undrained parameters ($c = c_u$ or s_u, $\phi = 0$, $\psi = 0$).

In method C, the analysis is performed based on total stresses, with undrained strength parameters ($c = c_u$ *or* s_u, $\phi = 0$, $\psi = 0$) and undrained stiffness parameters (E_u and $\nu = 0.495$).

It should be noted that not all methods of undrained behaviour are possible in every material model. Furthermore, every method (A, B and C) has its own advantages and disadvantages with regard to the available information on parameters, the computation of excess pore water pressures, effective stress paths, ...

7.4.3 NGI-ADP

With the NGI-ADP material model, the undrained C material behaviour type is used for an undrained analysis, with undrained parameters. The NGI-ADP model uses the undrained shear strength parameters (s_u^A) based on converted CPTu results. The cone factor for calculation of the shear strength was determined with field vane tests. Anisotropic conversion factors convert the field vane results to the required undrained shear strength value ($s_{u,ref}^A$).

The value $s^A_{u,ref}$ varies in the different layers defined in the model. The anisotropic conversion factors, with the corresponding plasticity index are used to establish the ratios s^P_u/s^A_u and s^{DSS}_u/s^A_u, as presented in Figure 6.14.

To be able to compare the results from the NGI-ADP material model and the HS material model calculations, a strain rate factor will be applied on the undrained shear strength in the NGI-ADP material model.

The assigned undrained shear strengths in the HS material model, are corrected with the Bjerrum correction factor, which, among others, includes a correction for the difference in rate of strain between field vane test and in situ slope failure. The influence of the rate of strain on the undrained shear strength depends on the plasticity index, as indicated in equations (6.3), (6.4) and (6.5). For the sludge elevation, the rate of strain effect is corrected with a factor of 0.8, based on the I_p of 30% and a time to failure of 10 000 min ($\approx$ 7 days) (in agreement with ASTM D2573). For the sludge foundation (I_p= 40%) a correction factor for the rate of strain of 0.77 is applied.

7.4.4 Hardening Soil

The hardening soil, undrained B material model requires both drained and undrained input parameters. In the HS model, the average laboratory undrained shear strength ($s_{u,Lab}$ or s_u) from triaxial compression, direct simple shear and triaxial extension, is the input parameter for shear strength. The undrained shear strength from field vane tests, corrected with the correction factor by Bjerrum [Bjerrum, 1972], is assumed to correspond to the average laboratory undrained shear strength. The conversion from CPTu results to $s_{u,Lab}$ profile, uses a cone factor, $N_{kt,Lab}$. The lab cone factor defined here differs from the cone factor $N_{kt,Lab}$ shown in table 7.2, which is derived from the average of the cone factors from the various stress states. In annex C the lab cone factor is calculated from the field vane test, corrected with the Bjerrum correction factor based on the plasticity index at the test locations. A lab cone factor of 12.3 is found.

It should be noted that the specific features of the advanced material models, such as the Hardening Soil model properties are mostly neglected in undrained B. Hence, the model basically behaves as a Mohr-Coulomb material model when regarding shear strengths.

Parameter	Symbol	Sludge elevation	Sludge foundation	Unit
General				
Material model	Model	NGI-ADP	NGI-ADP	
Type of material behaviour	Type	Undr. C	Undr. C	
Unsaturated unit weight	γ_{unsat}	17.5	16.5	[kN/m^3]
Saturated unit weight	γ_{sat}	17.5	16.5	[kN/m^3]
Initial void ratio	e	1.4	2.0	[-]
Parameters				
Ratio unloading/reloading shear modulus over active shear strength	G_{ur}/s_u^A	200	150	[-]
Shear strain in triaxial compression	γ_f^C	5	5	[%]
Shear strain in triaxial extension	γ_f^E	15	15	[%]
Shear strain in direct simple shear	γ_f^{DSS}	10	10	[%]
Reference active shear strength	$s_{u,ref}^A$	variable	variable	[kN/m^2]
Ratio of triaxial compression shear strength over active shear strength	$s_u^{C,TX}/s_u^A$	0.99	0.99	[-]
Ratio of passive shear strength over active shear strength	s_u^P/s_u^A	0.597	0.632	[-]
Initial mobilization	τ_0/s_u^A	0.7	0.7	[-]
Ratio of direct simple shear strength over active shear strength	s_u^{DSS}/s_u^A	0.746	0.762	[-]
Undrained Poisson's ratio	ν_u	0.495	0.495	[-]
Interfaces				
Interface strength (sludge-PVC liner)	R_{inter}	0.6	0.6	[-]

Table 7.3: Material properties of NGI-ADP material model for industrial sludge elevation and foundation

Parameter	Symbol	Sludge elevation	Sludge foundation	Unit
General				
Material model	Model	HS	HS	
Type of material behaviour	Type	Undr. B	Undr. B	
Unsaturated unit weight	γ_{unsat}	17.5	16.5	[kN/m^3]
Saturated unit weight	γ_{sat}	17.5	16.5	[kN/m^3]
Initial void ratio	e	1.4	2.0	[-]
Parameters				
Reference triaxial stiffness	E_{50}^{ref}	5500	2900	[kN/m^2]
Reference oedometer stiffness	E_{oed}^{ref}	2750	2300	[kN/m^2]
Reference un/reloading stiffness	E_{ur}^{ref}	24000	21000	[kN/m^2]
Power	m	0.9	0.9	[-]
Compression index	C_c	0.2	0.3	[-]
Swelling or reloading index	C_r	0.02	0.03	[-]
Undrained shear strength	s_u	variable	variable	[kN/m^2]
Poisson's ratio for un/reloading	ν_{ur}	0.2	0.2	[-]
Interfaces				
Interface strength (sludge-PVC liner)	R_{inter}	0.6	0.6	[-]

Table 7.4: Material properties of hardening soil material model for industrial sludge elevation and foundation

7.4.5 Results of slope analysis

The analysis of the sludge elevation using the NGI-ADP material model, indicated a factor of safety of 1.39. The failure mechanism is illustrated in Figure 7.6 by visualization of the incremental shear strains. A similar failure mechanism occurs with the hardening soil material model (Figure 7.7). A lower factor of safety, equal to 1.25, is found with the HS model.

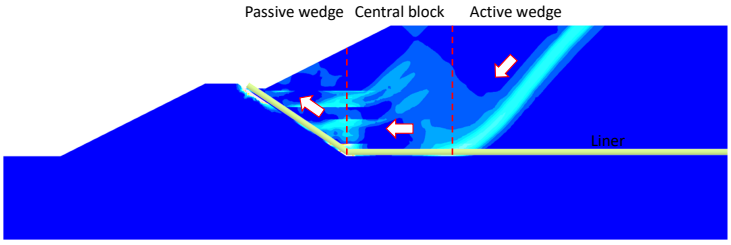

Figure 7.6: Indication of shear plane by visualisation of incremental shear strain at failure, NGI-ADP material model

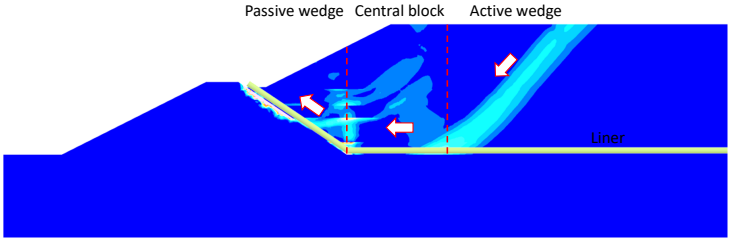

Figure 7.7: Indication of shear plane by visualisation of incremental shear strain at failure, HS material model

Due to the reduced friction at the bottom of the deposit (liner interface), a wedge-shaped failure mechanism occurs rather than a circular. In this case, an active wedge creates horizontal forces, a central bloc is displaced horizontally, and a passive wedge is pressed upwards. Both material models illustrate a nearly identical failure mechanism because of the liner interface governing the path of least resistance.

The difference in factor of safety is largely attributable to the assignment of the undrained shear strength. In the HS material model, an average undrained shear strength is assigned (mean of TC, DSS and TE) based on Bjerrum's correction factor, whereas in the NGI-ADP material model, different values are assigned to the various stress states, Active (TC), DSS and Passive (TE).

A large section of the shear plane consists of an active zone. The shear resistance in the horizontal (DSS) and passive zone is reduced along the PVC liner interface. Consequently, the shear strength of the active zone represents a significant part in the total shear resistance of the sludge elevation.

In the HS model, an average undrained shear strength is assumed, which is equal for active, DSS, and passive zone. In the NGI-ADP model the active undrained shear strength offers a higher shear strength in the active wedge, hereby significantly increasing the factor of safety.

A further elevation of the sludge embankment is possible according to the NGI-ADP analysis because of the, relatively, high factor of safety of 1.39. This indicates that there is some reserve in the shear resistance of the sludge.

The analysis with the HS model indicates a factor of safety of only 1.25. Adding additional material on top of the embankment would further decrease the safety, potentially risking slope failure. Hence, no further elevation of the embankment would be advised according to the HS material model analysis.

7.4.6 Sensitivity analysis

The variation of the factor of safety was calculated for different cone factors ($N_{kt,FV}$) and at varying plasticity index (I_p). The variation of the factor of safety (FS) is presented in Figure 7.8.

With the determined cone factor, $N_{kt,FV}$, of 11.0 and an average plasticity index of 30.2% ($\pm$7.6%) for the sludge elevation and 40% for the sludge foundation, a factor of safety of 1.39 was found using the NGI-ADP material model. Considering the variation of the plasticity index of the sludge, an increase or decrease of the FS is noticed. An increase in plasticity index by +10% leads to a lower FS of 1.19 ($-$15%). Whereas a lower plasticity index ($I_p - 10\%$) has a positive influence on the FS by increasing with 20% to 1.67.

A higher plasticity index results in less deviation (reduction of factor of safety) compared to a reduction of plasticity index. This disproportional deviation can be attributed to the influence of the plasticity index on the undrained shear strength ratio and therefore on the anisotropic correction factor (chapter 6, Figure 6.13 and 6.14).

The anisotropic correction factor is high for a low plastic soil, and lower for highly plastic soil. Since the relation is non-linear, the change in correction factor is not proportional to an equal increase or decrease of plasticity index.

The occurrence of slope failures commonly involves a large soil mass being displaced. The spread of parameters (such as plasticity index) will be levelled out by the vastness of the shear plane area. A good assumption for the average plasticity along the shear plane, will be the average plasticity of a group of soil samples.

Nevertheless, layers of noticeable higher or lower values of soil parameters should be identified as separate layers, as shear planes can preferentially develop in weaker areas. The implementation of the average plasticity index (of the elevation or foundation) can be justified by the levelling out of the influence on the factor of safety.

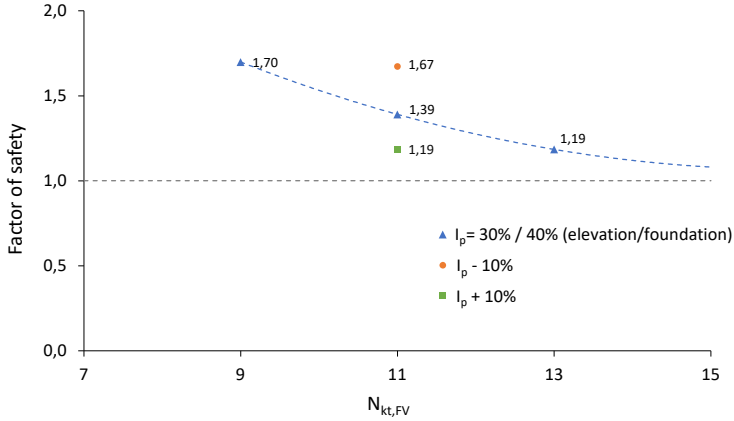

Figure 7.8: Influence of variation in cone factor ($N_{kt,FV}$) and plasticity index (I_p) on factor of safety for NGI-ADP material model calculations

To illustrate the influence of the variation of the cone factor on the factor of safety, the stability analysis was repeated with undrained shear strength determined with cone factors equal to 9 and 13. These cone factors correspond roughly to the minimum and maximum average cone factor determined at the five investigation locations, as described earlier. An increase of FS up to 1.70 (+22%) is the result of a lower cone factor of 9.0 instead of 11.0. A higher cone factor of 13.0 results in a decrease of FS (1.19 or −15%). The change in FS is significant, especially at low cone factors.

In addition, the determination of cone factor based on in situ (field vane tests) and laboratory tests (one-dimensional compression test and triaxial compression tests), see Chapter 5, indicated a large spread. The level of uncertainty of the method used for determining the cone factor is substantial. Caution is advised when using the described method because the variation in cone factor will greatly influence the result of the stability analysis.

7.5 Conclusions

In this chapter the stability of an embankment measuring 260 m × 135 m × 8 m, built with industrial CaF_2 sludge, is analyzed. The large variation of the material properties meant that the original design and calculations of the embankment, assuming a more homogeneous material, were no longer relevant. Because of the significant variation of the undrained shear strength of the different layers of the (partially) constructed embankment, it was chosen to assess the currently reached elevation height of the embankment with an undrained analysis. The recently developed NGI-ADP material model was compared to a classic undrained Hardening Soil model in the finite element program Plaxis.

The soil investigation program consisted of piezocone penetration tests, along with field vane tests at five locations. At these locations, samples were taken for triaxial and one-dimensional compression tests, described in chapter 5. For implementation of the material parameters in the NGI-ADP model, conversion factor for different stress states are needed.

The cone factor with field vane test as reference test, $N_{kt,FV}$, of 11.0 was converted with the anisotropic conversion factors determined in chapter 6, based on the dependency on the plasticity index. To represent the active undrained shear strength of the sludge, a cone factor of 7.4 and 8.7 (N_{kt}^{A}) was adopted for the sludge elevation (I_p= 30%) and sludge foundation (I_p= 40%) respectively. The average undrained shear strength for the HS model, is calculated using a cone factor of 12.3 ($N_{kt,Lab}$) based on field vane test, corrected with Bjerrum's correction factors.

The profiles of the undrained shear strength of the CPTu test with the determined cone factors, exhibit a large spread. Instead of a common Gauss distribution with standard deviation, an alternative method was used to determine the characteristic values of the undrained shear strength. The applied alternative method considers the spatial variation of local averages. Further clustering of the characteristic undrained shear strength profile with depth was executed for a simplified implementation in the finite element program.

Stability analyses of the built embankment were executed using, on one hand, an NGI-ADP material model and, on the other hand, a hardening soil material model. Both methods indicated a wedge and block shaped failure mechanism, formed due to the reduced resistance at the liner interface at the bottom of the sludge deposit. A significant difference in safety factor was found with the NGI-ADP model, resulting in a FS of 1.39, compared to the HS model with FS equal to 1.25.

In the NGI-ADP material model, the input data are the active undrained shear strength parameter (s_u^A) and ratios of s_u^P/s_u^A and s_u^{DSS}/s_u^A. The active undrained shear strength is based on the CPTu results, converted with the anisotropic conversion factors indicated in chapter 6, Figure 6.14. The cone factor is based on the (raw) field vane test results. An additional rate of strain correction factor was adopted. Note that when for example triaxial test results are used in analyses, rate of strain corrections are not common. However, it was chosen to correct the rate of strain for a better comparison with the HS model were a Bjerrum correction was used. This Bjerrum correction factor includes a rate of strain correction assuming a time to failure of 7 days.

The HS, undrained C model uses a single (average) undrained shear strength as input parameter. The cone factor for determining the undrained shear strength is based on field vane tests, corrected with the Bjerrum correction factors.

The presence of a liner on the bottom of the deposit and on the inside slope of the surrounding dike, reduced the influence of these shear zone on the total shear surface. Hence, the part where the active wedge is created represents the bulk of the shear resistance. In the NGI-ADP model, a higher undrained shear strength is obtained at active shear, whereas in the HS undrained C model, the average undrained shear strength is maintained along the entire shear surface. This results in a higher factor of safety with the NGI-ADP material model.

A sensitivity analysis indicated a disproportional influence of the plasticity index on the factor of safety. An increase in plasticity index results in a reduction of the factor of safety. Because the proposed anisotropic transformation factors do not show a linear relation with the plasticity index, a greater sensitivity is present at low plasticity. Since the occurrence of slope failures commonly involve large soil masses, the spread of soil parameters, such as the plasticity index, will be levelled out. Hence, the use of the average plasticity is justified. However, when soil layers with significant lower or higher plasticity are noticed during soil investigations, these layers should be considered as an individual layer in the further stability analysis.

The variation of the factor of safety depends strongly on the cone factor. The local averages at the five test locations for determination of $N_{kt,FV}$, range between 9 and 13, based on field vane test as reference. The overall average was 11.0. Because the calculation of the undrained shear strength uses the inverse of the cone factor, a significant increase on the factor of safety is found with a reduction of the $N_{kt,FV}$. A higher cone factor led to a lower factor of safety, however, the deviation was smaller.

The methodology used to determine the cone factors, based on in situ tests (field vane tests) and laboratory tests (oedometer and triaxial compression tests), shows a relatively large scatter for both. The level of uncertainty can be reduced by gathering more data and determining the cone factor based on test results spread over the terrain at multiple locations. Currently, the average cone factor, $N_{kt,FV}$, was used in the analysis. It may be considered to use a characteristic value of the cone factor. However, the undrained shear strength (calculated with $N_{kt,FV}$) is also reduced to the characteristic value. A double characteristic deduction may lead to an over conservative analysis.

Chapter 8

Summary of results and discussion

8.1 Overview

At the reorganisation of the company's old sludge deposits (complete removal of some deposits, elevation of one deposit above original dike level), the objective was to use a combination of naturally dried and consolidated sludge, filter pressed sludge and accelerated naturally dried sludge as construction material for the elevated embankments. By using the dried sludge itself as building material, the storage capacity of the remaining deposits can be increased. The low permeability and relatively fast elevation pace during the reconversion of the deposit sites, necessitates an undrained analysis. The re-stacking of previously consolidated sludge causes a highly unpredictable behaviour and strongly variable properties.

The purpose of this research was to evaluate different methods for characterisation of (historical) industrial sludge and to establish a cost-efficient, fast and reliable method to determine the parameters for the analysis of slope stability of (sludge) embankments. The industrial sludge shows similarities to (soft) clay, considering its low permeability and high water content. The sludge behaviour is based on material models and correlations which apply to clays, because of the lack of data and experience on this specific sludge material. However, deviant behaviour is possible, given the intrinsic differences in microscopic composition between clays and sludge. Furthermore, the sludge material's high variability of consolidation and large spread of the undrained parameters, needed to be taken into account.

Firstly, conclusions concerning the evaluation of the applied research methodology are summarised in 8.2.1 of which an important aspect concerns the method for determination of the cone factor.

Secondly, the accuracy of the most suitable method(s) is validated by performing a full-scale test. The stability results, obtained with the measured properties by the chosen test method, are then compared with the actual results of the full-scale test. The necessity of correction factors for the conversion from in situ or laboratory tests to full-scale test are determined.

Lastly, the established research methods and conversion parameters are applied on the stability analysis of a partially constructed embankment, built with CaF_2 sludge.

8.2 Conclusions

8.2.1 Soil characterisation

In situ and laboratory tests

The industrial CaF_2-sludge is regarded as a newly created waste material with soil-like properties. The method of stacking the industrial sludge in dunes and trenches, to enhance drying, in combination with a, strongly varying, fraction of glauconite containing sand, results in a material with heterogeneous properties. Hence, the characterisation of the material was mainly based on field investigations, accompanied by laboratory tests for reference.

A friction angle of 33.5% ($\pm$ 3.7%) and a cohesion of 8.0 kPa ($\pm$ 3.9 kPa) were found using the borehole shear test (BST) method. The results correspond to the friction angles obtained with triaxial compression tests, which indicated a peak angle of friction of 31.9% ($\pm$ 1.2%) or 30.5% ($\pm$ 2.0%) at ultimate strength, assuming a zero cohesion. The BST lacks pore water pressure measurements during pressurizing and shearing. Hence, the obtained parameters cannot be considered fully drained. The friction angle may therefore be underestimated and the cohesion overestimated, compared to fully drained parameters.

Piezocone penetration tests (CPTu) are essential in the profiling of soft soils in order to identify weak layers with potentially high pore water pressures. To estimate the cone factor for determination of undrained shear strength from net cone resistance of CPTu, a reference test must be at hand. In this research the cone factor was based on field vane tests and triaxial compression tests as reference.

Field vane tests were executed on the deposit sites which allows for a rapid estimating of the undrained shear strength, but at a lower accuracy compared to laboratory tests.

In addition to field tests, a series of triaxial compression tests and one-dimensional consolidation tests were executed. The investigation of the pre-consolidation stress (σ_p) with one-dimensional consolidation tests, shows a significant margin of error, thus decreasing the accuracy of estimation of the undrained shear strength at triaxial compression. One-dimensional consolidation tests can be replaced by CRS tests (Constant Rate of Strain) which could potentially increase the accuracy. Regarding the Critical State Soil Mechanic theory, a normal consolidation shear strength ratio (S) of 0.338 was obtained for the industrial sludge with the consolidated isotropic undrained triaxial compression tests.

Unlike the anisotropically consolidated undrained triaxial compression tests (CAU), proposed in literature, classic isotropic tests were performed on the industrial sludge. Limited availability and high cost of CAU triaxial testing currently restrict the usage to merely academic purposes or when the added value of the higher accuracy of CAU can result into a financial benefit in the further course of the project.

Determination of cone factor

The estimation of the cone factor for the determination of undrained shear strength from net cone resistance of CPTu tests, was based on reference tests with laboratory tests (triaxial compression tests and one-dimensional consolidation tests) and field vane tests. A cone factor of 11.0 was derived from field vane test ($N_{kt,FV}$). With laboratory tests, an average cone factor of 15.9 ($N_{kt,TC}$) was found. Comparison of literature data of cone factors of soils with similar plasticity index, indicated that the cone factor from field vane tests is on the low side, whereas ($N_{kt,TC}$) corresponds to a slightly overestimated value.

The cone factor from the triaxial compression test and one-dimensional consolidation test method has a large spread with results varying between 8.0 and 22.0. Determining the cone factor with this method has some advantages and disadvantages, as listed below.

- High quality data on the soil samples are obtained.
- The in situ effective vertical stress is to be estimated based on the soil volume weight, the position of the phreatic surface or estimations of the consolidation.

- The accuracy of the determination of the pre-consolidation stress at the one-dimensional consolidation test is limited to the chosen loading steps. An alternative method of determining the pre-consolidation stress is using constant rate of strain tests (CRS).
- Soil disturbance can occur while taking samples and/or when preparing samples for testing.
- The number of test points with the triaxial compression test and one-dimensional consolidation test method is limited due to the time-consuming sample taking and laboratory tests. More data points are preferable but will result in a costly research program.

The cone factor determined with field vane tests also exhibits a certain spread which can, partially, be attributed to the variation of the subsoil itself. The advantages and disadvantages of this method are listed below.

- A large set of data points can be obtained in a relatively short time span and at a low cost, which allows a better estimation of the spread. Furthermore, the larger dataset allows for a better comparison with the net cone resistance, resulting in a more accurate determination of the cone factor.
- The risk of sample/soil disturbance is limited since the soil is tested in situ. However, soil disturbance can occur when inserting the vane blades.
- The accuracy with field vane tests is lower compared to laboratory tests and the data acquired are limited to solely the undrained shear strength.
- Engineering judgement is required to distinguish erroneous measurements caused by disruptions in the subsoil.
- No information on over-consolidation can be obtained.

Taking into account the pros and cons of both methods and considering the large variation of the undrained shear strength in the sludge deposit, it was considered that the method with in situ field vane tests was the most suitable as reference test for the cone factor. For the presented case, it was considered that obtaining a larger data set will be more valuable compared to performing accurate laboratory tests on a limited number of samples.

8.2.2 Full-scale slope failure test

A full-scale slope failure test was performed and a back-calculation of the actual undrained shear strength of the industrial sludge at failure was executed. Field vane tests, executed on the test embankment, indicated a significant spread of the undrained shear strength. The large spread is mainly caused by the origin of the sludge material (sand inclusions, varying pre-consolidation, ...).

In a first back-analysis of the full-scale slope failure test, a Mohr-Coulomb material model was adopted and the raw field vane test results were corrected using a correction factor by Bjerrum [Bjerrum, 1972]. With the MC model, the results of the slope failure could not be reproduced with use of the corrected vane shear strengths. A lower crest load should have led to failure, hence the actual shear resistance is underestimated.

An alternative method was adopted where the different anisotropic stress states were implemented. The NGI-ADP material model was used to simulate the industrial sludge, in combination with anisotropic conversion factors for the vane shear test results. The NGI-ADP model well approached the results of the slope failure test, hence, proving the benefit of the material model and the implementation of anisotropic behaviour.

A second MC model was used which included the s_u^A value (active undrained shear strength) instead of the corrected undrained shear strength value. The second MC analysis gave a much better estimation of the failure load.

The use of anisotropic conversion factors is beneficial because the higher active shear strength is accounted for. Instead of an average undrained shear strength assumed along the shear plane, the different anisotropic shear strengths are assigned to the corresponding stress states along the shear surface.

Particularly for larger slopes the NGI-ADP model can be useful for undrained analysis since the different anisotropic shear strength ratios (active, DSS and passive) are implemented in the model. The average undrained shear strength of active, DSS and passive shear strength will be an underestimation of the average undrained shear strength along the entire shear surface if the active shear zone is larger compared to the DSS and passive zones.

8.2.3 Stability analysis of a sludge embankment

The elevation of sludge deposit Veldhoven S3-1, measuring 260 m $\times$ 135 m $\times$ 8 m build with industrial CaF_2 sludge, is analyzed using the adopted methods of anisotropic conversion and implementation in a NGI-ADP material model.

At several locations, the undrained shear strength was measured with piezocone tests. A cone factor (N_{kt}^{A}) of 7.4 was used for calculating the undrained shear strength in the NGI-ADP model, for calculating the active undrained shear strength (s_u^A) of the sludge in the elevation. In a hardening soil material model, a higher cone factor ($N_{kt,Lab} = 12.3$) was used for calculating the average undrained shear strength ($s_{u,ave}$), resulting in a lower shear strength.

The arbitrary profile of the CPTu required an alternative method for determining the characteristic parameters. By taking into account the spatial variation of local averages, a more realistic characteristic value is achieved in contrast to a Gauss distribution with standard deviation.

The sludge elevation was analyzed using on the one hand the NGI-ADP material model, and on the other hand the HS material model. Both methods indicated a similar failure mechanism. A higher factor of safety with the NGI-ADP model, compared to the HS model, can largely be attributed to assigning different strength parameters to the various stress states (active, passive, direct simple shear) in the soil.

The HS model uses an average undrained shear strength (average of active, passive, direct simple shear strength) for the entire shear surface. Nevertheless, the active shear zone is significantly larger compared to the other zones in the embankment. Since the active undrained shear strength is the highest shear strength ($s_u^A > s_u^{DSS} > s_u^P$), the NGI-ADP benefits from the large active shear zone, resulting in a higher factor of safety.

One should, however, be aware of strain compatibility along the slope. This mechanism implies that when peak resistance is achieved in a certain section along the shear surface, maximum resistance (ultimate or peak resistance) may not yet be reached in another part of the shear surface. This is due to the different strains at which active shear strength, direct simple shear strength and passive shear strength reaches their maximum value. After peak shear strength, softening can occur, resulting in a reduction of the shear strength for a certain stress state (e.g. active), whereas other stress states haven't reached peak or ultimate strength yet. Consequently, the factor of safety can be overestimated. It is advisable to verify the applied parameters (peak or ultimate values) and the corresponding shear strains for the various stress states.

A sensitivity analysis indicated a disproportional influence of the plasticity index on the slope stability. The factor of safety reduces with an increase in plasticity index. At low plasticity the variation is more significant. The reason for the disproportional influence lies in the proposed anisotropic transformation factors, which exhibit a non-linear relation with the plasticity index.

The factor of safety furthermore depends strongly on the cone factor. At the investigated site, the average cone factors, based on field vane shear tests, at the five investigated locations on Veldhoven S3 varied between 9 and 13. Compared to the safety factor of 1.39 for the overall average cone factor of 11, the factor of safety deviates up to 1.70 (+22%) for $N_{kt,FV} = 9$ and 1.19 (-15%) for $N_{kt,FV} = 13$. The variation is significant, especially at low cone factors.

The methods to determine the cone factor don't produce a highly reliable value. Taking into account the significant variation of the FS with the cone factor, caution is advised when defining a cone factor for a specific soil. In the present study, the average cone factor is adopted to calculate the undrained shear strength. If a characteristic value for the cone factor is used in the analysis, a lower level of uncertainty can be achieved. However, since the undrained shear strength (calculated with $N_{kt,FV}$) is also reduced to the characteristic value, a double characteristic deduction may lead to an over conservative design.

8.3 Recommendations for design, soil investigations and practice for construction of sludge embankments

For characterization of low permeability soils, such as industrial CaF_2 sludge, a combination of laboratory and field tests is advised. The execution of isotropically consolidated undrained triaxial compression (CIU) tests should provide the required parameters regarding the friction angle (ϕ') and undrained shear strength ratio (S). The more advanced anisotropically consolidated undrained triaxial compression test (CAU) would lead to a significant increase in research expenses, with a marginal benefit in accuracy and information. Only when a highly homogeneous material is present, it can be considered to execute some CAU test instead of several CIU tests.

Further testing would, among others, consists of one-dimensional consolidation tests (or constant rate of strain tests) for determining the compressibility and hydraulic conductivity, Atterberg's limits (plasticity index), ...

If the elevation is constructed on an existing sludge deposit, as in the presented study, in situ testing is necessary. Cone penetration tests are a simple and fast method for investigating a site at several locations and characterising the soil at greater depths. Any variation of the parameters can be mapped by spreading the tests across the terrain.

Piezocone testing is advised in low permeability soils since excess pore pressures arising during penetration are measured along with the present excess pore pressures in the soil. Hence, a more accurate measurement of the (net) cone resistance is obtained.

In order to calculate the undrained shear strength from the CPTu results, a cone factor needs to be determined. In heterogeneous soils, in situ tests (field vane tests) are advised since the variability can be taken into account. The accuracy of the in situ testing is, however, lower compared to laboratory tests. In contrast, a larger dataset can be obtain with fast and easy field vane tests, with a better understanding of the spread of the parameters.

A cone factor based on laboratory testing may have a higher accuracy if the soil samples are of good quality and are representative for the entire soil mass. Isotropic consolidated undrained triaxial compression test are used for determining the undrained shear strength ratio (S) along with one-dimensional consolidation tests for estimating the pre-consolidation pressure (σ'_p). Constant rate of strain test may enhance the estimation of the pre-consolidation pressure. Sufficient reference tests (lab or field vane tests) must be carried out for locations adjacent to CPTu tests in order to establish a reliable correlation.

For short term stability analyses, the NGI-ADP material model can be used. The use of the NGI-ADP material model has advantages regarding the direct input of undrained soil strength parameters and the anisotropic behaviour in the material model. The NGI-ADP material model is not suitable for accurately predicting the safety factor of slopes to be build, since the input parameter of the material model is the undrained shear strength. A hardening soil material model or soft soil model is advised for modelling the long term stability and to simulate the construction process with a staged construction method.

8.4 Recommendations for further research

In this thesis, the various aspects of different methods for determining the soil characteristics of the industrial CaF_2 sludge are discussed. After finishing the presented research, the following aspects for further study can be recommended.

Anisotropic conversion factors

The anisotropic conversion factors take into account the anisotropic behaviour of the soil at failure, with different shear strengths for different stress states (active, direct simple shear and passive).

In this thesis, the applied anisotropic conversion factors are solely based on literature data from soils with comparable properties (plasticity index). The results of safety analysis indicated a significant variability with the plasticity index, because of the used anisotropic conversion factors. At low plasticity, the variability is high and a small variation in plasticity index can result in a significant change in conversion factor.

To verify the assumed relation between conversion factor and plasticity index, a combination of triaxial compression and extension tests and direct simple shear tests are required. To improve the quality, tests with an anisotropic consolidation phase can be advised.

An extensive literature study of existing data on executed direct shear tests, triaxial compression and extension tests, could enhance the knowledge of the influence of anisotropy on the undrained shear strength regarding soils at different plasticity index. A verification of or adaptation to the anisotropic conversion factor defined in this thesis, based on [Ladd, 1991] and [Skempton, 1957], may benefit the accessibility of the NGI-ADP material model for undrained analysis.

Determination of cone factor

In this research only a limited study on the soil specific cone factor was executed. Significant variations of the cone factor were noticed with the used methods. Further research could focus on fine tuning the methods to determine the cone factor. Other in situ or laboratory testing is needed to establish a correlation with the measured net cone resistance by the piezocone.

Furthermore, the use of other methods for determining the undrained shear strength in a similar way to the cone penetration test may have potential. Full-flow penetrometers, such as the ball probe and T-bar probe, have a higher accuracy compared to the piezocone because of the greater projected area and were developed for measuring cone resistance in soft soils. Hence, the application may well be suited for the CaF_2 sludge.

Suction stresses

In partially saturated soils, suction stress can be present. The space between soil particles is partially filled with water and there is a negative pore water pressure. These suction stresses, which are cause by the absorption forces between water and soil particle, result in an increase in effective stress and, consequently, shear resistance.

The suction, or apparent cohesion, will influence the stability in a positive way, on the short term, but can disappear quickly by an sudden increase in water content (e.g. precipitation).

Some of the documented slope failures are triggered by a change in water level in the dewatering trenches. Tensiometers can be used to determine the suction stress and to asses the importance on the stability of slopes of dewatering trenches or embankments.

Sludge handling

An ongoing investigation at Veldhoven deposit involves the potential beneficial use of vertical drainage wicks to enhance the consolidation of sludge deposits, prior to excavation. The objective of the research is to reduce the water content of the sludge, hereby increasing the productivity of excavation and re-stacking works. Vertical wicks were installed in a 7 m thick sludge layer, which had been left to consolidate naturally for several decades. Limited natural consolidation had, however, taken place, still resulting in a high water content. The influence of vertical drainage wicks, combined with a vertical load (ballast) is being monitored by settlement measurements. The pore water pressure is monitored with open piezometer standpipes.

Besides the accelerated reduction in water content of the sludge drained by the vertical drainage wicks, the increase in shear resistance will be further evaluated by a combination of laboratory tests (triaxial compression tests, ...) and field tests (field vane tests, cone penetration tests, ...).

Appendix A

Results of piezocone penetration tests

This appendix contains the results of the piezocone penetration tests executed on deposit Veldhoven section S3-3.

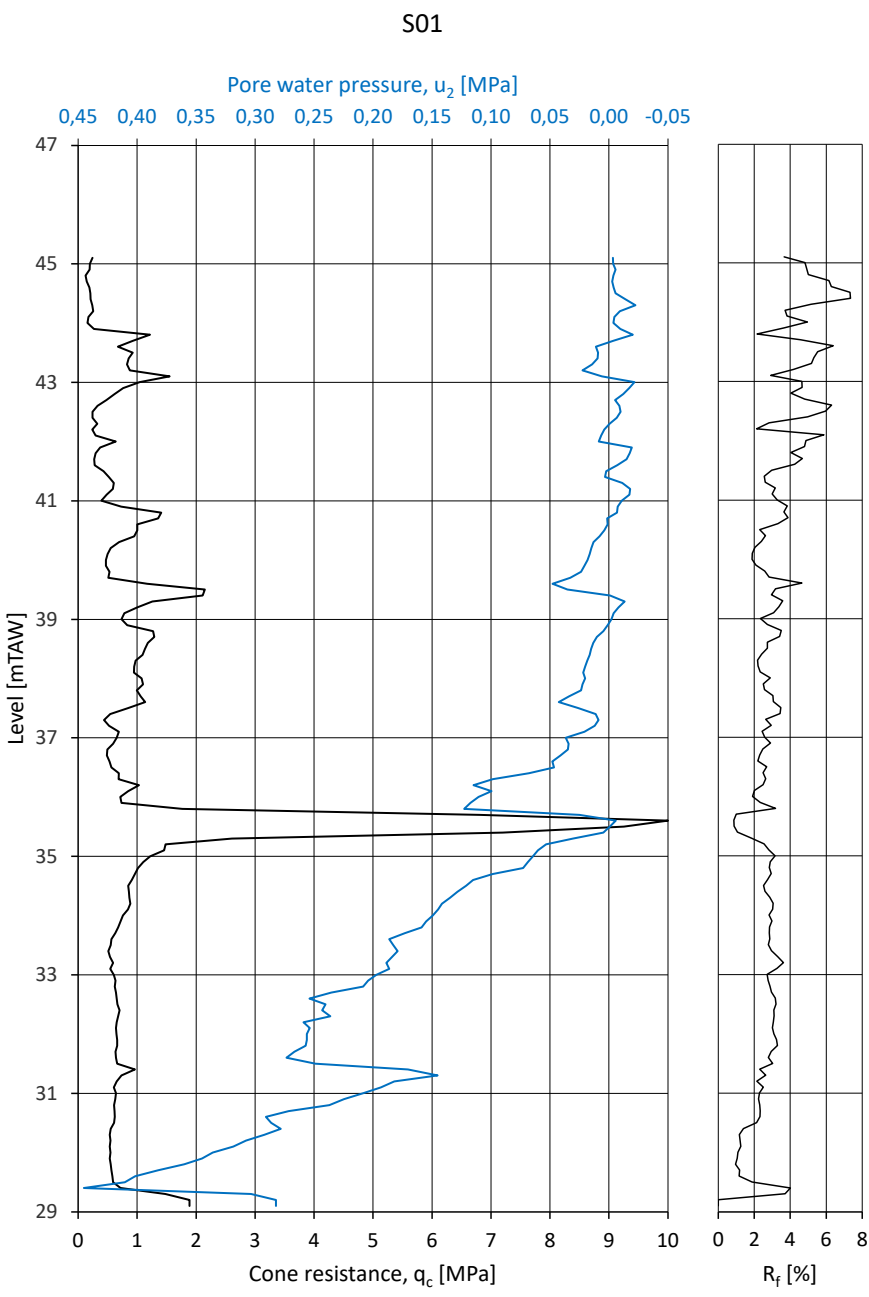

Figure A.1: Cone penetration test S01 on Veldhoven S3-3: Cone resistance (q_c), pore water pressure (u_2) and friction ratio (R_f)

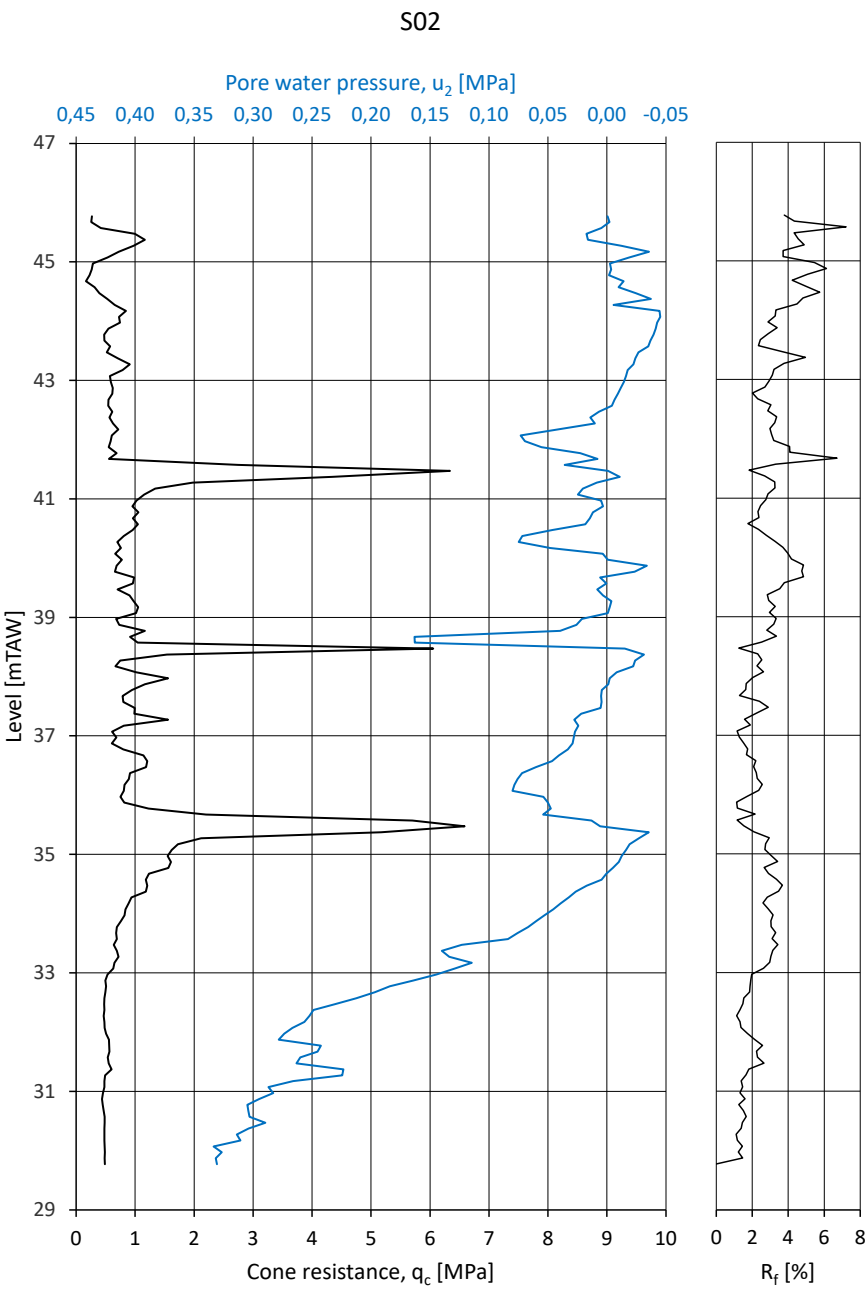

Figure A.2: Cone penetration test S02 on Veldhoven S3-3: Cone resistance (q_c), pore water pressure (u_2) and friction ratio (R_f)

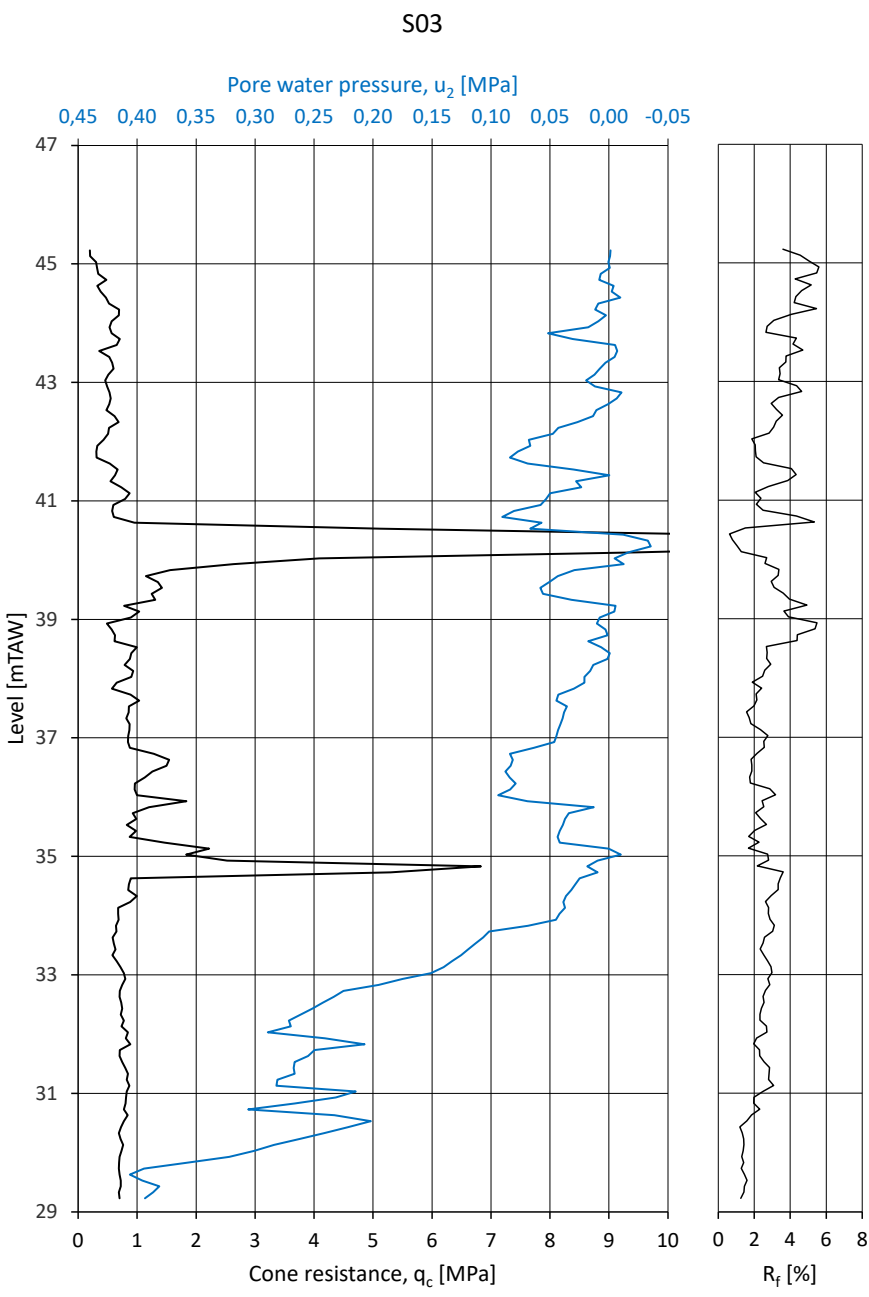

Figure A.3: Cone penetration test S03 on Veldhoven S3-3: Cone resistance (q_c), pore water pressure (u_2) and friction ratio (R_f)

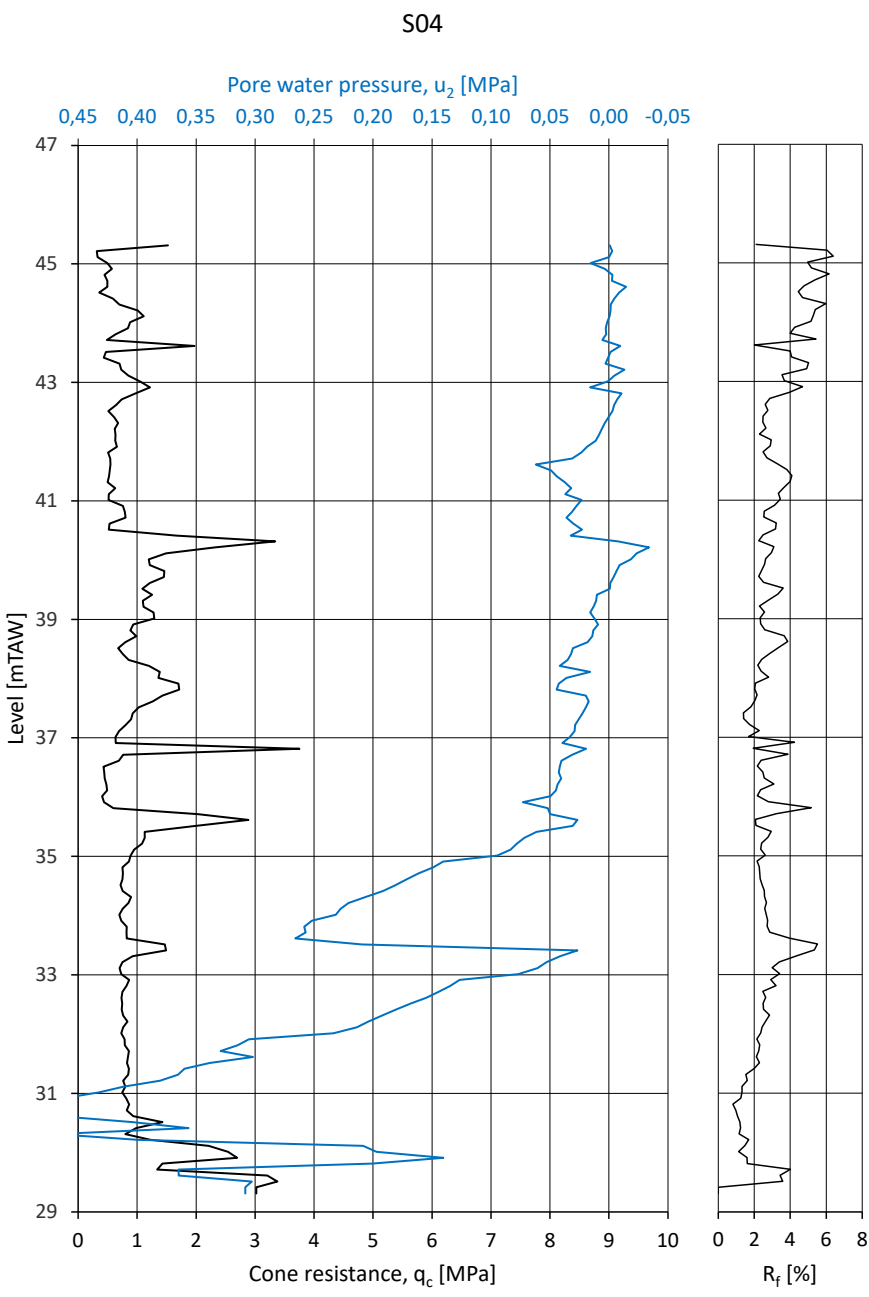

Figure A.4: Cone penetration test S04 on Veldhoven S3-3: Cone resistance (q_c), pore water pressure (u_2) and friction ratio (R_f)

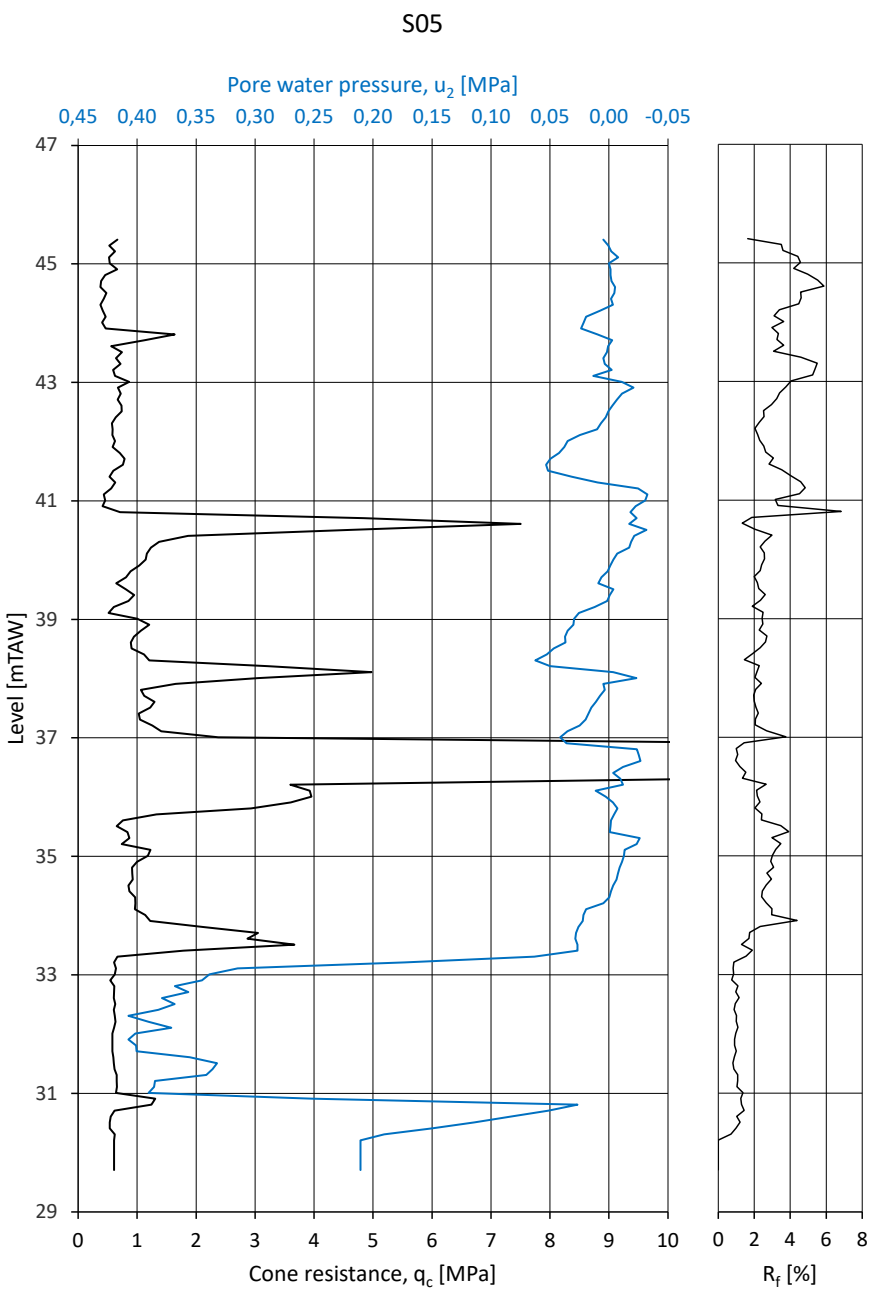

Figure A.5: Cone penetration test S05 on Veldhoven S3-3: Cone resistance (q_c), pore water pressure (u_2) and friction ratio (R_f)

Appendix B

Results of field vane tests

The field vane tests were executed with the Geonor H-70 apparatus, using a tapered vane measuring 60 mm × 120 mm. The measurement of the applied shear stress is limited to 160 kPa. The locations of the field vane tests are indicated on Figure 5.6.

Depth	Peak resistance	Residual resistance	Rod resistance	$s_{u,peak}$	$s_{u,res.}$	S_t
$[m]$	$[kPa]$	$[kPa]$	$[kPa]$	$[kPa]$	$[kPa]$	$[-]$
-0.5	15.0	10.0	0.0	15.0	10.0	1.5
-1.0	107.5	17.5	0.0	107.5	17.5	6.1
-1.5	120.0	25.0	15.0	105.0	10.0	10.5
-2.0	109.0	25.0	15.0	94.0	10.0	9.4
-2.5	74.0	27.5	15.0	59.0	12.5	4.7
-3.0	55.0	22.5	15.0	40.0	7.5	5.3
-3.5	48.0	22.5	20.0	28.0	2.5	11.2
-4.0	62.5	33.5	25.0	37.5	8.5	4.4
-4.5	72.5	37.5	32.5	40.0	5.0	8.0
-5.0	160.0	-	47.5	112.5	-	-

Table B.1: Results of field vane tests on location A

Depth	Peak resistance	Residual resistance	Rod resistance	$s_{u,peak}$	$s_{u,res.}$	S_t
$[m]$	$[kPa]$	$[kPa]$	$[kPa]$	$[kPa]$	$[kPa]$	$[-]$
-0.5	68.0	27.5	0.0	68.0	27.5	2.5
-1.0	62.0	30.0	7.5	54.5	22.5	2.4
-1.5	45.0	17.0	0.0	45.0	17.0	2.6
-2.0	77.5	15.0	5.0	72.5	10.0	7.3
-2.5	62.5	30.0	7.5	55.0	22.5	2.4
-3.0	69.0	36.0	17.0	52.0	19.0	2.7
-3.5	65.0	36.0	22.5	42.5	13.5	3.1
-4.0	119.0	50.0	27.0	92.0	23.0	4.0
-4.5	120.0	55.0	30.0	90.0	25.0	3.6
-5.0	117.5	60.0	42.0	75.5	18.0	4.2

Table B.2: Results of field vane tests on location B

Depth	Peak resistance	Residual resistance	Rod resistance	$s_{u,peak}$	$s_{u,res.}$	S_t
$[m]$	$[kPa]$	$[kPa]$	$[kPa]$	$[kPa]$	$[kPa]$	$[-]$
-0.5	20.0	5.0	6.3	13.8	0.0	-
-1.0	37.5	10.5	6.3	31.3	4.3	7.4
-1.5	69.0	17.5	14.5	54.5	3.0	18.2
-2.0	100.0	31.0	14.3	85.8	16.8	5.1
-2.5	82.5	52.5	15.5	67.0	37.0	1.8
-3.0	97.5	41.0	18.8	78.8	22.3	3.5
-3.5	126.0	14.0	21.3	104.8	-	-
-4.0	94.0	21.0	28.0	66.0	-	-
-4.5	110.0	47.5	31.3	78.8	16.3	4.8
-5.0	86.0	17.5	37.5	48.5	-	-

Table B.3: Results of field vane tests on location C

Depth	Peak resistance	Residual resistance	Rod resistance	$s_{u,peak}$	$s_{u,res.}$	S_t
$[m]$	$[kPa]$	$[kPa]$	$[kPa]$	$[kPa]$	$[kPa]$	$[-]$
-0.5	20.0	12.5	12.5	7.5	0.0	-
-1.0	41.0	10.0	12.5	28.5	0.0	-
-1.5	67.5	22.5	14.0	53.5	8.5	6.3
-2.0	65.0	27.5	13.5	51.5	14.0	3.7
-2.5	85.0	35.0	16.0	69.0	19.0	3.6
-3.0	107.5	47.5	22.5	85.0	25.0	3.4
-3.5	67.5	37.5	22.5	45.0	15.0	3.0
-4.0	83.0	40.0	31.0	52.0	9.0	5.8
-4.5	70.0	45.0	30.0	40.0	15.0	2.7
-5.0	>160					

Table B.4: Results of field vane tests on location D

Depth	Peak resistance	Residual resistance	Rod resistance	$s_{u,peak}$	$s_{u,res.}$	S_t
$[m]$	$[kPa]$	$[kPa]$	$[kPa]$	$[kPa]$	$[kPa]$	$[-]$
-0.5	57.5	11.0	0.0	57.5	11.0	5.2
-1.0	80.0	17.0	0.0	80.0	17.0	4.7
-1.5	68.0	15.0	5.0	63.0	10.0	6.3
-2.0	115.0	36.5	8.0	107.0	28.5	3.8
-2.5	77.5	40.0	12.0	65.5	28.0	2.3
-3.0	64.0	27.5	13.0	51.0	14.5	3.5
-3.5	70.0	28.5	15.0	55.0	13.5	4.1
-4.0	76.0	35.0	22.5	53.5	12.5	4.3
-4.5	142.5	30.0	26.0	116.5	4.0	29.1
-5.0	>160					

Table B.5: Results of field vane tests on location E

Appendix C

Determination of cone factor based on field vane tests

The cone factor is determined based on field vane test executed near piezocone penetration tests. The net cone resistance is determined for a layer thickness of 0.5 m. The following equations are used for the calculation of the cone factor.

$$q_t = s_u \cdot N_{kt} + \sigma_{v0} \tag{C.1}$$

$$q_t = q_c + u_2(1 - a) \tag{C.2}$$

$$q_{net} = q_t - \sigma_{v0} \tag{C.3}$$

$$s_{u,CPTu} = \frac{q_{net}}{N_{kt}} \tag{C.4}$$

$$N_{kt} = \frac{q_{net}}{s_{u,FV}} \tag{C.5}$$

For the calculation of the average cone factor, the following rules were used to exclude values.

- $q_{net} \geq 1500kPa$, potential sand layers
- $N_{kt} \geq 5$, mismatch of data, overestimation of shear resistance
- $N_{kt} \leq 30$, mismatch of data, underestimation of shear resistance

Other parameters:

- Volume weight of sludge 17.5 kN/m³ for upper part (46 - 36 mTAW)
- Volume weight of sludge 16.5 kN/m³ for lower part (36 - 29 mTAW)
- a factor = 0.75

Depth	$s_{u,FV}$	q_c	u_2	σ_{v0}	q_{net}	$N_{kt,FV}$	$s_{u,CPTu}$
$[m]$	$[kPa]$	$[kPa]$	$[kPa]$	$[kPa]$	$[kPa]$	$[-]$	$[kPa]$
-0.5	15.0	172.8	-4.3	8.8	163	10.9	14.1
-1.0	107.5	208.4	-10.8	17.5	188	(1.8)	(16.3)
-1.5	105.0	804.4	-2.7	26.3	777	7.4	67.2
-2.0	94.0	1031.6	-6.1	35.0	997	10.6	86.3
-2.5	59.0	486.4	-10.6	43.8	440	7.5	38.0
-3.0	40.0	348.4	2.4	52.5	297	7.4	25.6
-3.5	28.0	330.8	-11.3	61.3	267	9.5	23.1
-4.0	37.5	517.6	-10.8	70.0	445	11.9	38.5
-4.5	40.0	1101.2	-1.5	78.8	1022	25.6	88.4
-5.0	41.0	634.0	14.1	87.5	550	13.4	47.5
Average						**11.1 ± 5.6**	

Table C.1: Calculation of N_{kt} at location A, based on field vane test. $s_{u,CPTu}$ based on average N_{kt}.

Depth	$s_{u,FV}$	q_c	u_2	σ_{v0}	q_{net}	$N_{kt,FV}$	$s_{u,CPTu}$
$[m]$	$[kPa]$	$[kPa]$	$[kPa]$	$[kPa]$	$[kPa]$	$[-]$	$[kPa]$
-0.5	68.0	855.2	-1.9	9.0	846	12.4	84.8
-1.0	54.5	294.8	-8.2	18.0	275	5.0	27.5
-1.5	45.0	546.0	-24.3	27.0	513	11.4	51.4
-2.0	72.5	595.2	-41.0	36.0	549	7.6	55.0
-2.5	55.0	699.2	-25.2	45.0	648	11.8	64.9
-3.0	52.0	588.8	-11.5	54.0	532	10.2	53.3
-3.5	42.5	613.6	13.7	63.0	554	13.0	55.5
-4.0	92.0	597.2	45.8	72.0	537	5.8	53.8
-4.5	90.0	3348.0	10.6	81.0	3270	(36.3)	(327.7)
-5.0	75.5	1029.2	11.9	90.0	942	12.5	94.4
Average						**10.0 ± 3.0**	

Table C.2: Calculation of N_{kt} at location B, based on field vane test. $s_{u,CPTu}$ based on average N_{kt}.

Depth	$s_{u,FV}$	q_c	u_2	σ_{v0}	q_{net}	$N_{kt,FV}$	$s_{u,CPTu}$
$[m]$	$[kPa]$	$[kPa]$	$[kPa]$	$[kPa]$	$[kPa]$	$[-]$	$[kPa]$
-0.5	27.0	354.4	2.2	9.0	346	12.8	28.3
-1.0	33.5	552.4	2.3	18.0	535	16.0	43.7
-1.5	27.5	604.8	20.7	27.0	583	21.2	47.7
-2.0	44.0	514.8	2.3	36.0	479	10.9	39.2
-2.5	40.0	512.4	3.0	45.0	468	11.7	38.3
-3.0	41.5	562.4	28.3	54.0	515	12.4	42.1
-3.5	62.0	383.6	73.0	63.0	339	5.5	27.7
-4.0	74.0	690.4	26.2	72.0	625	8.4	51.1
-4.5	57.5	706.4	67.9	81.0	642	11.2	52.5
-5.0	50.0	10554.8	-6.0	90.0	10463	(209.3)	(855.4)
Average						**12.2 ± 4.4**	

Table C.3: Calculation of N_{kt} at location C, based on field vane test. $s_{u,CPTu}$ based on average N_{kt}.

Depth [m]	$s_{u,FV}$ [kPa]	q_c [kPa]	u_2 [kPa]	σ_{v0} [kPa]	q_{net} [kPa]	$N_{kt,FV}$ [$-$]	$s_{u,CPTu}$ [kPa]
-0.5	7.5	467.2	2.7	9.0	459	(61.2)	(34.0)
-1.0	28.5	630.4	-6.1	18.0	611	21.4	45.2
-1.5	53.5	792.4	2.3	27.0	766	14.3	56.7
-2.0	51.5	862.8	-4.0	36.0	826	16.0	61.1
-2.5	69.0	966.0	-1.1	45.0	921	13.3	68.1
-3.0	85.0	612.8	0.5	54.0	559	6.6	41.4
-3.5	45.0	594.0	18.6	63.0	536	11.9	39.6
-4.0	52.0	547.6	45.0	72.0	487	9.4	36.0
-4.5	40.0	678.4	31.0	81.0	605	15.1	44.8
-5.0	>160.0	1676.8	8.8	90.0	1589	(209.3)	(117.6)
Average						**13.5 ± 4.5**	

Table C.4: Calculation of N_{kt} at location D, based on field vane test. $s_{u,CPTu}$ based on average N_{kt}.

Depth [m]	$s_{u,FV}$ [kPa]	q_c [kPa]	u_2 [kPa]	σ_{v0} [kPa]	q_{net} [kPa]	$N_{kt,FV}$ [$-$]	$s_{u,CPTu}$ [kPa]
-0.5	57.5	585.0	-1.1	4.5	580	10.1	61.6
-1.0	80.0	484.0	-2.0	12.6	471	5.9	50.0
-1.5	63.0	436.0	3.5	21.6	415	6.6	44.1
-2.0	107.0	840.0	10.5	30.6	812	7.6	86.2
-2.5	65.5	665.2	4.2	39.6	627	9.6	66.6
-3.0	51.0	733.6	-10.5	48.6	682	13.4	72.5
-3.5	55.0	622.8	9.0	57.6	567	10.3	60.3
-4.0	53.5	692.8	43.6	66.6	637	11.9	67.7
-4.5	116.5	550.4	7.1	75.6	477	(4.1)	(50.6)
-5.0	>160.0	2786.0	-22.4	84.6	2696	(16.8)	(286.3)
Average						**9.4 ± 2.6**	

Table C.5: Calculation of N_{kt} at location E, based on field vane test. $s_{u,CPTu}$ based on average N_{kt}.

Bibliography

[Aas et al., 1986] Aas, G., Lacasse, S., Lunne, T., and Høeg, K. (1986). Use of in-situ tests for foundation design on clay. In Clemence, S. P., editor, *Proceedings of In Situ '86, Use of in Situ Tests in Geotechnical Engineering (ASCE)*, pages 1–30, Blacksburg, Virginia, US.

[Almeida and Parry, 1983] Almeida, M. S. S. and Parry, R. H. G. (1983). Tests with centrifuge vane and penetrometer in a normal gravity field, technical report, soils tr 141. Technical report, Cambridge University. SOILS TR 141.

[Andresen, 2002] Andresen, L. (2002). *Capacity analysis of anisotropic and strain-softening clay.* PhD thesis, University of Oslo, Institue of Geology.

[Andresen and Jostad, 1999] Andresen, L. and Jostad, H. (1999). Application of an anisotropic hardening model for undrained response of saturated clay. In Ppande, G. N., Pietruszczak, S., and Schweiger, H. F., editors, *International Symposium on Numerical Models in Geomechanics. NUMOG VII*, pages 581–585.

[ASTM D2435 / D2435M-11, 2011] ASTM D2435 / D2435M-11 (2011). *Standard Test Methods for One-Dimensional Consolidation Properties of Soils Using Incremental Loading.* American Society of Testing and Materials (ASTM) International, West Conshohocken, PA, 2011.

[ASTM D2573 / D2573M-18,] ASTM D2573 / D2573M-18. *Standard Test Method for Field Vane Shear Test in Saturated Fine-Grained Soils.* American Society of Testing and Materials (ASTM) International, West Conshohocken, PA, 2018.

[ASTM D4318-17e1, 2017] ASTM D4318-17e1 (2017). *Standard Test Methods for Liquid Limit, Plastic Limit, and Plasticity Index of Soils.* American Society of Testing and Materials (ASTM) International, West Conshohocken, PA, 2017.

[ASTM D4767-11, 2011] ASTM D4767-11 (2011). *Standard Test Method for Consolidated Undrained Triaxial Compression Test for Cohesive Soils*. American Society of Testing and Materials (ASTM) International, West Conshohocken, PA, 2011.

[Azzouz et al., 1983] Azzouz, A. S., Baligh, M. M., and Ladd, C. C. (1983). Corrected field vane strength for embankment design. *ASCE Journal of Geotechnical Egineering*, 109(5):730–734.

[Balasubramaniam et al., 2010] Balasubramaniam, A. S., Cai, H., Zhu, D., Surarak, C., and Oh, E. Y. N. (2010). Settlement of embankments in soft soils. *Geotechnical Engineering Journal of the SEAGS & AGSSEA*, 41(1):61–78.

[Baligh et al., 1987] Baligh, M. M., Azzouz, A. S., and Chin, C. T. (1987). Disturbances due to ideal tube sampling. *Journal of Geotechnical Engineering*, 113(7):739–757.

[Becker et al., 1987] Becker, D. E., Crooks, J. H. A., Been, K., and Jefferies, M. G. (1987). Work as a criterion for determining in situ and yield stresses in clays. *Canadian Geotechnical Journal*, 24(4):549–564.

[Bhatia and Kasturi, 1996] Bhatia, S. K. and Kasturi, G. (1996). Comparison of PVC and HDPE geomembranes (interface friction performance). *Report for PVC Geomembrane Institute, Syracuse University*.

[Billington, 1988] Billington, E. W. (1988). Generalized isotropic yield criterion for incompressible materials. *Acta mechanica*, 72(1-2):1–20.

[Bishop, 1955] Bishop, A. W. (1955). The use of the slip circle in the stability analysis of slopes. *Géotechnique*, 5(1):7–17.

[Bjerrum, 1972] Bjerrum, L. (1972). Embankments on soft ground. In *Conference on Perfomance of Earth and Earth-supported Structures (ASCE)*, volume 2, pages 1–54, Purdue University.

[Bjerrum, 1973] Bjerrum, L. (1973). Problems of soil mechanics and construction on soft clays. In *Proceeding of 8th internation conference on soil mechcanisc and foundation, state of the art report*, volume 3, pages 111–159.

[Brinkgreve and Ragi Manoj, 2019] Brinkgreve, R. B. J. Zampich, L. M. and Ragi Manoj, N. (2019). Plaxis 2D connect edition V20 manual. Technical report, Plaxis bv, Bentley Systems, incorporated.

[Burmister, 1950] Burmister, D. M. (1950). Principles and techniques of soil identification. In *Proceedings of the 29th annual meeting of the Highway Research Board*, volume 29, pages 402–433.

[Calle et al., 2008] Calle, E., Vrouwenvelder, T., Lindenber, J., Hannink, G., and Bruijn, E. (2008). Representatieve waarden voor grondparameters in de geotechniek. *Geotechniek*, (2):24–29. In Dutch.

[Casagrande, 1936] Casagrande, A. (1936). The determination of the pre-consolidation load and its practical significance. In *Proceedings of the International Conference on Soil Mechanics and Foundation Engineering*, volume 3, pages 60–64, Harvard University, Cambridge.

[Chandler, 1988] Chandler, R. J. (1988). The in situ measurement of the undrained shear strenght of clays using the field vane. In *Proceeding of the International Symposium on Vane Shear Strength Testing in Soils*, pages 13–44.

[Craeynest and Suys, 2010] Craeynest, E. and Suys, E. (2010). Onderzoek naar het structureel gedrag van een industrieel slib. Master's thesis, Department of Civil Engineering, KU Leuven.

[De Beer, 1977] De Beer, E. (1977). Static cone penetration testing in clay and loam. In *Proceedings of Sonder Symposium, Fugro*, pages 15–23.

[Deschamps and Yankey, 2006] Deschamps, R. and Yankey, G. (2006). Limitations in the back-analysis of strength from failures. *Journal of Geotechnical and Geoenvironmental Engineering (ASCE)*, 132(4):532–536.

[Duncan et al., 2014] Duncan, J. M., Wright, S. G., and Brandon, T. L. (2014). *Soil strength and slope stability*. John Wiley & Sons.

[Grimstad et al., 2012] Grimstad, G., Andresen, L., and Jostad, H. P. (2012). NGI-ADP: Anisotropic shear strength model for clay. *International Journal for Numerical and Analytical Methods in Geomechanics*, 36(4):483–497.

[Handy, 1986] Handy, R. L. (1986). Borehole shear test and slope stability. In Clemence, S. P., editor, *Proceedings of In Situ '86, Use of in Situ Tests in Geotechnical Engineering (ASCE)*, pages 161–175, Blacksburg, Virginia, US.

[Hinchberger and Rowe, 1998] Hinchberger, S. D. and Rowe, R. K. (1998). Modelling the rate-sensitive characteristics of the gloucester foundation soil. *Canadian Geotechnical Journal*, 35(5):769–789.

[Hunter and Fell, 2003] Hunter, G. and Fell, R. (2003). Prediction of impending failure of embankments on soft ground. *Canadian geotechnical journal*, 40(1):209–220.

[Indraratna et al., 2005] Indraratna, B., Sathananthan, I., Bamunawita, C., and Balasubramaniam, A. S. (2005). Chapter 2 theoretical and numerical

perspectives and field observations for the design and performance evaluation of embankments constructed on soft marine clay. In Indraratna, B. and Chu, J., editors, *Ground Improvement — Case Histories*, volume 3 of *Elsevier Geo-Engineering Book Series*, pages 51 – 89. Elsevier.

[Jaky, 1944] Jaky, J. (1944). The coefficient of earth pressure at rest (in hungarian). *Journal of the Society of Hungarian Architects and Engineers*, pages 355–358.

[Jamiolkowski et al., 1985] Jamiolkowski, M., Ladd, C. C., Germaine, J. T., and Lancelotta, R. (1985). New devolopments in field and laboratory testing of soils. In *Proceedings of the 11th Conference on Soil Mechanics and Foundation Engineering*, volume 1, pages 57–153, San Francisco.

[Karlsrud et al., 2005] Karlsrud, K., Lunne, T., Kort, D. A., and Strandvik, S. (2005). CPTU correlations for clays. In *Proceedings of the 16th International Conference on Soil Mechanics and Geotechnical Engineering*, volume 2, pages 693–702. Balkema.

[Karstunen et al., 2005] Karstunen, M., Krenn, H., Wheeler, S. J., Koskinen, M., and Zentar, R. (2005). Effect of anisotropy and destructuration on the behavior of murro test embankment. *International Journal of Geomechanics*, 5(2):87–97.

[Koutsoftas and Ladd, 1985] Koutsoftas, D. C. and Ladd, C. C. (1985). Design strengths for an offshore clay. *Journal of Geotechnical Engineering*, 111(3):337–355.

[La Rochelle et al., 1988] La Rochelle, P., Zbdi, P. M., Leroueil, S., Tavenas, F., and Virely, D. (1988). Piezocone tests in sensitive clays of eastern canada. In *Proceedings of the International Symposium on Penetration Testing. ISOPT-1*, volume 2, pages 831–841, Orlando.

[Ladanyi, 1967] Ladanyi, B. (1967). Deep punching of sensitive clays. In *Proceedings of the 3rd Pan American Conference on Soil Mechanics and Foundation Engineering, Sociedad Venezolana de Mecánica del Suelo e Ingeniería de Fundaciones*, pages 533–546.

[Ladd, 1969] Ladd, C. C. (1969). The prediction of in situ strees-strain behaviour of soft saturated clay during undrained shear. *Proceedings NGI Bolkesjo Symposium*, pages 14–20.

[Ladd, 1991] Ladd, C. C. (1991). Stability evaluation during staged construction. *Journal of geotechnical engineering*, 117(4):540–615.

[Ladd and Degroot, 2003] Ladd, C. C. and Degroot, D. J. (2003). Recommended practice for soft ground site characterization. In Culligan, P. J., Einstein, H. H., and Whittle, A. J., editors, *12th Panamerican Conference on Soil Mechanics and Geotechnical Engineering (PCSMGE)*, volume 1, pages 3–58.

[Ladd and Foott, 1974] Ladd, C. C. and Foott, R. (1974). New design procedure for stability of soft clays. *Journal of Geotechnical and Geoenvironmental Engineering*, 100(7):763–786.

[Ladd et al., 1977] Ladd, C. C., Foott, R., Ishihara, K., Schlosser, F., and Poulos, H. G. (1977). Stress-deformation and strength characteristics. In *Proceeding of the 9th International Conference on Soil Mechanics and Foundation Engineering*, volume 3, pages 421–494, Tokyo, Japan.

[Ladd and Lambe, 1963] Ladd, C. C. and Lambe, T. W. (1963). The strength of "undisturbed" clay determined from undrained tests. In *Symposium on Laboratory Shear Testing of Soils*, pages 342–371, Ottawa, Canada.

[Larsson and Mulabdic, 1991] Larsson, R. and Mulabdic, M. (1991). Piezocone tests in clay. Technical Report Report No 42, Swedish Geotechnical Institute, Linköping, Sweden.

[Lefebvre et al., 1983] Lefebvre, G., Ladd, C. C., Mesri, G., and Tavenas, F. (1983). Report of the testing committee. Technical report, Committee of Specialists on Sensitive Clays on the NBR Complex.

[Löfroth, 2008] Löfroth, H. (2008). *Undrained shear strength in clay slopes - Influence of stress conditions. A model and field test study.* PhD thesis, Chalmers university of technology, Department of Civil and Environmental Engineering.

[Lunne and Kleven, 1981] Lunne, T. and Kleven, A. (1981). Role of CPT in North sea foundation engineering. *Symposium on Cone Penetration Engineering Division (ASCE)*, pages 907–912.

[Lunne et al., 1997] Lunne, T., Robertson, P. K., and Powell, J. J. M. (1997). *Cone-penetration testing in geotechnical practice.* CRC Press.

[Magnus et al., 2005] Magnus, R., Teh, C. I., and Lau, J. M. (2005). *Report of the committee of inquiry into the incident at the MRT Circle Line worksite that led to the collapse of the Nicoll Highway on 20 April 2004*, volume 1. Ministry of Manpower.

[Mansikkamäki, 2015] Mansikkamäki, J. (2015). *Effective stress finite element stability analysis of an old railway embankment on soft clay.* PhD thesis, Julkaisu-Tampere University of Technology.

[Mayne, 1980] Mayne, P. W. (1980). Cam-Clay predictions of undrained strength. *Journal of Geotechnical Engineering (ASCE)*, 106(11):1219–1242.

[Mayne and Mitchell, 1988] Mayne, P. W. and Mitchell, J. K. (1988). Profiling of overconsolidation ratio in clays by field vane. *Canadian Geotechnical Journal*, 25(1):150–157.

[Mesri, 1975] Mesri, G. (1975). New design procedure for stability of soft clays. *Journal of Geotechnical and Geoenvironmental Engineering*, 101(Discussion).

[Nakase, 1983] Nakase, A. Kamei, T. (1983). Undrained shear strength anisotropy of normally consolidated cohesive soils. *Soils and Foundations*, 23(1):91–101.

[Op't Eynde and Michiels, 2005] Op't Eynde, S. and Michiels, T. (2005). Stabiliteitsonderzoek van dijken gebouwd met en op industrieel slib. Master's thesis, Department of civil engineering, KU Leuven.

[Plaxis, 2015] Plaxis (2015). Phi-c reduction and comparison with bishop's method. Technical report, Plaxis.

[Powell and Quarterman, 1988] Powell, J. J. M. and Quarterman, R. S. T. (1988). The interpretation of cone penetration tests in clays, with particular reference to rate effects. In *International Symposium on Penetration Testing*, volume 2, pages 903–910, Orlando, Florida.

[Rad and Lunne, 1988] Rad, N. S. and Lunne, T. (1988). Direct correlations between piezocone test results and undrained shear strength of clay. In *International Symposium on Penetration Testing*, volume 2, pages 911–917, Orlando, Florida.

[Rampton and Paradis, 1981] Rampton, V. N. and Paradis, S. (1981). Quaternary geology of Woodstock - Map area 21H, New Brunswick. techreport, Mineral Development Branch, Department of Natural Resources, Fredericton, New Brunswick. Map Report 81-3.

[Rémai, 2013] Rémai, Z. (2013). Correlation of undrained shear strength and CPT resistance. *Periodica Polytechnica Civil Engineering*, 57(1):39–44.

[Rowe et al., 1995] Rowe, R. K., Gnanendran, C. T., Landva, A. O., and Valsangkar, A. J. (1995). Construction and performance of a full-scale geotextile reinforced test embankment, Sackville, New Brunswick. *Canadian Geotechnical Journal*, 32(3):512–534.

[Rowe et al., 2001] Rowe, R. K., Gnanendran, C. T., Valsangkar, A. J., and Landva, A. O. (2001). Performance of a test embankment constructed on an organic clayey silt deposit. *Canadian Geotechnical Journal*, 38(6):1283–1296.

[Schofield and Wroth, 1968] Schofield, A. N. and Wroth, P. (1968). *Critical state soil mechanics*, volume 310. McGraw-Hill London.

[Senneset et al., 1982] Senneset, K., Janbu, N., and Svanø, G. (1982). Strength and deformation parameters from cone penetration tests. In *European symposium on penetration testing. ESOPT-II*, volume 2, pages 863–870, Amsterdam.

[Skempton, 1951] Skempton, A. (1951). The bearing capacity of clays. In *Proceedings of the Building Research Congress, Natianal Research Council*, pages 180–189.

[Skempton, 1957] Skempton, A. W. (1957). Discussion. In *Proceedings of the Institution of Civil Engineers*, volume 7, pages 305–307.

[Skempton and Northey, 1952] Skempton, A. W. and Northey, R. D. (1952). The sensitivity of clays. *Géotechnique*, 3(1):30–53.

[Taylor, 1948] Taylor, D. W. (1948). *Fundamentals of soil mechanics*, volume 66. JohnWiley & Sons, New York.

[Technische adviescommissie voor de waterkeringen, 1989] Technische adviescommissie voor de waterkeringen (1989). Leidraad voor het ontwerp van rivierdijken, deel 2: Benedenriviergebied. Technical report, Technische adviescommissie voor de waterkeringen, 's Gravenhage. In dutch.

[Teh, 1987] Teh, C. (1987). *An analytical study of the cone penetration test*. PhD thesis, Oxford University.

[Tennekoon, 2007] Tennekoon, J. (2007). *Geotechnical characterisation of an industrial sludge and mumerical analysis of sludge dam behaviour*. PhD thesis, Department of Civil Engineering, K.U. Leuven.

[Terzaghi, 1943] Terzaghi, K. (1943). *Theoretical soil mechanics*. JohnWiley & Sons, New York.

[Terzaghi et al., 1996] Terzaghi, K., Peck, R. B., and Mesri, G. (1996). *Soil mechanics in engineering practice*. John Wiley & Sons, New York, 3th edition.

[Tielemans and Van Herck, 2017] Tielemans, J. and Van Herck, J. (2017). Evaluatie van de shansep methode voor het ontwerp en de controle van ophogingen met industrieel slib. Master's thesis, Faculteit industriële ingenieurswetenschappen, KU Leuven.

[Tresca, 1868] Tresca, M. H. (1868). Mémoires sur l' écoulement des corps solides. In *Mémoires présentés par divers savant à l'Académie royale des Sciences*, volume 18, pages 733–799. Imprimerie impériale.

[Vaid and Campanella, 1974] Vaid, Y. P. and Campanella, R. G. (1974). Triaxial and plane strain behavior of natural clay. *Journal of Geotechnical engineering division*, 100(3):207–224.

[Van Autenboer, 1993] Van Autenboer, T. (1993). Slibbekkens ham, milieu effect rapport. Technical report, Limburgs Universitair Centrum.

[Van Der Veken, 2002] Van Der Veken, J. (2002). Bouwen van dijken met en op industrieel slib. Master's thesis, Department of Civil Engineering, KU Leuven.

[Van Duinen, 2014] Van Duinen, T. A. (2014). Handreiking voor het bepalen van schuifsterkte parameters, wti 2017 toetsregels stabiliteit. Technical report, Technical Report 1209434-003, Deltares.

[Varathungarajan et al., 2009] Varathungarajan, D. A., Garfield, S. M., and Wright, S. G. (2009). Characterization of undrained shear strength profiles for soft clays at six sites in texas. Technical report, University of Texas at Austin. Center for Transportation Research.

[Vermeer and Meier, 1998] Vermeer, P. A. and Meier, C. P. (1998). Standsicherheit und verformungen bei tiefen baugruben in bindigen böden. *Geotechnik V., Deutsche G. fur (Hrsg.): Vorträge der Baugrundtagung in Stuttgart, Verlag Gl uckauf*, pages 133–148.

[Vesić, 1975] Vesić, A. S. (1975). *Principles of pile foundation designs*. Duke University.

[Von Mises, 1913] Von Mises, R. (1913). Mechanik der festen Körper im plastisch deformablen Zustand. *Nachrichten von der Gesellschaft der wissenschaften zu Göttingen. Math Phys Klasse*, 1:582–592.

[Wheeler et al., 2003] Wheeler, S. J., Näätänen, A., Karstunen, M., and Lojander, M. (2003). An anisotropic elastoplastic model for soft clays. *Canadian Geotechnical Journal*, 40(2):403–418.

[Yonatan et al., 2009] Yonatan, P. H., Maertens, J., Van Gemert, D., Houtmeyers, J., and Goorden, M. (2009). Industrieel slib voor bouwen van een dijk: geotechnisch gedrag en numerieke simulaties. *Geotechniek*, 13(2):46–54.

[Zwanenburg et al., 2012] Zwanenburg, C., Den Haan, E. J., Kruse, G. A. M., and Koelewijn, A. R. (2012). Failure of a trial embankment on peat in Booneschans, the Netherlands. *Géotechnique*, 62(6):479–490.

Curriculum vitae

Kristof VERREYDT Guido Gezellestraat 49 B-2560 NIJLEN

° 23/01/1988, Lier (Belgium)

Married to Nicky Bastiaens (° 24/04/1989, ⚭ 24/10/2015)
Father of Finn (° 26/09/2016) and Ella (° 18/02/2019)

Education

2014 - 2021
PhD student, Department of Civil Engineering, K.U. Leuven

2006 - 2010
MSc in Engineering Technology: Construction, Faculty of Engineering Technology, KU Leuven

2000 - 2006
Secondary education, Economics-Mathematics, Sint-Gummaruscollege Lier

Employment

2010 - present
Project Engineer, Triconsult nv

List of publications

Articles in internationally reviewed scientific journals

Verreydt, K., Van Gemert, D., Rauwoens, P., Houtmeyers, J., Claes, T., and Villalobos, F. A. (2020). Discussion: Analysis of a full-scale slope failure test on a sludge embankment. *Proceedings of the Institution of Civil Engineers - Geotechnical Engineering*, 173(6), 562–564. ISSN (Online) 1751-8563, ISSN (print) 1353–2618.

Verreydt, K., Van Gemert, D., Rauwoens, P., Houtmeyers, J., and Claes, T. (2019). Analysis of a full-scale slope failure test on a sludge embankment. *Proceedings of the Institution of Civil Engineers - Geotechnical Engineering*, 172(5), 417–431. ISSN (Online) 1751-8563, ISSN (print) 1353–2618.
Awarded with Crampton prize

Van Gemert, D., Taerwe, L., and Verreydt, K. (2017). Comparison of evolution of pop-out damage by mixed in burnt lime nodules in precast concrete in outside and inside exposure conditions. *International Journal for Restoration of Buildings and Monuments*, 23(1), 29–40.

Van Gemert, D., Brosens, K., Ignoul, S., Verreydt, K., and Heirman, G. (2014). Cathodic protection of steel elements in reinforced concrete and in masonry constructions. *International Journal for Restoration of Buildings and Monuments*, 20(4), 219–246.

Papers at international conferences and symposia, published in full in proceedings

Verreydt, K., Van Gemert, D., Rauwoens, P. (2020). Design parameters for construction of dikes with treated sludge at redevelopment of sludge reservoirs. *2020 Geotechnical Engineering Proceedings Lecture (ICE-BGA)*, webinar, 18 November 2020.

Deckers, T., Verreydt, K., Brosens, K., and Van Gemert, D. (2018). Draagvermogen van historische constructies. Praktijkcases beschouwd vanuit een ingenieursstandpunt. *WTA-Symposium: Draagvermogen van historische constructies. Een sterk verhaal*, Dordrecht, 20 April 2018. <in Dutch>

Brosens, K., Van Gemert, D., and Verreydt, K. (2016). Durable consolidation by cathodic protection of steel elements in historical concrete and masonry buildings. K. Van Balen and E. Verstrynge (eds.), *Proceedings of the 10th International Conference on Structural Analysis of Historical Constructions* (SAHC 2016), pp. 887–894, Leuven, 13–15 September 2016.

Verreydt, K., Brosens, K., Loomans, K., and de Bouw, M. (2016). Analysis of a historical metal structure at Merksplas Colony (B). K. Van Balen and E. Verstrynge (eds.), *Proceedings of the 10th International Conference on Structural Analysis of Historical Constructions* (SAHC 2016), pp. 1644–1649, Leuven, 13–15 September 2016.

Brosens, K., Van Gemert, D., and Verreydt, K. (2015). Historische funderingen: Overzicht, standzekerheidsproblematiek en technieken voor versterking. WTA-Symposium *Schade aan bouwkundig erfgoed door bewegingen in de ondergrond*, pp. 18–34, Antwerpen, 20 November 2015. <in Dutch>

Verreydt, K., Van Gemert, D., Houtmeyers, J., and Van Waelderen, J. (2014). Redevelopment of old sludge reservoirs. *Proceedings of 7th International Congress on Environmental Geotechnics*, ICEG 2014, pp. 644–649, Melbourne, Australia, 10–14 November 2014.

Verreydt, K., Van Gemert, D., Houtmeyers, J., and Van Waelderen, J. (2014). Redevelopment of old sludge reservoirs. Xuan L. (ed.), *Proceeding of 5th International Conference on Environmental Science and Development*, ICESD 2014, Vol.10, pp. 177–181, Singapore, 19–21 February 2014.

Ignoul, S., Verreydt, K., De Backer, L., and Van Gemert, D. (2013). Innovatieve toepassingen van hout: een overzicht van kapconstructies tot de Tweede Wereldoorlog. Studiedag *Bouwmaterialen & constructietechnieken in het interbellum*, WTA Nederland-Vlaanderen, Leuven, 8 November 2013. <in Dutch>

Papers at national conferences and symposia, published in full in proceedings

Van Gemert, D., Ignoul, S., Verreydt, K., and Heirman, G. (2013). Oude en nieuwe funderingssystemen en archeologische artefacten. Onderlinge impact van archeologie en funderingen. *Seminarie Onroerend Erfgoed Brussel*, 16 May 2013. <in Dutch>

Brosens, K., Verreydt, K., and Dereymaeker, J. (2011). Het gebruik van SCRP voor het versterken van betonstructuren - Recente ontwikkelingen en piloottoepassing van voorgespannen SCRP wapening. Studiedag *Nieuwe generatie gelijmde wapening*, ie-net, Genootschap Civiele Techniek, Antwerpen, 29 November 2011. <in Dutch>

Book chapters

Verreydt, K., Brosens, K., Loomans, K., de Bouw, M., and Van Gemert, D., (2019). Technieken voor revitalisering van constructies met respect voor historische waarden. Deel 2: Analyse en versterking van de historische staalconstructie in de kapel van Merksplas-Kolonie. In: A. De Nayer, D. Van Gemert, J. Elsen, Y. Vanhellemont, E. Verstrynge (eds.), *Handboek Onderhoud, Renovatie en Restauratie*. Chapt. II.1, afl. 74, pp. 157–178. Mechelen: Kluwer. <in Dutch>

Van Gemert, D., Taerwe, L., and Verreydt, K. (2017). Evolutie van popoutschade in beton ten gevolge van ingemengde, gebrande kalkkorrels. In: A. De Nayer, D. Van Gemert, J. Elsen, Y. Vanhellemont, E. Verstrynge (eds.), *Handboek Onderhoud, Renovatie en Restauratie*, Chapt. II.5.2, afl. 68, pp. 163–199. Mechelen: Kluwer. <in Dutch>

Van Gemert, D., Brosens, K., Ignoul, S., Verreydt, K., and Heirman, G. (2015). Kathodische bescherming van wapeningen in gewapend beton en van stalen elementen in metselwerkconstructies. In: A. De Nayer, D. Van Gemert, J. Elsen, Y. Vanhellemont, E. Verstrynge (eds.), *Handboek Onderhoud, Renovatie en Restauratie*, Chapt. III, afl. 61, pp. 69–116. Mechelen: Kluwer. <in Dutch>

Ignoul, S., Verreydt, K., and Van Gemert, D. (2014). Innovatieve toepassingen van hout: een overzicht van kapcontructies tot de Tweede Wereldoorlog. In: A. De Nayer, D. Van Gemert, Y. Vanhellemont, H. De Clerck (eds.), *Handboek Onderhoud, Restauratie, Renovatie*, Chapt. II.4, pp. 1–34. Mechelen: Kluwer. <in Dutch>

Van Gemert, D., Ignoul, S., Verreydt, K., Brosens, K., and Heirman, G. (2013). Standzekerheidsproblemen bij oude funderingssystemen, deel 1. In: A. De Nayer, D. Van Gemert, H. De Clercq, Y. Vanhellemont (eds.), *Handboek Onderhoud, Restauratie, Renovatie*, Chapt. II.5.3 Degradatie van structuren, pp. 125–162. Mechelen: Kluwer. <in Dutch>

Van Gemert, D., Ignoul, S., Verreydt, K., Brosens, K., and Heirman, G. (2013). Standzekerheidsproblemen bij oude funderingssystemen, deel 2. In: A. De Nayer, D. Van Gemert, H. De Clercq, Y. Vanhellemont (eds.), *Handboek Onderhoud, Restauratie, Renovatie*, Chapt. II.5.3 Degradatie van structuren, pp. 162–192. Mechelen: Kluwer. <in Dutch>



FACULTY OF ENGINEERING TECHNOLOGY
DEPARTMENT OF CIVIL ENGINEERING
BUILDING MATERIALS AND BUILDING TECHNOLOGY DIVISION
Kasteelpark Arenberg 40, box 2448
B-3001 Leuven
kristof.verreydt@kuleuven.be
http://www.bwk.kuleuven.be/mat